AN ABSTRACT OF THE DISSERTATION OF

Hadi Hasan for the degree of Doctor of Philosophy in Industrial Engineering presented on March 23, 2006.
Title: Development of Microchannel Arrays in Aluminides.

Abstract approved:

Signature redacted for privacy.

Brian K. Paul

Micro Energy and Chemical Systems (MECS) devices enable at least two areas of benefit due to the accelerated heat and mass transfer that can be accomplished in microchannels. First, MECS devices enable process intensification; the ability to reduce the volume of space needed to implement systems of thermal and chemical unit operations. Second, MECS devices permit new capabilities for material synthesis and process control not possible at larger scales. Recent interest in high temperature MECS applications, such as catalytic combustion, fuel reforming, and waste heat recovery, has given rise to the need for materials that support high temperature microreactors. This dissertation investigates new microlamination methods for producing economical, intermetallic microchannel arrays that can resist high temperatures and have a high aspect ratio. The first part of the research shows the capability of fabricating two fluid microchannel array design from $Ni_3Al$ and FeAl foils, produced using existing

aluminide foils. FeAl foil is found to be superior from an economical vantage. However, NiAl is a much better choice for high temperature catalytic reactions. Therefore, the second part of this dissertation investigates the effects of foil and processing conditions, primarily surface roughness and Ni plating, on diffusion bonding of reactively synthesized NiAl foils. Carbon inclusion is minimized in the matrix and better surface roughness obtained by using pyrolytic boron nitride platens of smoother texture. Void free bonds and better homogenization are accomplished by virtue of smoother surface roughness and thinner nickel layer. It is expected that economical NiAl foils could be produced using powder roll compaction techniques. The roughness wavelength and perhaps the amplitude of foils made in this manner would need to have less than 20% variation with excellent bonding results anticipated at around 5% variation.

# Development of Microchannel Arrays in Aluminides

by

Hadi Hasan

A DISSERTATION

submitted to

Oregon State University

in partial fulfillment of
the requirements for the
degree of

Doctor of Philosophy

Presented March 23, 2006
Commencement June 2006

Doctor of Philosophy dissertation of Hadi Hasan presented on March 23, 2006

APPROVED:

Signature redacted for privacy.

Major Professor, representing Industrial Engineering

Signature redacted for privacy.

Head of the Department of Industrial and Manufacturing Engineering

Signature redacted for privacy.

Dean of the Graduate School

I understand that my dissertation will become part of the permanent collection of Oregon State University libraries. My signature below authorizes release of my dissertation to any reader upon request.

Signature redacted for privacy.

Hadi Hasan, Author

ACKNOWLEDGEMENTS

My heartiest gratitude to Dr. Brian K. Paul for his guidance, encouragement, and financial support throughout the course of my study. May Lord Jesus Christ, peace be upon his name, bless his heart. I would like to thank all my committee members, Dr. Sundar Atre, Dr. David Porter, Dr. Kevin Drost, and Dr. John Sessions for their guidance and commitment. Special thanks to Dr. Yunlong Sun of Electro Scientific Industries for helping me with my concepts, and to Dr. Skip Rochefort for giving me unlimited access to his lab. I am grateful to Steve Etringer, our developmental engineer, for all his help at critical moments in this research.

I thank all the wonderful friends at Oregon State University. Many thanks to Tom Tseng for the lively discussions which helped me gain a better understanding of the physical mechanisms. Thanks a million to Raghavendaran Nagarajan, truly a Godsend (Guru Prasad), who helped me with my mathematical concepts throughout the course of my study and asked me tough questions when it mattered.

My appreciation to my mother, soul of my late father, and parents of my wife for their patience and prayers, and to all my brothers, especially to Ali Hasan who always gave me good advice and helped me focus on the big picture. Last but not the least, I express my gratitude to my best fried, soul mate, and wife Najia Ali Hyder whose patience and contribution to this Ph.D. is too enormous to mention. From the very first day to the last, she earned this degree with me every step of the

way. Therefore, I dedicate this dissertation to her. Finally, I express my gratitude to the Almighty and His favorites by saying:

*As Salam Aay Rasan-O-Tauq-O-Salasil Kay Aseer*

TABLE OF CONTENTS

TABLE OF CONTENTS (Continued)

TABLE OF CONTENTS (Continued)

LIST OF FIGURES

LIST OF FIGURES (Continued)

LIST OF FIGURES (Continued)

LIST OF TABLES

# DEVELOPMENT OF MICROCHANNEL ARRAYS IN ALUMINIDES

# CHAPTER 1

# INTRODUCTION

## 1.1. Microfluidic Devices

Micro Energy and Chemical Systems (MECS) are multiple length-scale (multi-scale) fluidic devices, which rely on highly-paralleled, embedded microchannels for the distributed processing of bulk mass and energy. Through the accelerated heat and mass transfer that can be accomplished in microchannels, MECS devices enable at least two areas of benefit. First, MECS devices enable process intensification; the ability to reduce the volume of space needed to implement systems of thermal and chemical unit operations. These spatially-intensified devices permit the distributed processing of mass and energy including applications such as on-board fuel reforming for automotive fuel cells, man-portable heat pumps and tissue-based toxicity sensing. Second, MECS devices permit new capabilities for material synthesis and process control not possible at larger scales. Examples of improved

capabilities at the micro-scale include more uniform mixing, much higher operating pressures and better temperature control including rapid quenching.

MECS devices differ from other microfluidic applications involving biological or chemical assaying. MECS devices are used to process bulk amounts of fluid compared with micro total analysis systems (μTAS) which analyze small samples. Consequently, MECS devices are much larger than μTAS devices. The overall size of MECS devices can range between a few millimeters for portable power systems to almost one meter for distributed fuel reformers. They are typically based on arrays of microchannels in order to handle much larger volumes of fluid and also typically have more demanding chemical and thermal property requirements. Critical microchannel features tend to vary between 25 and 250 μm.

## 1.2. Applications

Various potential applications of MECS technologies have been identified. Past and current development efforts have targeted broad ranging applications including high flux heat exchangers, microscale combustion systems, compact chemical reactors (Drost, Call, Cuta, and Wegneg, 1997), compact gas/liquid contactors, compact biological reactors, thermal management systems, hydrogen production for portable and distributed power generation, portable and distributed heat actuated cooling systems, distributed chemical reactors for environmental restoration (Ameel, Warrington, Wegneg,

and Drost, 1997), in-situ resource processing for space applications (TeGrotenhuis, Wegeng, Vanderwiel, Whyatt, Viswanath, and Schielke, 2000), $CO_2$ remediation and sequestration systems (VanderWiel, Zilka-Marco, Wang, Tonkovich, and Wegneg, 2000), and biological sensors for chemical and biological warfare applications (Marshall, 2002). Current technologies under development include distributed and portable heat pumps to be used in automobile engines; microreactors for molecular manufacturing; microreactors for the production of biodiesels; and portable kidney dialysis systems.

MECS are typically fabricated by microlamination involving the patterning, registration and bonding of thin layers (laminae) of metal, ceramics, and/ or polymers (Paul and Peterson 1999). Lamina patterning may employ laser micromachining, wet etching, electrochemical machining, embossing etc. Laminae registration entails stacking a number of laminae together to ensure proper alignment and dimensional accuracy. Laminae bonding may include solid state diffusion bonding, diffusion soldering and brazing, polyimide sheet adhesive, microprojection welding etc.

Recent interest in high temperature MECS applications, such as catalytic combustion, fuel reforming, and waste heat recovery, has given rise to the need for materials to support high temperature microreactors (Knitter, Bauer, Linner-Kramer, and Hanjosten, 1999). Because of their high-temperature corrosion resistance, ceramics have been an obvious choice in the fabrication of such devices. Ceramic laminae are formed in the unfired state by

consolidating ceramic powder into the desired shape with a binder material. However, binder removal in unsupported ceramic laminae can cause warpage or low fractional densities.

## 1.3. Objectives

The objective of this dissertation is to investigate new microlamination methods for producing economical, intermetallic microchannel arrays that can resist high temperatures with high aspect ratio. Key objectives are to show improved bonding conditions (less time, temperature and pressure) along with better bond quality (better homogeneity and fewer voids). The first part of this research explores the possibility of fabricating two fluid microchannel array designs out of $Ni_3Al$ and FeAl foils produced using existing aluminide foil technology. The second part investigates the effects of surface roughness and Ni plating on heterogeneous diffusion bonding of reactively synthesized NiAl foils.

## 1.4. Literature Review

A brief literature review of ceramic processing techniques for fabrication of microfluidic devices, and diffusion bonding efforts in intermetallics is presented in this section.

### 1.4.1. Ceramic Processing

Advantages of using a green ceramic tape include easy patterning, no need for oxide removal, since it is essentially in an oxide form, and bonding in a non-vacuum environment unlike metallic laminae that require vacuum or inert atmosphere. The downside of using ceramic tape includes sagging of the green tape into the adjacent channels in case of high aspect ratio microchannels. Sometimes, a sacrificial material, such as glass, has been employed to mitigate the sagging problem (Matson, Martin, Bennett, Stewart, and Bonham 1999). However, glass removal can be problematic. Matson et al. (1999) fabricated ceramic microchannel array devices out of commercially available green ceramic tape: Ferro type A6-C-10. The material is comprised of ceramic/glass composite with organic binder to improve flexibility in the thin sheet form. After patterning a 250 μm thick green ceramic tape with $CO_2$ laser, the ceramic laminae were preconditioned by baking at 50° C for 30 minutes. The patterned shims were stacked together and bonded by uniaxially pressing the stack at 2000 psi and 70° C for 10 minutes. Next, the binder was removed in soaking cycles at an elevated temperature, followed by sintering at 875° C for 30 minutes.

Wilcox et al. (2002) listed various techniques to avoid sagging in ceramic microfluidic devices. An insertion of fugitive materials, by placing a patterned insert within the green sheets, withstands the high pressure required for the lamination conditions in ceramic devices. These materials volatilize at

high temperature, resulting in the desired geometry or microchannel. Secondly, an interlayer of polymer between the successive layers of ceramic accelerates the bonding between the layers by decreasing the required pressure of bonding up to 5 times. The decrease in the lamination pressure minimizes the distortion in the ceramic structure. The polymer PEOX has good adhesive properties and volatilizes during the sintering process. Thirdly, pressure sensitive adhesives (PSA) have been utilized for near room temperature and zero pressure lamination of the ceramic layers.

Recently, a new nano-ceramic material known as HAS-CERCANAM has been developed at Ceramatec Inc. The material has a high surface area (80-100 $m^2/g$) and a nanopore network that remains stable at temperatures as high as 1000° C. Its unique properties allow the incorporation of microchannels, with the help of sacrificial inserts, into the monolithic material using a simple step. This procedure eliminates the need for slow, dry or wet etching required in conventional ceramics such as silicon carbide. The material is cast in molds after mixing the ingredients and reagents to facilitate reaction bonding, followed by undisclosed proprietary techniques. The sacrificial inserts or microfeatures can be incorporated prior to the casting step. Next, the green part is fired at 200° C or 800° C to give the material the desired strength (Akash et al., 2004).

Although, some issues regarding the warpage and fractional densities are being resolved, ceramic processing requires special bonding and sintering

techniques. In comparison with solid intermetallic foils, ceramic processing requires more steps, thus posing a potential for higher production costs.

### 1.4.2. Intermetallic Foils

Intermetallics are another group of materials whose physical properties are comparable to those of ceramics. By definition, intermetallics are metallic compounds which have crystal structures different from the constituent metals, usually having high covalency (Sauthoff, 1995). Aluminide intermetallics exhibit good physical properties, e.g., large high temperature modulus, excellent high temperature corrosion resistance, low to moderate thermal conductivities, and in some cases, low densities and inexpensive elemental constituents. Room temperature processing of these materials is generally difficult due to their brittleness. Aluminide intermetallics have been shaped both through conventional metallurgy processes such as casting and forging, as well as powder metallurgy processes such as hot isostatic pressing and extrusion (German and Iacocca, 1996). Powder extrusion entails gas atomization of intermetallic powders followed by hot extrusion of green cross-sections and densification within a sintering furnace at an elevated temperature, resulting in fine-grained microstructures (Ray, 1990; Wright and Knibloe, 1990; German and Iacocca, 1996). Stoloff and Alman (1991) demonstrated reactive hot isostatic pressing and reactive sintering of mixed elemental powders as a means for forming shaped aluminide compounds and

composites. Microporosity was an issue which was somewhat counteracted by hot isostatic pressing.

Hot rolling of aluminides is difficult owing to the limited ductility in these systems (Sikka, 1996). Two routes have successfully been taken to fabricate intermetallic foils. These include cold rolling of single crystal $Ni_3Al$ to yield an $Ni_3Al$ foil, and powder processing of FeAl sheets by roll compaction.

Demura et al. (2000) fabricated thin ductile foils of $Ni_3Al$ single crystal ranging from 53 to 300 μm in thickness by cold rolling. Rods of boron-free binary stoichiometric $Ni_3Al$ were grown in a furnace. The crystal growth was kept constant by controlling the power of the lamps to achieve high single crystallinity. The grown rods, 12 mm in diameter and 150 mm in length, were sectioned into thin sheets along the direction of the growth by means of electric discharge machining. The sheets, initially 1 or 2 mm thick, were polished and cold-rolled to a thickness of 300 μm by using four-high mills with a work roll diameter of 110 mm. Further rolling was achieved by using 75 mm diameter cemented carbide rolls. Both rolling operations were conducted without using any intermediate annealing or lubricant.

Deevi (2000) fabricated 200 μm thick iron aluminide sheets (Fe-40 at% Al) via the powder metallurgy route. FeAl powder was obtained through water atomization using a molten alloy of FeAl, containing 24-26% Al, 0.005% of Boron, 0.05% of C, 0.42% of Mo, and 0.1% of Zr by weight, as the feedstock.

Green sheets of 660 μm FeAl were obtained by roll compaction from a blended mixture of the atomized powder and binder. Debindering of the FeAl green sheets was carried out at a 350-600° C temperature range in a nitrogen atmosphere for 8 hours. Sintering was conducted at 1260° C. Successive annealing and cold rolling were conducted in three stages at 1150° C, 1260° C and again 1150° C. The sheets were passed through the roller leveler to obtain uniform flatness. Finally, the sheets were annealed at 700° C in vacuum for 2 hours.

NiAl is not commercially available in the form of a foil though it is of particular interest as it has the highest melting temperature among commercial aluminides. As such, an alternative route is to synthesize NiAl foils out of thin elemental foils by means of a self-propagating, high temperature synthesis reaction (Rawers, Hansen, Alman, and Hawk, 1994).

### 1.4.3. Intermetallic Bonding

Owing to tenacious surface oxide films, aluminides are difficult to join. Due to this fact, a limited amount of literature is available on the weldability of aluminides and the characterization of aluminide joints. Santella and David (1985) studied the heat affected zone cracking in the electron beam, laser and gas tungsten arc welding of ductile aluminides of at% Ni-10% Fe-20% Al-0.25%-B (IC-25) and Ni-10% Fe-20% Al-0.10% B (IC103). Annealed sheet stocks of the material were characterized after autogenous welds by electron beam welding, laser welding, and gas tungsten arc welding. A rapid decrease

in ductility was observed for both alloys between 600° and 800° C, which did not recover upon cooling. Cracking was observed in both the fusion zone and heat affected zone. It was determined that cracking was a function of the welding parameters, where high input conditions at low speeds produced fewer cracks. In a subsequent study Santella, David, and Horton (1986) observed that increasing the 10 at% Fe in the alloys decreased the heat affected zone cracking and the composition of boron also had a significant effect on the cracking phenomenon. Samples containing 200 ppm of boron retained high temperature ductility better than samples containing 500 ppm, and produced fewer cracks.

Li and Chaki (1993, 1995) studied the autogenous gas tungsten arc welding of $Ni_3Al$ alloy plates. The plates were cut from the cast ingot of the alloy and had an at% composition as $Ni_{73.08}Al_{15.82}Cr_{8.33}Mo_{1.68}Zr_{0.52}B_{0.05}$. Cracks were observed in the heat affected zone described as liquation cracks around the dendritic boundaries and eutectic cells. Microcracks were observed in the fusion zone around the eutectic cells. Enrichment of the alloy with zirconium formed eutectic alloys with Nickel and the dendritic boundaries melted at 1150° C. Further annealing at 1100° C in Argon for 23 hours reduced the melting temperature to 1125° C and increased the liquation cracking in the heat affected zone.

Moore and Kalinowski (1993) used the diffusion brazing process to join NiAl bars. Aluminum was evaporated from the specimen by annealing it

at about 1550° C for 1 to 3 minutes, leaving a nickel rich layer. The specimen was brazed at about the same temperature for 15 minutes under nominal pressure, followed by hot isostatic pressure of 138 MPa at 1340° C for 4 hours in a vacuum environment. The specimen was further annealed at 1530° C for 6 hours to homogenize the matrix. Metallographic studies of butt joints did not show a discernable difference between the parent material and the brazed joints.

Banovic, DuPont, Tortorelli, and Marder (1999, 2001) while cladding carbon steel substrates with FeAl, employing the gas tungsten arc and gas metal arc welding process, observed that FeAl cladding was directly related to the aluminum composition within the deposit. FeAl with less than 10wt % aluminum was readily weldable, whereas higher concentration of aluminum produced poor welds and cracks in the interface.

Dunford and Wisbey (1993) noted that titanium readily absorbs its own surface oxide layer above 750° C thus its alloys are easily bonded above this temperature in an inert or vacuum environment. They reported that $Ti_3Al$ based alloys can be bonded at 900° C to 1100° C. Diffusion bonding of TiAl was deemed more difficult than that of $Ti_3Al$ based alloys, since aluminum modified titanium oxides are formed in the former which may restrict the grain boundary migration along the interface.

Clemens, Lorich, Eberhardt, Glatz, Knable, and Kestler (1999) presented the results of solid-state diffusion bonding of $\gamma$-TiAl based alloys.

About 1 mm thick γ-TiAl sheets were diffusion bonded at 1000° C under 40 MPa for 1 to 8 hours. Metallographic studies showed a good bond interface without any voids.

Wallis, Ubhi, Bacos, Josso, Lindqvist, Lundstrom, and Wisbey (2004) joined γ-TiAl sheets using a Ti-Cu-Ni braze alloy at the interface. Brazing was conducted at 1040° C for 10 minutes. Bonding temperatures of 1000° C under various pressures of 0.003 MPa, 0.8 MPa and 3 MPa with a dwell time of 30 minutes were employed. Shear tests revealed a shearing strength of 220 to 230 MPa for the various bonding pressures.

Nakao, Shinozaki, and Hamada (1991) diffusion bonded TiAl bars at 1273 to 1473 K under a varying pressure of 10 to 30 MPa with a varying bonding time of 16 minutes to 64 minutes. Diffusion bonding diagrams were drawn to show the bonding conditions for void free joints. Tensile strength of 225 MPa was obtained for the joints at room temperature.

All of these prior attempts to join intermetallics were carried out in the bulk. Very few efforts have been made to embed micro-scale geometries within a bulk intermetallic sample. Kanlayasiri and Paul (2004) researched reactive diffusion bonding parameters to microlaminate a leak-free, parallel flow microchannel array using reactively diffused NiAl foils. Non-homogeneous bonds were achieved using a 7 μm thick Ni foil interlayer. Bonding conditions were extreme, resulting in fin warpage and long bonding cycles.

## 1.5. Overview of Research

This research deals with issues related to the development of high temperature microchannel arrays from aluminide foils. Due to their high strength to weight ratio and excellent resistance to corrosion at high temperatures, aluminide intermetallics are a good candidate for making high temperature devices. Furthermore, a functional aspect ratio of 28:1 has been successfully fabricated in NiAl foils (Kanlayasiri, 2003). The research is conducted on three intermetallic aluminide foils: single crystal $Ni_3Al$ foil, an ordered intermetallic phase in the nickel aluminide system; FeAl, an ordered phase in the iron-aluminide system; and NiAl synthesized from commercially pure Ni and Al, the other ordered intermetallic phase in the nickel aluminide system.

In the first part of this study, the potential for making high temperature microchannel devices is demonstrated through the use of pre-fabricated single crystal $Ni_3Al$ foil. A two-fluid counter flow microchannel array is fabricated from cold rolled, single crystal $Ni_3Al$ foil. A leak-proof device is successfully fabricated. Metallographic studies of the cross-section of the bonded foils do not show any bond line or voids at the bonding interface. However, cost is a major issue in mass production of high temperature devices from single crystal $Ni_3Al$ foils.

The second part of this research investigates the potential for fabricating two-fluid counter flow microchannel array from more economical

FeAl foil, made from a powder roll compaction method. Metallographic studies of the array show void free, sound bond interfaces. However, a marked deformation is observed in the microchannel geometry. This deformation and warpage could be the effect of the applied bonding pressure at an elevated temperature and may be eliminated by optimizing the bonding conditions.

The third part of this research deals with the diffusion bonding of synthesized NiAl foils from commercially pure Ni and Al foils. One motivation for this research is to explore the possibility for other types of aluminide foils, for instance NiAl, to be produced by following the same route as the FeAl foil. In particular, the research investigates the effect of foil surface roughness on bond quality in the diffusion bonding process. An isostatic diffusion bonding model is synthesized from the literature and employed to understand the effect of different bonding parameters in the diffusion bonding process. The prediction of the theoretical model is found to be consistent with experimental results. An improvement in the bond quality and the homogeneity of the bonded laminae, over previous research by Kanlayasiri (2003), is demonstrated by decreasing the surface roughness of the mating surfaces through the use of smoother pyrolytic boron nitride platens. A significant reduction in carbon contamination is also achieved by using PBN platens instead of graphite platens to hold the laminae. A thin nickel layer is deposited on NiAl laminae as a diffusion aid, by means of electroplating, to expedite the diffusion bonding process. General observations are made on foil

surface requirements for future NiAl foils produced by powder roll compaction methods.

## 1.6. References

Akash, A., Nair, B., Minnick, K., Wilson, M., and Hartvigsen, J., (2004), "HAS-CERCANAM: A New Material with a Continuous Nanopore Network," Materials Research Society Symposium, 788: 359-363.

Ameel, T. A., Warrington, R. O., Wegneg, R. S., and Drost, M. K., (1997), "Miniaturization Technologies Applied to Energy System," Energy Conversion Management, 38(10-13): 969-982.

Banovic, S. W., DuPont, J. N., Tortorelli, P.F., and Marder, A.R., (1999), "Role of Aluminum on the Weldability and Sulfidation Behavior of Iron-Aluminum Cladding," Welding Journal, 78(1): 23s-30s.

Banovic, S. W., Dupont, J.N., and Marder, A. R., (2001), "Experimental Evaluation of Fe-Al Claddings in High-Temperature Sulfidizing Environments," Welding Journal, 80(3): 63s-70s.

Clemens, H., Lorich, A., Eberhardt, N., Glatz, W., Knabl, W., and Kestler, H., (1999), "Technology, Properties and Applications of Intermetallic γ-TiAl Based Alloys," Zeitschrift fuer Metallkunde/Materials Research and Advanced Techniques, 90(8): 569-580.

Deevi, S. C., (2000), "Powder Processing of FeAl Sheets by Roll Compaction," Intermetallics, 8: 679-685.

Demura, M., Kyosuke, K., Umezawa, O., George, E. P., and Hirano, T., (2001), "Ductile Thin Foil of $Ni_3Al$," ASTM Special Technical Publication, n 1413, Mechanical Properties of Structural Films, 248-261.

Drost, M. K., Call, C. J., Cuta, J. M., and Wegneg, R. S., (1997), "Microchannel Integrated Evaporator/Combustor Thermal Processes," Microscale Thermophysics Engineering, 1(4): 321-333.

Dunford, D. and Wisbey, A., (1993), "Diffusion Bonding of Advanced Aerospace Metallics," Materials Research Society Symposium Proceedings, 314: 39-50

German, R. M. and Iacocca, R. G., (1996), "Powder Metallurgy Processing," Physical Metallurgy and Processing of Intermetallic Compound, Chapman & Hall, NewYork, pp. 605.

Kanlayasiri, K. and Paul, B. K., (2004), "A Nickel Aluminide Microchannel Array Heat-Exchanger for High Temperature Applications," Journal of Manufacturing Processes, 6(1): 17-25.

Knitter, R., Bauer, W., Linner-Kramer, B., and Hansojosten, E., (1999), "Rapid Manufacturing of Ceramic Microcomponents," EUROMAT 99, September 27-30, Munche, 14-18.

Li, H., and Chaki, T. K., (1993), "Welding of a Two-Phase $Ni_3Al$ Alloy," Materials Research Society Symposium Proceedings, 288: 1167-1172.

Li, H., and Chaki, T. K., (1995), "Grain Boundary Melting and Hot Cracking in Weld HAZ of a Two-Phase $Ni_3Al$ Alloy Containing Zr," Materials Research Society Symposium - Proceedings, 364(1): 375-380.

Marshall, P. D., (2002), "Advanced Sensor Technologies for Micro- to Nano-Scale Biological Measurements," Proceedings of IEEE Sensors, 1(1): 466-471.

Matson, D. W., Marin, P. M., Bennett, W. D., Stewart, D. C., and Bonham, C. C., (1999), "Laminated Ceramic Ccomponents for Micro Fluidic Applications," Proceedings of SPIE - The International Society for Optical Engineering, 3877: 95-100.

Moore, T. J. and Kalinowski, J. M., (1993), "Diffusion Brazing NiAl With Self-Generated Filler Metal" Materials Research Society Symposium Proceedings, 288: 1173-1178.

Nair, B., Wislon, M., Akash, A., Crandallm J., Lewinsohn, C., Cutler, R., and Flinders, M., (2004), "Ceramic Microfabrication Techniques for Microdevices with Three-Dimensional Architecutre," Materials Research Society Symposium Proceedings, 782: 205-210.

Nakao, Y., Shinozaki, K., and Hamada, M., (1991), "Diffusion Bonding of Intermetallic Compound TiAl," ISIJ International, 31(10): 1260-1266.

Paul, B. K., and Peterson, R. B., (1999), "Microlamination for Microtechnology Based Energy, Chemical, and Biological Systems," American Society of Mechanical Engineers, Advanced Energy Systems Division (Publication) AES, 39: 45-52.

Paul, B. K., Hasan, H., Dewey, T., Alman, D., and Wilson, R. D., (2002), "An Evaluation of Two Methods for Producing Intermetallic Microchannels," American Society of Mechanical Engineers, Micro-Electromechanical Systems Division Publication (MEMS), 261-266.

Rawers, J. C., Hansen, J. S., Alman, D. E., and Hawk, J. A., (1994), "Formation of Sheet Metal-Intermetallic Composites by Self-Propagating High-Temperature Reactions," Journal of Materials Science Letters, 13:1357-1360.

Ray, R., (1990), "Dipersion Strengthened Nickel Aluminide (NiAl) Alloys via Advanced Melt Spinning Technology," Metal Powder Report, 45(1): 56-59.

Santella, M. L, and David, S. A., (1985), "Study of HAZ Cracking in Ductile Aluminides," Abstracts **of** Papers Presented at 66th AWS Annual Meeting, 228-230.

Santella, M. L., David, S. A., and Horton, J. A., (1986), "Weldability of and Ni3Al Alloy," Advances in Welding Science and Technology - TWR '86: Proceedings of an International Conference on Trends in Welding Research, 629-633.

Sauthoff, G., (1995), "Intermetallics," Weinhem, New York, pp. 1-2, 38-40.

Sikka, V. K., (1996), "Processing of Aluminides," Physical Metallurgy and Processing of Intermetallic Compound, Chapman & Hall, New York, pp. 561-562.

Stoloff, N. S. and Alman, D. E., (1991), "Powder Processing of Intermetallic Alloys and Intermetallic Matrix Composites," Material Science and Engineering A, 144(1-2): 51-62.

TeGrotenhuis W. E., Wegneg, R. S., Vanderwiel, D. P., Whyatt, G. A., Viswanath, V. V., Schielke, K. P. ,(2000), "Microreactor System Design for NASA In Situ Propellant Production Plant on Mars," AICHE Spring National Meeting, Atlanta, GA.

Wallis, I. C., Ubhi, H. S., Bacos, M. P., Josso, P., Lindqvist, J., Lundstrom, D., and Wisbey, A., (2004), "Brazed Joints in $\gamma$ TiAl Sheet: Microstructure and Properties," Intermetallics, 12(3): 303-316.

Wilcox, D. L., Burdon, J. W., Changrani, R., Chou, c., Dai, S., Koripella, R., Oliver, M., Sadler, D., Allmen, P. V., and Zenhauasern, F., (2002), "Add Ceramic "MEMS" to the Pallet of Microsystem Technologies," Materials Research Society Symposium Proceedings, 687: 225-242.

Wright R. N., and Knobloe, J. R., (1990), "Influence of Alloying on the Microstructure and Mechanical Properties of P/M $Ni_3Al$," Acta Metalllurgica, 38(10): 1993-2001.

# CHAPTER 2

# DEVELOPMENT OF $Ni_3Al$ MICROCHANNEL ARRAYS FOR HIGH-TEMPERATURE MICROREACTORS AND MICRO-SCALE HEAT EXCHANGERS

## 2.1. Introduction

Micro Energy and Chemical Systems (MECS) are multi-scale fluidic systems that rely on embedded microchannels for their function. The overall size of MECS devices places them in the mesoscopic regime, i.e., in a size range between macro objects such as automobile engines and laboratory vacuum pumps, and the intricate MEMS-based sensors that reside on a silicon chip. Thus MECS, although having nano and micro-scale features, are large by MEMS standards, straddling the size range between the macro- and micro-worlds.

It is expected that these miniature devices can be produced in high volumes at low cost following the lead of IC devices and MEMS sensors. However, IC and MEMS manufacturing rely heavily on silicon-based processing where submicron features are routinely implemented in production. The microfluidic components in MECS generally do not require the extremely small feature sizes available by silicon micromachining (although

nanotechnology could be employed in the deposition of engineered catalysts on microreactor walls). Furthermore, for many MECS applications, silicon is not the favored base material (Peterson, 1998 and 1999). It has a much higher thermal conductivity than is desired for many energy-based applications and the material, although strong, is brittle, expensive, and cannot always be tailored to specific environmental conditions. In contrast, the functionality of MECS typically requires that they have the thermal, chemical, and physical properties of more traditional engineering materials such as metals or ceramics.

One subclass of MECS devices, which is attracting a growing amount of research interest, is high-temperature microreactors and micro-scale heat exchangers. Because of the environments in which these devices are used, they require materials with high melting temperatures and high-temperature corrosion resistance. A microchannel catalytic combustor/ reactor and a gasoline vaporizer have been produced at Pacific Northwest National Laboratories (Matson, Martin, Stewart, Tonkovich, White, Zilka, and Roberts, 1999). The material used in this application was type 316 stainless steel with microchannel widths on the order of 250 μm. Researchers in Germany created a microchannel heat exchanger that is used in a miniaturized reactor for the synthesis of HCN (Hessel, Ehrfeld, Golbig, Hoffmann, Lowe, and Storz, 1999). The microchannels were fabricated in stainless steel and were on the order of 60 μm wide.

As these devices were fabricated in stainless steel, the maximum operating temperature of these devices is in the range of 550-600°C. Operation above these temperatures over a sustained period of time would cause loss of device effectiveness due to creep. However, there exist numerous applications for microchannel devices at temperatures higher than this. Additional applications of current interest for high temperature (> 600 C) microchannels include (Chaumat, Moret, and Gasse, 1995):

- Steam superheating for driving turbines
- Hydrogen steam reforming
- Gasification of coals and heavy oils
- Flue gas desulphurization
- Chemical, petroleum, petrochemical and metallurgical process waste heat recovery and process heating
- Incineration, especially of hazardous materials
- Domestic furnace waste recovery
- Jet engine heat recovery

Ceramics have been identified as a possible structural material for these devices because of their very high melting temperatures, low thermal conductivity, and corrosion resistance. Some work has been conducted with the use of multi-layer ceramics to form microchannel conduits (Kim, Yi, Zhong, Bau, Hu, and Ananthasuresh, 1998). Problems with ceramics include

warpage due to shrinkage during binder removal, warpage due to sagging, and low fractional densities.

Wilcox et al. (2002) listed various techniques to avoid sagging in ceramic microfluidic devices. An insertion of fugitive materials, by placing a patterned insert or screen printing within the green sheets, sustains the high pressure required for the lamination conditions in ceramic devices. These materials volatilize at high temperature, resulting in the desired geometry or microchannel. Secondly, an interlayer of polymer between the successive layers of ceramic accelerates the bonding between the layers by decreasing the required pressure of bonding up to 5 folds. The decrease in the lamination pressure minimizes the distortion in the ceramic structure. The polymer PEOX has good adhesive properties and volatilizes during the sintering process. Thirdly, pressure sensitive adhesives (PSA) have been utilized for near room temperature and zero pressure lamination of the ceramic layers.

Recently, a new nano-ceramic material known as HAS-CERCANAM has been developed at Ceramatec Inc. The material has a high surface area (80-100 $m^2/g$) and a nanopore network that remains stable at temperatures as high as 1000° C. Its unique properties allow the incorporation of microchannels, with the help of sacrificial inserts, into the monolithic material using a simple step. This procedure eliminates the need for slow, dry or wet etching required in conventional ceramics such as silicon carbide. The material is cast in molds after mixing the ingredients and reagents to facilitate reaction bonding,

followed by undisclosed proprietary techniques. The sacrificial inserts or microfeatures can be incorporated prior to the casting step. Next, the green part is fired at 200° C or 800° C to give the material the desired strength (Akash et al., 2004).

Another group of materials with physical, chemical and thermal properties similar to those of ceramics are aluminide intermetallics (Brandes and Brook, 1992; Golberg, Demura, and Hirano, 1998). However, like ceramics, intermetallics generally have poor formability at room temperature which makes foil formation difficult. Recent intermetallics research has found mechanisms to overcome these problems. Researchers at the National Institute for Materials Science (NIMS) in Japan have recently found methods for producing ductile thin foils of $Ni_3Al$ from single crystals (Demura et al. 2001; Demura et al. 2000). Demura et al. (2001) fabricated thin ductile foils of $Ni_3Al$ single crystal ranging from 53 to 300 μm in thickness by cold rolling. Rods of boron-free binary stoichiometric $Ni_3Al$ were grown in a furnace. The crystal growth was kept constant by controlling the power of the lamps to achieve high single crystallinity. The grown rods, 12 mm in diameter and 150 mm in length, were sectioned into thin sheets along the direction of the growth by means of electric discharge machining. The sheets, initially 1 or 2 mm thick, were polished and cold-rolled to a thickness of 300 μm by using four-high mills with a work roll diameter of 110 mm. Further rolling was achieved by

using 75 mm diameter cemented carbide rolls. Both rolling operations were conducted without using any intermediate annealing or lubricant.

As shown in Figure 2.1, these materials possess excellent high-temperature mechanical properties. Therefore, one approach to aluminide microchannel array formation would be to pattern these foils in their ductile state and diffusion bond them together at high temperature. The objective of this research was to explore some of the issues associated with producing microchannel arrays from this foil.

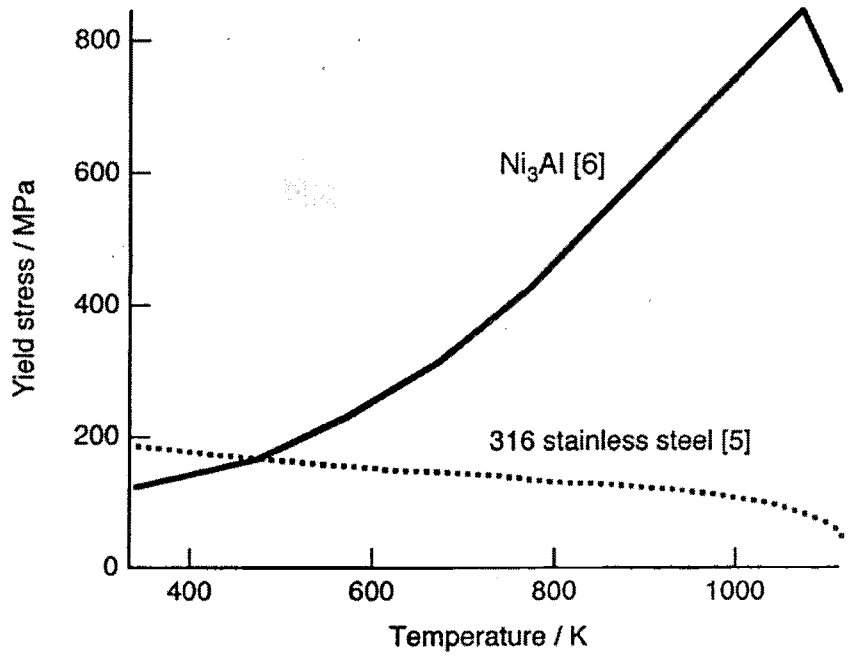


Figure 2.1. Temperature dependence of yield strength of Ni3Al single crystal <100> tensile direction compared with those of 316 stainless steel (Demura et al., 2001)

Table 2.1. Comparison of physical and mechanical properties of some aluminide intermetallics.

| Property | NiAl | $Ni_3Al$ | TiAl | $Ti_3Al$ | FeAl | $Fe_3Al$ |
|---|---|---|---|---|---|---|
| Melting point, K | 1955 | 1663 | 1733 | 1873 | 1523-1673 | 1813 |
| Density, $g/cm^3$ | 5.86 | 7.50 | 3.91 | 4.2 | 5.56 | 6.58 |
| Young's modulus, $10^6$ psi | 42.7 | 25.9 | 25.5 | 21.0 | 37.8 | 23 |
| Thermal expansion, $10^{-6}$/ K at 873 K | 13.2 | 12.5 | 12.2 | - | - | 20 |
| Specific heat, J/g . K | 0.64 | 0.61 | | - | - | |
| Thermal conductivity, W/m.K | 76 | 28.9 | 22 | 15 | - | 10.9 |

## 2.2. Device Design and Fabrication

### 2.2.1. Materials

The equilibrium binary phase diagram for the Nickel-Aluminum system is shown in Figure 2.2 (Massalski, 1990). In particular, the NiAl and $Ni_3Al$ phases are of interest for engineering applications. Table 2.1 compares some physical, mechanical and thermal properties of various aluminide intermetallics (Stoloff and Sikka, 1996; ASM Metal Handbook 1990). The nickel-aluminides tend to have the highest melting temperature while the titanium-aluminides have the lowest density and the iron-aluminides have perhaps the best high-temperature corrosion resistance. This data illustrates the excellent high temperature properties of nickel-aluminides. In particular, $Ni_3Al$ has excellent high-temperature wear resistance, excellent oxidation resistance, carburization resistance, nitridation resistance, high temperature strength, cavitation erosion resistance, and fatigue resistance. Major industrial applications for $Ni_3Al$ based alloys include furnace fixtures, turbochargers for diesel engines, hydroturbines, catalytic converter substrates, and manufacturing tooling (Sikka, 1996).

The $Ni_3Al$ single crystal foil used in this investigation was supplied by Dr. Toshiyuki Hirano at NIMS in Japan (Demura, Suga, Umezawa, Kishida, George, and Hirano, 2001). The Al content was confirmed to be close to the stoichiometric composition (25 at% Al). The $Ni_3Al$ foil provided was about 76

mm long, 36 mm wide, and 85 μm thick and had a significant warp due to the cold rolling process. Deformation of the foil was difficult due to the grain boundaries to assist dislocation movement.

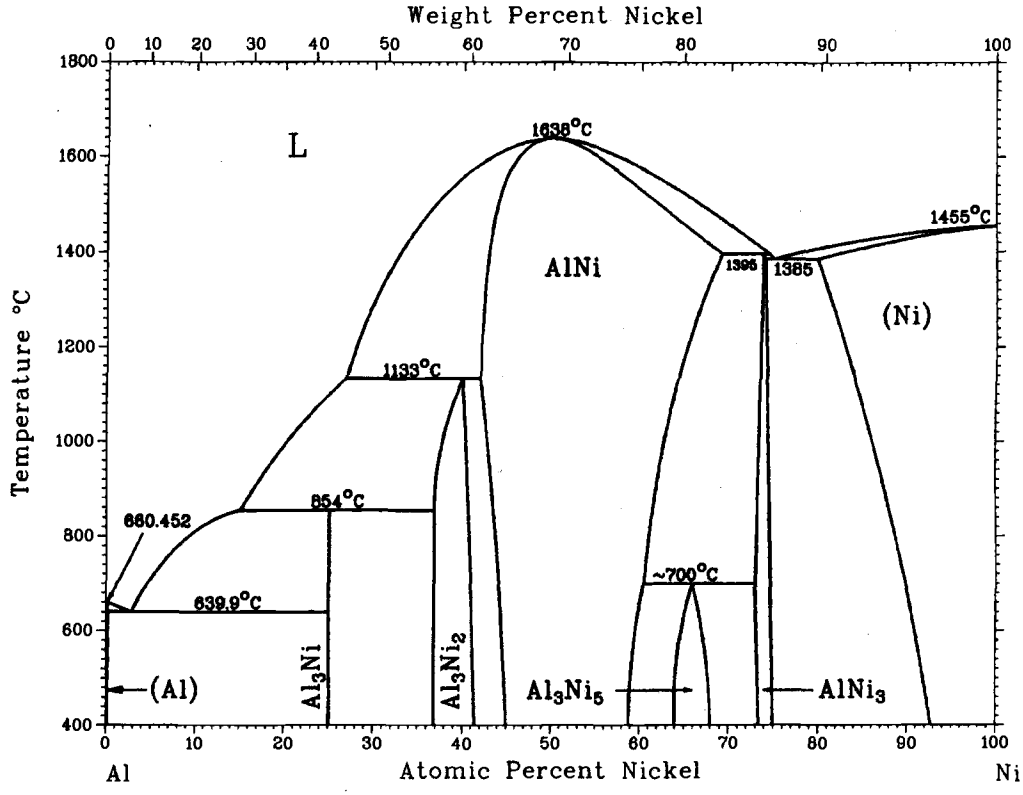


Figure 2.2. The phase diagram for the Ni-Al system (Massalski, 1990)

### 2.2.2. Device Design

To evaluate the $Ni_3Al$ procedure, a counterflow microchannel design was implemented as shown in Figure 2.3. The major dimensions of the laminae were nominally 15 mm by 15 mm. Channel dimensions were 2 mm wide by 10 mm long in the counterflow and 700 μm wide in the neck between

the channel and the header. One reason for the slight dimensions was that very little material was available for sample preparation. Laminae were cut from an 85 μm thick $Ni_3Al$ single crystal foil supplied by Dr. Toshiyuki Hirano at NIMS in Japan. All results reported are from the first attempt at this procedure with a small amount of material. Another reason for the slight dimensions is that oversized dimensions in the width of the neck of counterflow microchannels have been known to cause leakage in two-fluid microchannel systems. Width dimensions in the neck were sized based on known manufacturability rules for two-fluid systems in 304 stainless steel (Paul, Hasan, Thomas, Wilson, and Alman, 2001).

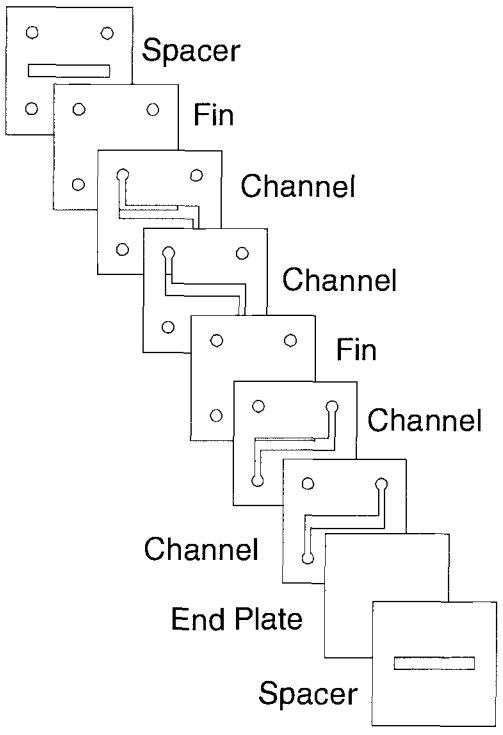


Figure 2.3. An exploded view illustrating the microlamination procedure used to produce an $Ni_3Al$ intermetallic counterflow heat exchanger.

A microlamination procedure was used to implement the counterflow design. This procedure involved laminae patterning, registration, and bonding. At the start of the experiment, very little was known about the machinability and weldability of the foils. Considering the small amount of foil, a conservative approach was taken. The blanks were cleaned using acetone, methanol, and deionized water. An ESI 4420 Laser Micromachining System with a 266 nm UV laser rail was used to pattern the blanks. Optical microscopy of the foils, shown in Figure 2.4, after patterning revealed no cracking in the regions immediately adjacent to the cut but did show some ejecta along the edges.

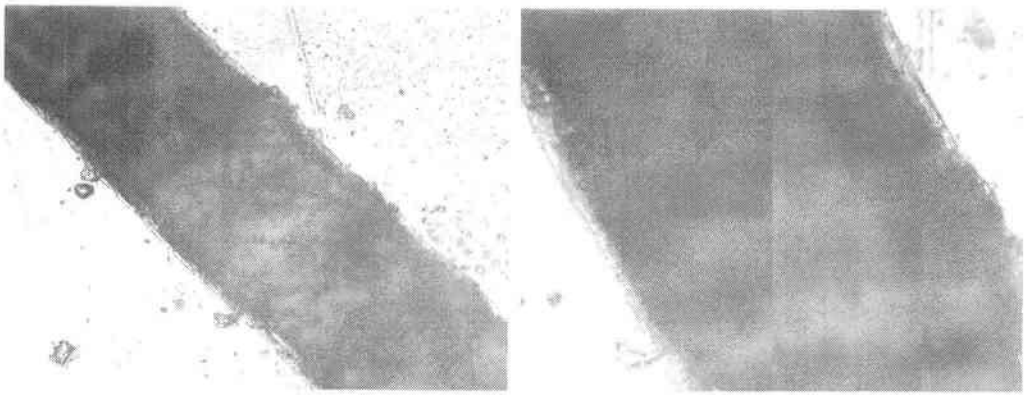

Figure 2.4. Micrographs of laser-machined $Ni_3Al$ foil

Laminae registration was accomplished using a thermally-enhanced edge registration (TEER) technique to minimize misalignment while avoiding buckling which is induced during high-temperature bonding (Thomas and Paul, 2002). Diffusion bonding of the laminae was achieved in a vacuum hot press at elevated temperature and pressure. The sample was fixtured between two graphite platens with 900 psi pressure and heated at a rate of 10°C per minute to a temperature of 900° C in atmospheric gases at $3x10^{-4}$ torr. The sample was held at this temperature for 4 hours to ensure that the intermetallic foils would bond. Temperature profile for the $Ni_3Al$ diffusion bonding cycle is shown in Figure 2.5.

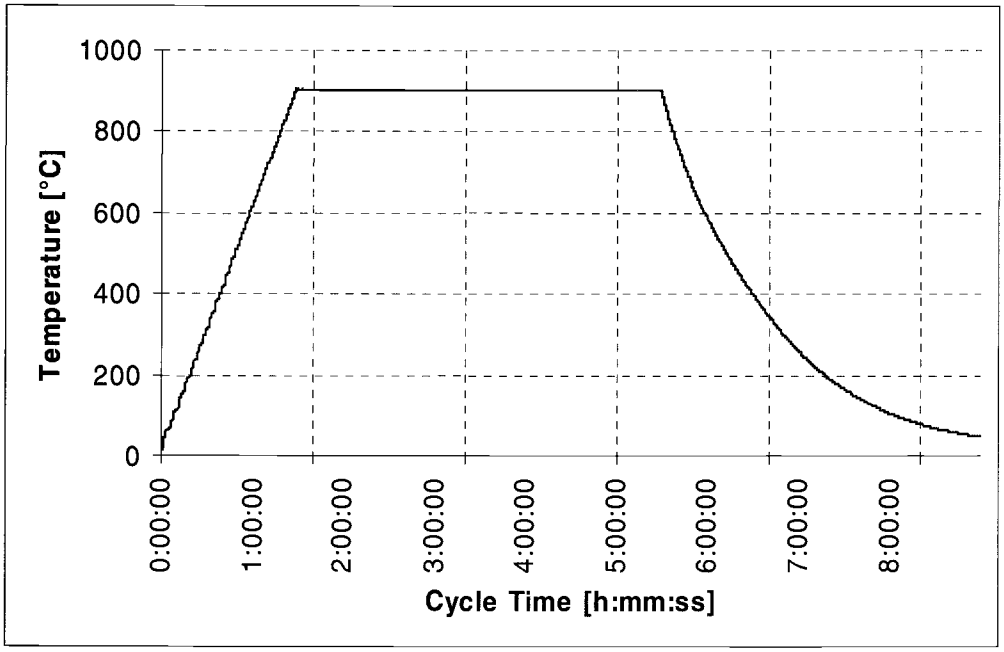


Figure 2.5. Temperature profile of Ni3Al diffusion bonding cycle

## 2.3. Results

The device was found to be brittle after diffusion bonding of the laminae. A leak test was performed on the device to assure soundness of the approach. As stated before, two-fluid systems are known to have particular leakage problems and, therefore, are a good check of the process capability. The test was performed to determine if leakage existed between the counterflow channels. Leakage testing involved hooking pressurized air to one of the inlets and blocking its outlet. The other inlet and outlet were left open and the device and test fixture were submerged under water.

A micrograph of the fabricated $Ni_3Al$ device is shown in Figure 2.6. The device was tested for leakage under more than one atmosphere of gauge

pressure without any sign of bubbles. No leakage was observed between the channels as well as along the edges of the device.

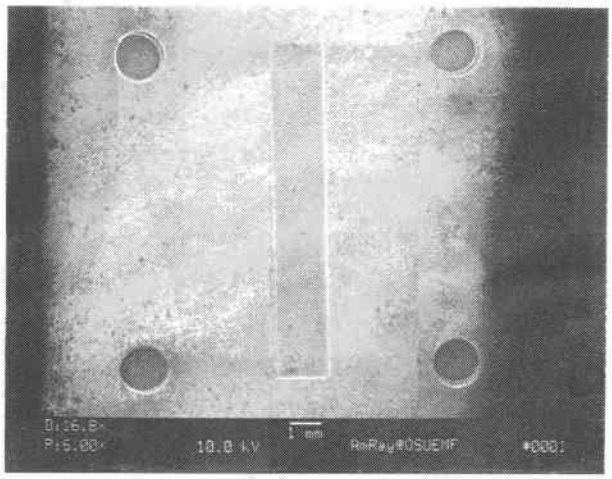


Figure 2.6. Micrograph of the fabricated $Ni_3Al$ counterflow heat exchanger

Micrographs of the cross-section of two $Ni_3Al$ laminae are shown in Figures 2.7. and 2.8. No bond line or voids are visible at the interface indicating a sound bond.

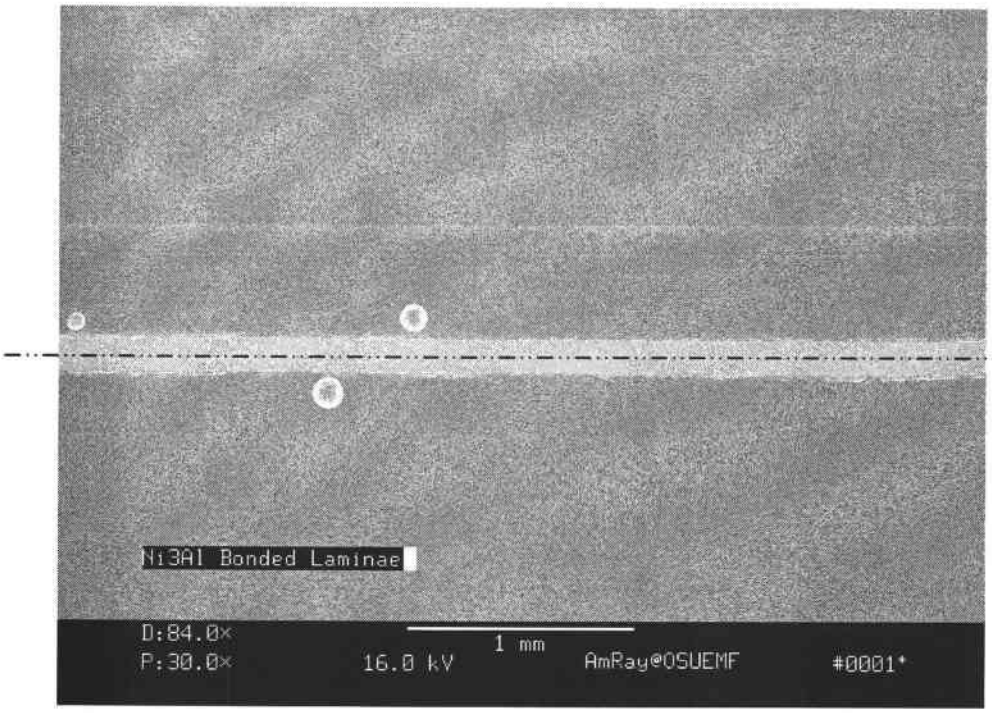


Figure 2.7. Scanning electron micrograph of diffusion bonded $Ni_3Al$ laminae (30X)

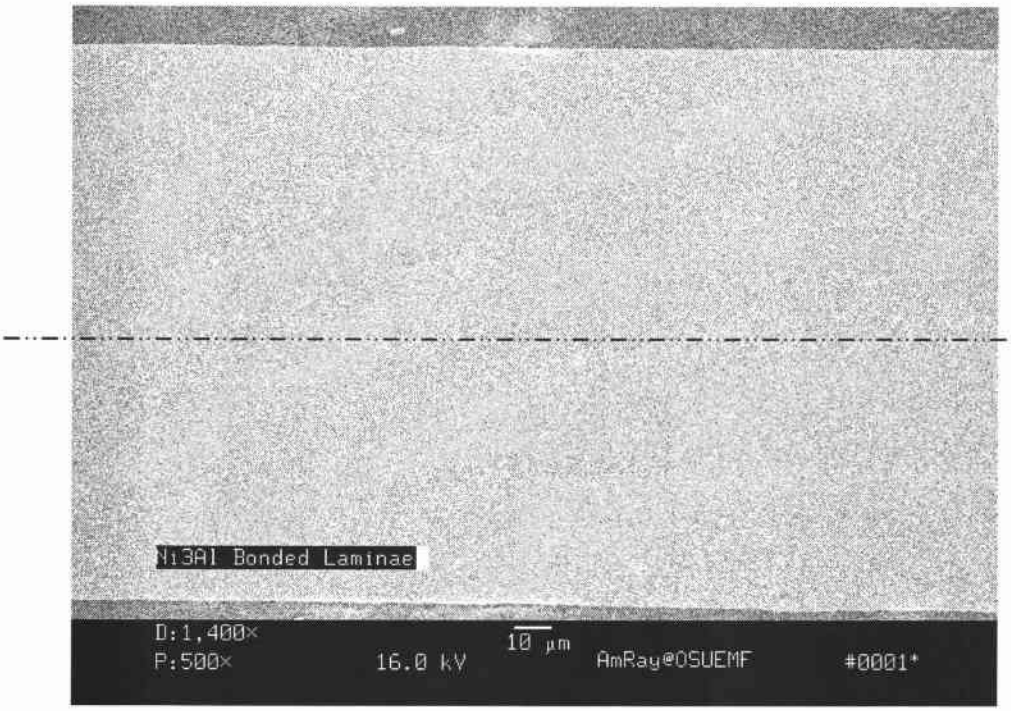


Figure 2.8. Scanning electron micrograph of diffusion bonded $Ni_3AL$ laminae (500X)

## 2.4. Conclusion

The work presented here demonstrates a fabrication technique used to make a two-fluid microchannel device from an $Ni_3Al$ single crystal foil. This method has the advantage of eliminating volumetric shrinkage due to binder removal when compared to ceramic micro-scale devices. The microlamination procedure using $Ni_3Al$ single-crystal foil was found to be leak-proof. It was determined that laser micromachining can be used as a patterning technique without causing thermal cracking in the foil. Metallographic study of the bond quality showed no voids at that bond interface. However, cost is a major issue in mass production of high temperature devices from single crystal $Ni_3Al$ foils.

## 2.5. Acknowledgements

The author would like to acknowledge the generous contribution of $Ni_3Al$ foil by Dr. Toshiyuki Hirano at the National Institute for Materials Science (NIMS), 1-2-1, Sengen, Tsukuba, Ibaraki 305-0047, Japan.

## 2.6. References

Akash, A., Nair, B., Minnick, K., Wilson, M., and Hartvigsen, J., (2004), "HAS-CERCANAM: A New Material with a Continuous Nanopore Network," Materials Research Society Symposium, 788: 359-363.

Alman, D.E. and Dogan, C.P., (1995), "Intermetallic Sheets Synthesized from Elemental Ti, Al, and Nb Foils," Metallurgical and Materials Transactions A, 26A: 2759-62.

Alman, D.E., (1996), "Fabrication, Structure and Properties of Aluminum-Aluminide Layered Composites," Materials Research Society Symposium – Proceeding, 434: 255-260.

"ASM Metal Handbook, Volume 2, Properties and Selection: Nonferrous Alloys and Special Purpose Materials," (1990), American Society for Metals, Metals Park, Ohio, pp. 914-920.

Brandes, E.A. and Brook, G.B. (Ed.), (1992), "Smithells Metals Reference Book," 1992, 7th edition.

Chaumat, G., Moret, F., and Gasse, A., (1995), "SiC Brazing for Ceramic Heat Exchangers," DVS-Berichte, 166:217-219.

Demura, M., Kishida, K., Umezawa, O., George, E.P. and Hirano, T., (2000), "Ductile Thin Foil of $Ni_3Al$," Mechanical Properties of Structural Films, STP 1413, American Society for Testing and Materials, 248-261.

Demura, M., Kyosuke, K., Umezawa, O., George, E. P., and Hirano, T., (2001), "Ductile Thin Foil of $Ni_3Al$," ASTM Special Technical Publication, n 1413, Mechanical Properties of Structural Films, 248-261.

Demura, M., Suga, Y., Umezawa, O., Kishida, K., George, E. P., and Hirano, T., (2001), "Fabrication of $Ni_3Al$ Thin Foil by Cold-Rolling" Intermetallics, 9(2):157-167.

Golberg, D., Demura, M. and Hirano, T., (1998), "Effects of Al-rich off-stoichiometry on the yield stress of binary Ni3Al single crystals," Acta Materialia, 46: 2695-2703.

Hessel V., Ehrfeld, W., Golbig, K., Hoffmann, C., Lowe, H., and Storz, M., (1999), "High Temperature HCN Gerneration in a Complex Integrated Micro-Reaction System," Proceedings of IMRET3, 3RD International Conference on Microreaction Technology, Frankfurt.

Kim, M., Yi, M. Zhong, J., Bau, H.H., Hu, H. and Ananthasuresh, S.G.K., (1998) "The Fabrication of Flow Conduits in Ceramic Tapes and the Measurement of Fluid Flow through These Conduits," Proceedings of the ASME Dynamic Systems and Controls Division, DSC, 66:171-177.

Massalski, T. B., Singleton, M. F., Marray, J. L., and Nash, P., (1990), "Binary Alloy Phase Diagrams," American Society for Metals, Metals Park, Ohio, pp.183.

Matson, D. W., Martin, P., Stewart, D., Tonkovich, A., White, M., Zilka J., and Roberts, G., (1999), "Fabrication of Microchannel Chemical Reactors Using a Metal Lamination Process," Proceedings of IMRET3, 3RD International Conference on Microreaction Technology, Frankfurt.

Paul, B.K., Hasan, H., Thomas, J., Wilson, R., and Alman, D., (2001), "Limits on Aspect Ratio in Two-fluid Micro-scale Heat Exchangers," Transactions of NAMRC XXIX, Gainesville, FL. 461-468.

Peterson, R. B, (1999), "Numerical Modeling of Conduction Effects in Microscale Counterflow Heat Exchangers," Microscale Thermophysical Engineering, 3(1):17-30.

Peterson, R. B., (1998), "Size Limits for Regenerative Heat Engines," Microscale Thermophysical Engineering, 2: 121-131.

Sikka, V. K., (1996), "Processing of Aluminides," Physical Metallurgy and Processing of Intermetallic Compound, Chapman & Hall, NewYork, pp. 598-599.

Stoloff, N. S., and Sikka V. K. (editors) (1996), "Physical Metallurgy and Processing of Intermetallic Compounds," Chapman and Hall, New York, NY, pp. 217.

Thomas, J. and Paul, B. K., (2002), "Thermally-Enhanced Edge Registration (TEER) for Aligning Metallic Microlaminated Devices," Transactions of NAMRC XXX, West Lafayette, IN, 21-24.

Wilcox, D. L., Burdon, J. W., Changrani, R., Chou, c., Dai, S., Koripella, R., Oliver, M., Sadler, D., Allmen, P. V., and Zenhauasern, F., (2002), "Add Ceramic "MEMS" to the Pallet of Microsystem Technologies," Materials Research Society Symposium Proceedings, 687: 225-242.

# CHAPTER 3

# FABRICATION OF ALUMINIDE MICROCHANNEL ARRAYS USING FeAl FOILS SYNTHESIZED BY A POWDER ROLLING AND ANNEALING APPROACH

## 3.1. Introduction

For their excellent corrosion resistance, iron aluminides have drawn the attention of researchers for several decades. They offer outstanding oxidation and sulfidation resistance at a relatively low material cost than many stainless steels. Their high tensile strength, comparable to many stainless steels, lower density and higher strength to weight ratio, than many stainless steels, make them a good candidate as a structural material (Sikka, Viswanathan, and McKamey, 1993). Table 3.1 compares some physical, mechanical and thermal properties for various aluminide intermetallics (Stoloff and Sikka, 1996; ASM Metal Handbook 1990) with 316L stainless steel.

Table 3.1. Comparison of physical and mechanical properties of some aluminide intermetallics.

| Property | NiAl | $Ni_3Al$ | TiAl | $Ti_3Al$ | FeAl | $Fe_3Al$ | 316L SS |
|---|---|---|---|---|---|---|---|
| Melting point, K | 1955 | 1663 | 1733 | 1873 | 1523-1673 | 1813 | 1302 |
| Density, $g/cm^3$ | 5.86 | 7.50 | 3.91 | 4.2 | 5.56 | 6.58 | 8.1 |
| Young's modulus, $10^6$ psi | 42.7 | 25.9 | 25.5 | 21.0 | 37.8 | 23 | 29 |
| Thermal expansion, $10^{-6}$/ K at 873 K | 13.2 | 12.5 | 12.2 | - | - | 20 | 16.2 |
| Specific heat, J/g . K | 0.64 | 0.61 | | - | - | | 0.5 |
| Thermal conductivity, W/m.K | 76 | 28.9 | 22 | 15 | - | 10.9 | 16 |

Thermal conductivity of $Fe_3Al$ is low and electric resistivity is high as compared to other structural alloys. Thermal expansion is similar to 300-series steels up to a temperature of 800° C; above this temperature the expansion of $Fe_3Al$ is higher than the steels. Increasing aluminum concentration in $Fe_3Al$ based alloys results in an increase in the coefficient of thermal expansion (McKamey, 1996). $Fe_3Al$ also exhibits an outstanding high magnetic permeability (Sauthoff, 1995). The magnetic properties in iron aluminides also depend on the aluminum content, where magnetization decreases with increasing aluminum content (McKamey, 1996). FeAl based alloys exhibit excellent corrosion and oxidation resistance in harsh environments and a high strength-to-weight ratio when compared to common structural materials such as stainless steel (Jordan et al., 1999). The two shortcomings of iron aluminides included low ductility at room temperature and a sharp drop in strength above 600° C. Later research shows that a controlled composition and microstructure can improve the ductility 10-15 % in iron aluminides (Sikka, 1993). FeAl-based alloys are hot workable between a temperature range of

900° to 1100° C and can be warm finished at temperatures as low a s 650° C. However, they are not cold workable (Sikka et al., 1993).

The commercial application of iron aluminides generally involves corrosive, high temperature environments. Applications include heating elements, automotive gas turbine engines, coal gasification systems, dies for superplastic formation of titanium-based alloys, catalytic converters, etc. (Sikka et al., 1993).

The equilibrium binary phase diagram for the Iron-Aluminum system is shown in Figure 3.1 (Massalski, 1990). Although iron and aluminum form many intermetallic phases, the ordered phases of FeAl and $Fe_3Al$ are of interest because of their properties.

FeAl-based alloys may also be applied towards the fabrication of recuperators for microturbines. Recuperators are compact heat exchangers that boost the efficiency of microturbines. Recuperators are used to preheat incoming air to the combustor. The application requires high temperature durability including high strength and corrosion resistance. Although, the recuperator technology for microturbines is well established, the maximum operating temperature is limited to 600°-650° C because of the stainless steel construction (Pint et al, 2001). The inlet pressure for the recuperator gas is about 450 kPa for a 100 kW microturbine (Lagerstrom, 2003). One way to improve the recuperator efficiency is to increase the turbine rotor inlet temperature, which will also increase the temperature requirements of the

recuperator. Because of its good corrosion resistance, low density, high melting point and high strength as compared to the stainless steel, FeAl is a good candidate for the fabrication of recuperators for mircoturbines.

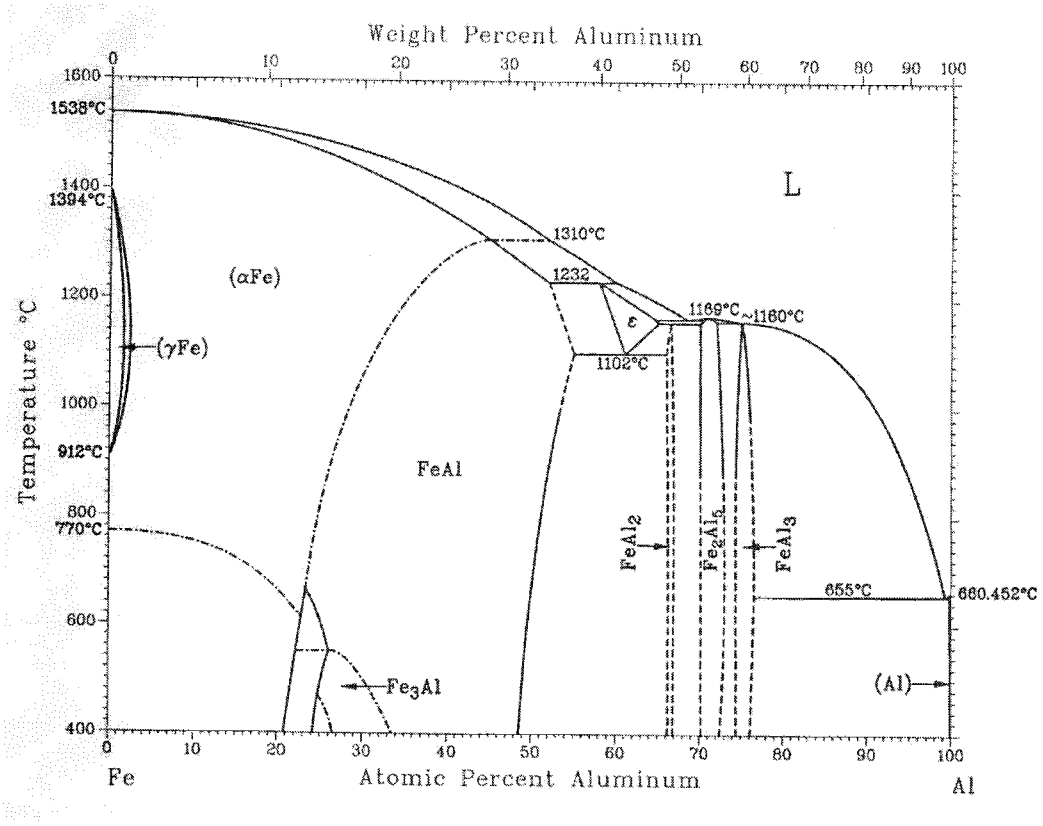


Figure 3.1. Iron-Aluminum binary phase diagram. (Massalski, 1990)

A literature review of research conducted on the bonding of iron aluminides is presented here. David et al. (1999) undertook electron beam welding and gas tungsten arc welding of several $Fe_3Al$ based alloys with 27 to 30 at% Al content. The alloys had varying content of Cr, Nb, Mn, B, $TiB_2$ which were not disclosed due to proprietary reasons. Hot cracking was

observed in case of gas tungsten arc welding. In case of electron beam welding cracks were observed at higher welding speeds whereas good welds were obtained at slower speeds. Few attempts have been made to diffusion bond $Fe_3Al$ to other dissimilar materials. Juan, Yajiang, and Huiqiang (2001 and 2002) diffusion welded $Fe_3Al$ intermetallic compound and Q235 carbon steel. The bonding parameters were a target temperature of 1080° C, holding time of 60 minutes, under a pressure of 9.8 MPa in a vacuum of $5 \times 10^{-6}$ Torr. SEM analysis showed no obvious brittle phases, voids or cracks at the bond interface between $Fe_3Al$ and Q235 carbon steel.

Wang, Li, and Liu (2003) diffusion bonded $Fe_3Al$ and 18-8 stainless steel. The $Fe_3Al$ intermetallic sample was prepared by induction melting in the vacuum and hot-rolling. The sample was machined into a 100 x 20 x 20 mm strip, whereas steel was a 100 x 20 x 8 mm strip. Diffusion bonding was carried out at a temperature of 1040° C for 60 minutes under a pressure of 15 MPa in a vacuum environment. A TEM analysis of the bonding interface revealed that sound bonding was achieved without any cracks and voids on the bonding interface.

In case of FeAl based alloys, both cold and hot cracking have been reported at the weld interface when attempted to bond via gas tungsten arc welding (Maziasz et al., 1992). Addition of 0.24 at% boron, which increased the room temperature ductility and strength at 600° C, also resulted in hot cracks in the fusion zone.

Banovic, DuPont, Tortorelli, and Marder (1999, 2001) while cladding carbon steel substrates with FeAl, employing the gas tungsten arc and gas metal arc welding process, observed that FeAl cladding was directly related to the aluminum composition within the deposit. FeAl with less than 10wt % aluminum was readily weldable, whereas higher concentration of aluminum produced poor welds and cracks in the interface. As evident from literature review, while several attempts have been made to join FeAl by means of conventional welding methods, no known efforts have been made to study the diffusion bonding of FeAl foils.

As described earlier, low room temperature ductility and poor high temperature creep strength are major issues restricting the application of iron aluminides. In recent years, powder processing of FeAl sheets by roll compaction has been developed to overcome these shortcomings. Deevi (2000) fabricated 200 μm thick iron aluminide sheets (Fe-40 at% Al) via the powder metallurgy route. FeAl powder was obtained through water atomization using a molten alloy of FeAl, containing 24-26% Al, 0.005% of Boron, 0.05% of C, 0.42% of Mo, and 0.1% of Zr by weight, as the feedstock. Green sheets of 660 μm FeAl were obtained by roll compaction from a blended mixture of the atomized powder and binder. Debindering of the FeAl green sheets was carried out at a 350-600° C temperature range in a nitrogen atmosphere for 8 hours. Sintering was conducted at 1260° C. Successive annealing and cold rolling were conducted in three stages at 1150° C, 1260° C and again 1150° C. The

sheets were passed through the roller leveler to obtain uniform flatness. Finally, the sheets were annealed at 700° C in vacuum for 2 hours.

Foil obtained through this process has a tensile strength greater than stainless steel whereas the yield strength is comparable to stainless steel at 800° C. The ductility is improved from 2.2 % to 5% at room temperature. There is also a significant improvement in the creep strength (Deevi, Sastry, and Sikka, 2001). These improvements enable the possibility of fabricating high temperature microfluidic devices with FeAl foil through the microlamination route. A review of available literature reveals no known diffusion bonding studies of FeAl foils.

The objective of this study is to explore the range of diffusion bonding parameters, i.e., temperature, pressure, and dwell time needed for powder-rolled and annealed FeAl foil with application to microchannel arrays. The value of this research is in its ability to demonstrate:

1. Diffusion bonding in FeAl foils.
2. The application of FeAl foils to produce a microchannel device, which in turn paves the way to explore the possibility that:
    a. Other types of aluminide foils, for instance NiAl, can be produced by following the same route as FeAl.
    b. Aluminides, because of their low density, are ideal materials for MECS applications and a good replacement for stainless steel.

## 3.2. Experimental Approach

The FeAl foil used in this investigation has been supplied by Dr. Clive Scorey at Ametek Inc. The foil is confirmed to be 24 wt % Al which translates to about 40 at% Al. The foil is about 203 μm thick. To fabricate an FeAl microchannel array, a counter flow microchannel design was implemented as shown in Figure 3.2. The major dimensions of the laminae were nominally 15 mm by 15 mm. Channel dimensions were 1.5 mm wide by 9.75 mm long in the counterflow and 750 μm wide in the neck between the channel and the header. Width dimensions in the neck were sized based on known manufacturability rules for two-fluid systems in 304 stainless steel (Paul, Hasan, Thomas, Wilson, and Alman, 2001).

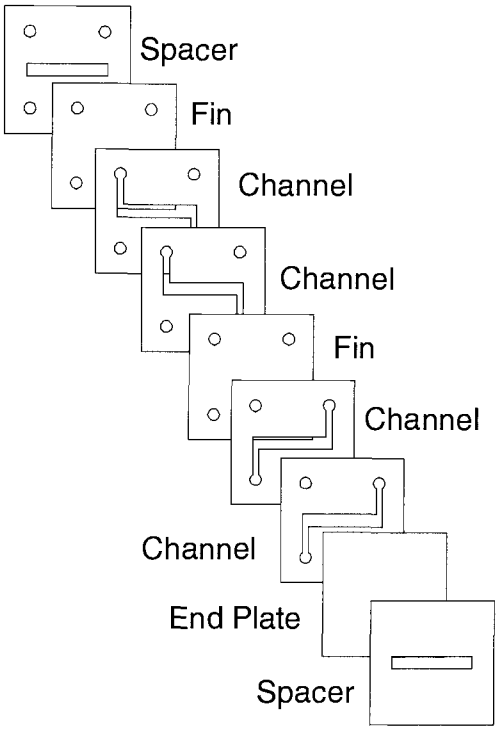


Figure 3.2. An exploded view illustrating the microlamination procedure used to produce an FeAl intermetallic counterflow heat exchanger.

A microlamination procedure was used to implement the counterflow design. This procedure involved laminae patterning, registration, and bonding. The blanks were cleaned using acetone, methanol, and deionized water in an ultrasound cleaner for 5 minutes each. An ESI 4420 Laser Micromachining System with a 355 nm UV laser rail was used to pattern the blanks. The average power of 5.8 watts, with a repetition rate of 30 KHz, a beam diameter of 30 μm, and a velocity of 20 mm/sec were used in four steps of 0 μm, 60 μm, 120 μm, and 180 μm, with 27 passes each. Laminae registration was accomplished using a thermally-enhanced edge registration (TEER) technique to minimize misalignment while avoiding buckling which is induced during high-temperature bonding (Thomas and Paul, 2002). Diffusion bonding of the

laminae was achieved in a vacuum hot press at elevated temperature and pressure. The sample was fixtured between two graphite platens with 9.8 MPa and heated at a rate of 10°C per minute to a temperature of 1050° C in atmospheric gases at $3x10^{-4}$ torr. The sample was held at this temperature for 2 hours to ensure that the intermetallic foils would bond. The temperature profile of diffusion bonding is shown in Figure 3.3.

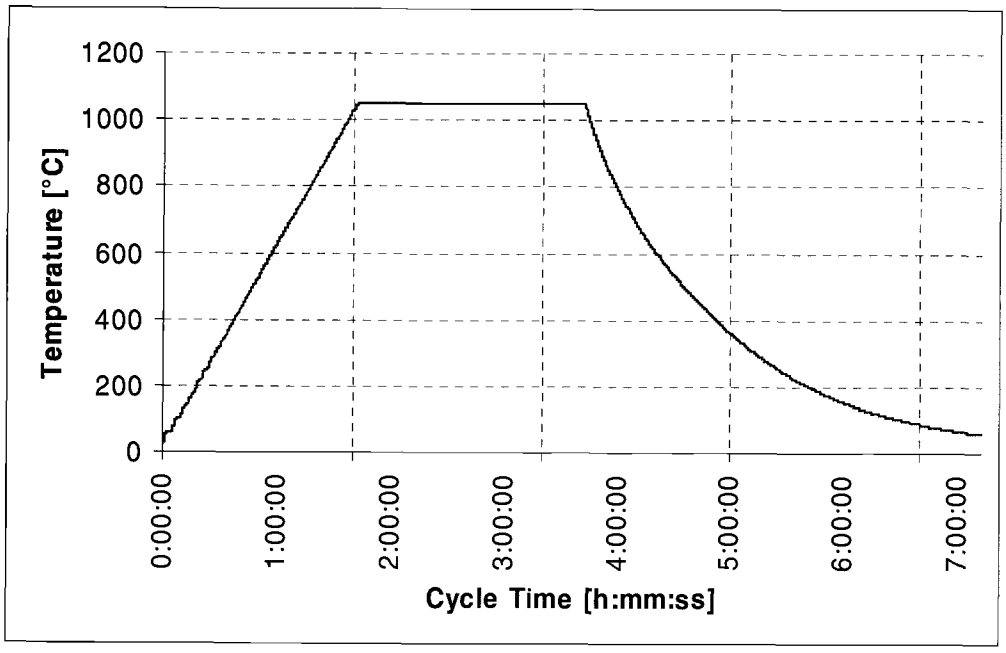


Figure 3.3. Temperature profile of FeAl diffusion bonding

## 3.3. Results

Two microchannel array devices were fabricated at 1050° C under 9.8 MPa for 2 hours. Prior to bonding, the laminae were flattened under a pressure of 36 MPa at room temperature for 5 minutes.

Micrographs of a cross section of the other device are shown in Figures 3.4 and 3.5. Bond lines are not visible between the laminae and there are no voids at the bonding interfaces, indicating a sound bond. However, a marked warpage of channels is obvious due to excessive bonding pressure. In future research, this warpage may be minimized through streamlining of the bonding pressure.

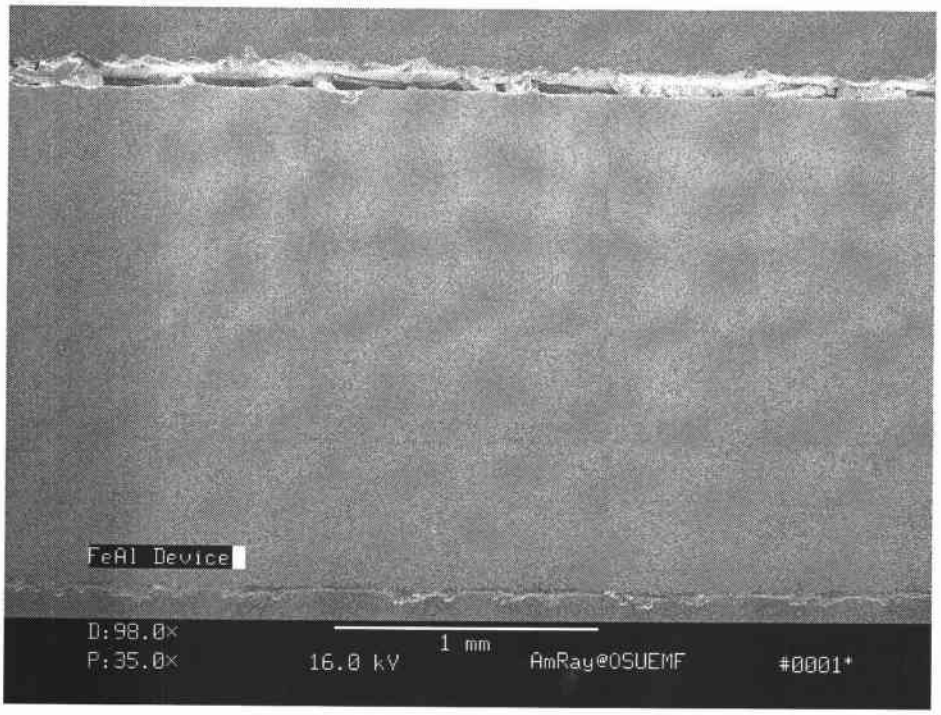


Figure 3.4. Scanning electron micrograph of a cross-section of diffusion bonded FeAl device (98X)

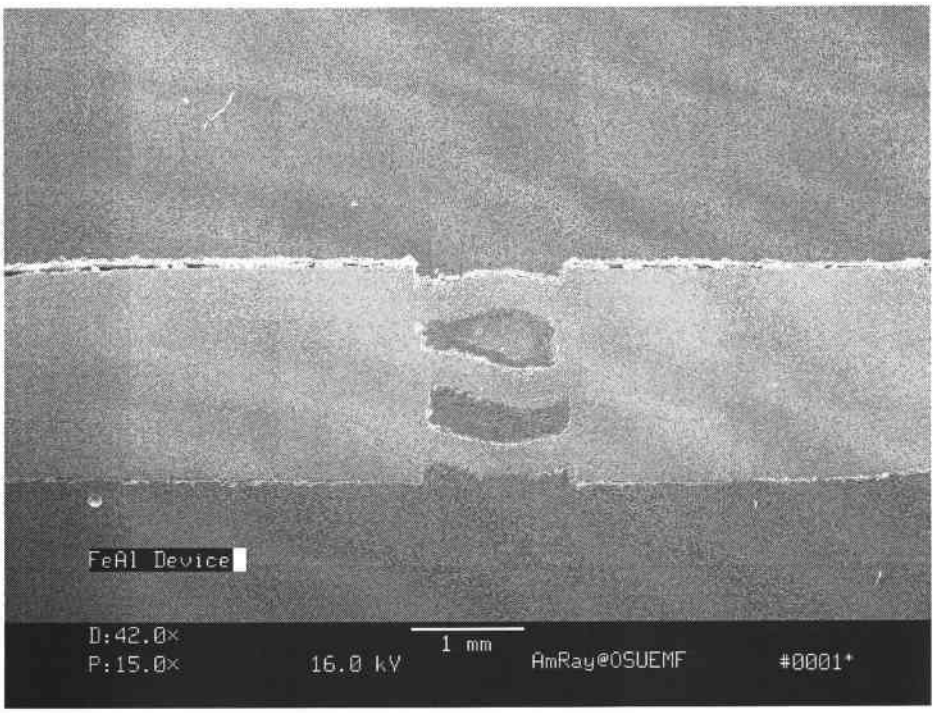


Figure 3.5. Scanning electron micrograph of a cross-section of diffusion bonded FeAl device (42X)

## 3.4. Conclusion

The work presented here demonstrates the potential of employing FeAl foils to fabricate mircochannel arrays. Two FeAl microchannel array devices were successfully fabricated. Metallographic studies of one of the devices showed a sound bond. Warpage in the channels was observed which can be minimized by optimizing the bonding pressure. This deformation and warpage could be the effect of the applied bonding pressure at an elevated temperature and may be eliminated by optimizing the bonding conditions. Another issue with this foil was its surface flatness at room temperature. The foils were

flattened under an excessive pressure for a short duration, at room temperature, which may have introduced some stresses in the foil.

## 3.5. References

"ASM Metal Handbook, Volume 2, Properties and Selection: Nonferrous Alloys and Special Purpose Materials," (1990), American Society for Metals, Metals Park, Ohio, pp. 914-920.

Banovic, S. W., DuPont, J. N., Tortorelli, P.F., and Marder, A.R., (1999), "Role of Aluminum on the Weldability and Sulfidation Behavior of Iron-Aluminum Cladding," Welding Journal, 78(1): 23s-30s.

David, S. A., Horton, J. A., McKamey, C. G., Zacharia, T., and Reed, R. W., (1989) "Welding of Iron Aluminides," Welding Journal, 68(9): 372s-381s.

Deevi, S. C., (2000), "Powder Processing of FeAl Sheets by Roll Compaction," Intermetallics, 8: 679-685.

Deevi, S. C., Sastry, D. H., and Sikka, V.K., (2001), "Alloy Development and Industrial Processing of Iron Aluminide Sheets," Proceedings of the International Symposium on Structural Intermetallics, 111-119.

Ghezel-Ayagh, H., Daly, J. M., and Wang, Z. H., (2003), "Advances in Direct Fuel Cell / Gas Turbine Power Plants," American Society of Mechanical Engineers, International Gas Turbine Institute, Turbo Expo (Publication) IGTI, 2: 625-629.

Jordan, A. D., Uwakweh, O. N. C., Maziasz, P. J., and Reed, R. W., (1999), "Weld Thermal Simulation and its Effect upon the Microstructure of As-Cast FeAl-Based Materials," Materials Characterization, 43(4): 227-233.

Juan, W., Yajiang, L., and Huiqiang, W., (2002), "Fine Structure at the Diffusion Welded Interface of $Fe_3Al$/Q235 Dissimilar Materials," Bulletin of Materials Science, 24(6): 639-642.

Juan, W., Yajiang, L., Huiqiang, W., and Jiangwei, R., (2002), "Micro-Image Analysis in the Diffusion-Bonded Zone of $Fe_3Al$/Q235 Carbon Steel Dissimilar Materials," Bulletin of Materials Science, 25(5): 367-370.

Juan, W., Yajiang, L., and Peng, L., (2003), "XRD and TEM Analysis on the$Fe_3AL$/18-8 Stainless Steel Diffusion Bonded Interface," Materials Letters, 57: 4323-4327.

Lagerstrom, G. and Xie, M., (2002), "High Performance and Cost Effective Recuperator for Micro-Gas Turbines," American Society of Mechanical Engineers, International Gas Turbine Institute, Turbo Expo (Publication) IGTI, 1: 1003-1008.

Massalski, T. B. (Editor-in-Chief), (1990), "Binary Alloy Phase Diagrams," ASM International, Materials Park, Ohio, pp. 148.

Maziasz, P. J., Goodwin, G. M., Liu, C. T., and David, S. A. (1992), "Effects of Minor Alloying Elements on the Welding Behavior of FeAl Alloys for Structural and Weld-Overlay Cladding Applications," Scripta Metallurgic, 27(12): 1835-1840.

McKamey, C. G., (1996), "Iron Aluminides," Physical Metallurgy and Processing of Intermetallic Compound, Chapman & Hall, New York, pp. 351-391.

Paul, B.K., Hasan, H., Thomas, J., Wilson, R., and Alman, D., (2001), "Limits on Aspect Ratio in Two-fluid Micro-scale Heat Exchangers," Transactions of NAMRC XXIX, Gainesville, FL. 461-468.

Pint, B. A., Swindeman, R. W., More, K. L., Tortorelli, P. F., (2001) "Materials Selection for High Temperature (750°-1000°C) Metallic Recuperators for Improved Efficiency Microturbines," ASME Paper #2001-GT-445, presented at the International Gas Turbine & Aeroengine Congress & Exhibition, New Orleans, LA,

Sauthoff, G., (1995), "Intermetallics," Weinhem, New York, pp. 84-87.

Sikka, V. K., Viswanathan, S., and McKamey, C. G., (1993), "Development and Commercialization Status of $Fe_3Al$ Based Intermetallic Alloys," Proceedings of the First International Symposium on Structural Intermetallics Structural Intermetallics," The Materials Society, Warrendale, PA, pp. 483-491.

Stoloff, N. S., and Sikka V. K. (editors) (1996), "Physical Metallurgy and Processing of Intermetallic Compounds," Chapman and Hall, New York, NY, pp. 217.

# CHAPTER 4

# EFFECT OF SURFACE ROUGHNESS AND NICKEL FILM THICKNESS ON DIFFUSION BONDING OF NICKEL ALUMINIDE FOILS

## 4.1. Introduction

Aluminide intermetallics exhibit good physical properties, e.g., large high temperature modulus, excellent high temperature corrosion resistance, low to moderate thermal conductivities, and in some cases, low densities and inexpensive elemental constituents. Room temperature processing of these materials is generally difficult due to their brittleness.

Table 4.1 compares some physical, mechanical and thermal properties for various aluminide intermetallics (Stoloff and Sikka, 1996; ASM Metal Handbook 1990). The nickel-aluminides tend to have the highest melting temperature while the titanium-aluminides have the lowest density and the iron-aluminides have perhaps the best high-temperature corrosion resistance. The thermal conductivity of NiAl as compared to other aluminides is on the higher side which could be important for some heat exchanger applications. The coefficient of thermal expansion is lower which may be important for dimensional stability inside of microchannels. For nickel-aluminides, the

physical, mechanical and thermal properties and corrosion resistance of NiAl are most desirable for the majority of high-temperature MECS applications.

Table 4.1. Comparison of physical and mechanical properties of some aluminide intermetallics.

| Property | NiAl | $Ni_3Al$ | TiAl | $Ti_3Al$ | FeAl | $Fe_3Al$ |
|---|---|---|---|---|---|---|
| Melting point, K | 1955 | 1663 | 1733 | 1873 | 1523-1673 | 1813 |
| Density, $g/cm^3$ | 5.86 | 7.50 | 3.91 | 4.2 | 5.56 | 6.58 |
| Young's modulus, $10^6$ psi | 42.7 | 25.9 | 25.5 | 21.0 | 37.8 | 23 |
| Thermal expansion, $10^{-6}$/ K at 873 K | 13.2 | 12.5 | 12.2 | - | - | 20 |
| Specific heat, J/g . K | 0.64 | 0.61 | | - | - | |
| Thermal conductivity, W/m.K | 76 | 28.9 | 22 | 15 | - | 10.9 |

The equilibrium binary phase diagram for the Nickel-Aluminum system is shown in Figure 4.1 (Massalski, 1990). The stoichiometric NiAl phase is perhaps most desirable because of its high temperature resistance and good corrosion resistance. Although the melting temperature of NiAl is not much higher than that of Ni, the high temperature mechanical properties of NiAl are much better. NiAl has a substantially lower density and a higher Young's modulus than Ni. This could be important to reduce weight for portable applications. In addition NiAl has excellent oxidation and sulfidation resistance at high temperatures which is critical for high temperature reactions.

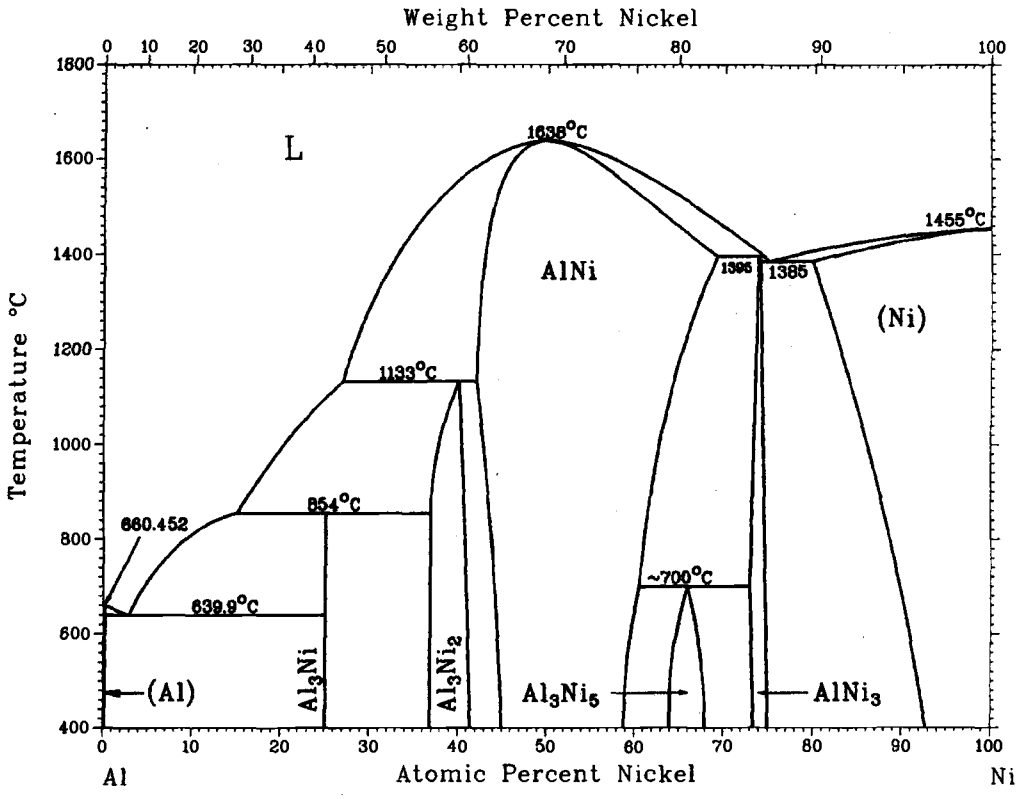


Figure 4.1. The phase diagram for the Ni-Al system (Massalski, 1990)

One potential application of NiAl is portable microreactors for hydrocarbon steam reforming. Apart from reducing the size of the reformer, employing NiAl microchannels instead of stainless steel allows the operation at higher temperatures. This in turn improves the reaction kinetics which requires fewer microchannels for the same hydrogen production rate. Microchannels cause higher heat and mass transfer as well as minimize coke formation because of low residence time. These microreactors can be utilized in automotive fuel cells and environmentally safe systems for the destruction of hazardous chlorinated hydrocarbons (Ehrfeld, Hessel, and Lowe, 2000;

Ortego, Richardson, and Twigg, 1997). Janikowski, Gombert, Soelberg, Harrup, and Jovanovic (2002) evaluated a technique to destroy hazardous compounds that may be discharged during the process. Palladium was deposited as a layer of catalyst on NiAl, FeAl, and TiAl coupons. Water and halocarbon such as $CCl_2$ were pumped into the system at a predetermined rate. After the initiation of the reaction the contents were ramped up to 750° C and were held at that temperature for one week. Only the NiAl system was found to withstand these conditions. The other coupons underwent corrosive degradation.

Diffusion bonding is one approach to fabricate NiAl microchannel arrays. Past research has shown that extreme temperature and pressure conditions are necessary for diffusion bonding which can cause significant deformation. Wattanutchariya (2002) showed that 20% deformation to a typical microchannel cross-section could cause as much as a 50% increase in the number of channels needed, resulting in a 50% increase in the size of devices that are designed for portability. Kanlayasiri (2003) showed the Ni-assisted reactive diffusion bonding resulted in a significant improvement in the flatness of the fins over previous research, however, the bond lines were characterized as inhomogeneous with many voids. In addition to the warpage and poor quality bond lines, problems with this approach included the difficulty of handling 7.5 μm Ni foil as a diffusion aid mechanism to assist in diffusion bonding. The objective of this study is to explore the effects of

surface conditions and Ni film thickness on the quality of NiAl diffusion bond. A reduction in the bonding time, pressure, and temperature will facilitate better geometric accuracy and will also help in decreasing production cost.

## 4.2. Diffusion Bonding

Diffusion bonding or diffusion welding has been described as joining of two similar or dissimilar surfaces at an elevated temperature in which the primary source of strength of joints is regarded as the diffusion of the atoms across the joining interface and secondary source as the plastic deformation of the faying surfaces. (Kazakov, 1985; Kalpakjian and Schmid, 2001). Schwartz (1979) suggests an optimal temperature range of 60% to 80% of the melting temperature for most of the bonded metals to realize a good diffusion bond.

Kearns (1980) divided the diffusion bonding progression into three stages. The first stage entails the plastic deformation of the mating surfaces, formation of grain boundaries and voids along the mating surfaces, and initiation of surface diffusion. In the second stage, grain boundary diffusion takes over, closing the voids at the grain boundaries. In the third stage, volume diffusion of the atoms into the remaining voids at the interface takes place. These three stages could overlap in a diffusion bonding process. Diffusion bonding of dissimilar materials may entail chemical reactions at the bond interface followed by the diffusion of chemical species and is therefore termed as reactive diffusion (Philibert, 1991).

Self-propagating, high-temperature synthesis (SHS), also termed in the literature as reaction synthesis and combustion synthesis, relies on a reaction between elemental constituent to form ceramic or intermetallic compounds (Rawers, Hansen, Alman, and Hawk, 1994). Due to the high thermal stability of the forming compound as the driving force, heat is liberated when the reaction begins, and the reaction becomes self sustaining and self propagating (Alman, 1994). Alman, Dogan, Hawk, and Rawers, 1995 explain that the SHS reactions in aluminides are initiated at around the melting temperature of aluminum. The reaction lasts for a few seconds and is accompanied by the formation of liquid transient phase. The advantages of SHS foil lamination technique include lower processing time, temperature and pressure to produce well-bonded composites and ease of processing.

There are four important processing parameters that control the diffusion bonding process; temperature, pressure, time of contact, and the surface conditions. The ambient environment can be regarded as a fifth parameter for the process. A detailed account of the first three parameters has been collated by Kanlayasiri (2003) in a state of the art study on nickel aluminide diffusion bonding. They are summarized from Kazakov (1985) as follows: The bonding temperature should be anywhere between 50 to 70% of the melting point of the most fusible metal in the composition. Elevated temperature not only aids the interdiffusion of atoms across the interface of the

weld but also assists the crushing of surface asperities during surface deformation.

The bonding pressure should be enough to ensure deformation of surface asperities and to fill the voids in the weld zone. It should ensure an intimate and tight contact between the two mating surfaces being bonded. The bonding pressure also breaks the oxide layer on the surfaces to aid diffusion and coalescence.

The time of contact or holding time at elevated temperature and pressure should be sufficient so that the intimate contact between the mating surfaces is formed and the diffusion process takes place completely. The holding time should be kept at a minimum for physical and economic considerations. In the case of bonding dissimilar materials, excessive holding time may leave voids in the bonding interface and may also change the composition of the material.

The ambient environment of the diffusion bonding sample is usually vacuum, which is kept around $10^{-1}$ to $10^{-3}$ Pa. Sometimes, a high purity inert gas like argon or helium is used as the atmosphere for diffusion bonding, although very high purity gases are expensive and so usually inert gases are not as effective at protecting bond joints during processing.

The fourth bonding parameter, the surface condition is presented in some detail below. Kearns (1980) characterizes surface conditions into surface roughness, oxidized layer on the mating surfaces, contaminants such as oil,

grease, dirt or any other randomly distributed solid or liquid impurities, and absorbed gas and/or moisture. Surface finish is usually described by three important terms namely roughness, waviness, and lay. Roughness can result from machining or other manufacturing operations and is comprised of finely spaced surface irregularities. Roughness is a closely-spaced digression from the surface's ideal form. Waviness has greater spacing between the irregularities as compared to the roughness and is usually caused by vibration, warping, or spindle deflection in machining or other processing. Lay is used to specify the surface pattern produced during a machining process, it is comprised of parallel ridges and valleys having a common direction (Farago, 1982).

## 4.3. Surface Roughness

Surface roughness is commonly specified as either arithmetic average (center line average roughness) or root mean square average roughness. The arithmetical average, denoted in ISO 4287 as $R_a$, is the average deviation of the surface from a mean line or centerline. The arithmetical average deviation from the mean line is

$$R_a = \frac{1}{l}\int_0^l |y| dl$$

where

$R_a$ = arithmetical average deviation from the mean line

$y$ = ordinate of curve of profile

$l$ = length over which average is taken

An approximate of the average roughness may be obtained by adding the y increments, as shown in Figure 4.2 (Dallas, 1976), without regard to sign and dividing the sum by the number of increments taken:

$$R_a = \frac{\sum_{i=1}^{i=n} y_i}{n}$$

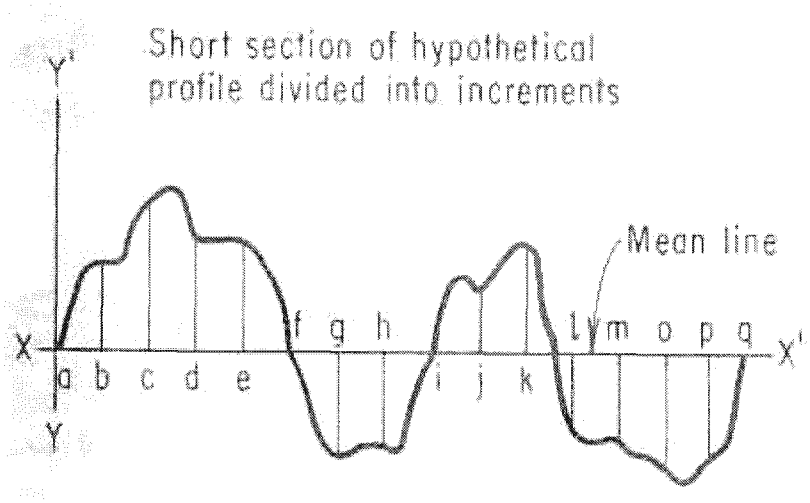


Figure 4.2. Short section of hypothetical profile, divided into increments (Dallas, 1976)

The root mean square average roughness, denoted in ISO 4287 by $R_q$, is calculated by taking a series of measurements of deviations from the center line and taking their root mean square. It is defined mathematically as:

$$R_q = \left[\frac{1}{l}\int_0^l y^2 dl\right]^{1/2}$$

An approximation of the root mean square average roughness may be obtained by adding the square of the y increments shown in Figure 4.2, dividing the sum by the number of increments taken, and extracting the square root:

$$R_q = \left[ \frac{\sum_{i=1}^{i=n} y_i^2}{n} \right]^{1/2}$$

$R_q$ is more sensitive to occasional high and low peaks, and gives more weight to higher peaks. Other important specifications include maximum peak to valley roughness height and ten point height. Maximum peak to valley roughness is denoted in ISO 4287 as $R_t$ and is the distance between two lines parallel to the center line that contacts the extreme upper and lower points on the profile within the sampling length. (Dallas, 1976; ISO 4287, 1997)

Roughness sampling length is the distance between the successive data points being recorded in a scan whereas the evaluation length is basically the length of the scan being taken to measure the surface roughness. Table 4.2, taken from ISO 4288, specifies the roughness sampling lengths and roughness evaluation lengths for a given center line average roughness (ISO 4288, 1996).

Table 4.2. Roughness sampling and evaluation lengths for different ranges of $R_a$

| $R_a$ μm | Roughness sampling length mm | Roughness evaluation length mm |
|---|---|---|
| $(0.006) < R_a \leq 0.02$ | 0.08 | 0.4 |
| $0.02 < R_a \leq 0.1$ | 0.25 | 1.25 |
| $0.1 < R_a \leq 2$ | 0.8 | 4 |
| $2 < R_a \leq 10$ | 2.5 | 12.5 |
| $10 < R_a \leq 80$ | 8 | 40 |

Compared with the surface roughness, waviness requires a longer evaluation length. There is no standard for how long is long enough or how to break the waviness into separate sample lengths as is done for roughness. Waviness is usually evaluated for one sample length equal to the longest trace possible on a particular part with a particular instrument.

Surface roughness can be measured by a number of contact and non-contact methods. Surface texture measurement with a stylus type instrument is most widely used. Surface profile measuring system or a profilometer is a stylus type instrument widely used in industry and fits into the first category. The essential components of a surface profile measuring system include precision scan head, precision sample stage, video camera, video monitor, and

a computer console. Measurements are made electromechanically by moving the sample beneath a diamond tipped stylus according to user programmed scan length and speed. The stylus is coupled to a LVDT (Linear Variable Differential Transformer). As the stage moves the sample, the stylus ride over the sample surface. Surface variations cause the stylus to move vertically. Electrical signals corresponding to the stylus movement are produced as the position of the LVDT changes. An analog signal proportional to the position change is produced by the LVDT, which in turn is converted to a digital format by a digital converter. The digitized signal from the scan thus obtained is displayed on the video monitor and can be stored in a computer. The advantage of this kind of system is the cost as compared to the non-contact method. Since it is a contact measuring technique, it may give erroneous readings if the stylus is not in an optimal condition. Furthermore, the diameter of the tip of the stylus puts a limit on the accurate measurement of the valleys. Regardless of the size of the tip, the stylus can scan over the peaks, but if the tip is bigger than the valleys it will not be able to discern them (Farago, 1982; Veeco, 2000).

Interferometry is a powerful non-contact technique that can be used for surface roughness measurements. The technique involves illuminating the surface of a sample and measuring the reflected intensity. The system may be used as a simple reflectometer, in which case interfaces between materials with different refractive indices can be detected by the resultant step change in the

reflectivity signal. The essential components of an interferometry system include an interferometer that integrates a laser source, signal detector, and a CCD camera with an associated illuminator. Measurement of surface roughness by light inference has several advantages over the contact method. It gives us a much better resolution than a surface profilometer. As it is a non-contact method it can be used on softer materials which are hard to scan with a profilometer. It is more accurate than any of the contact methods and does not require frequent recalibration. Its limitations include its adaptability to external surfaces that can be accessible by the microscope, and the sample should be comprised of relatively smoother surface. Other non-contact methods include scanning electron microscopy, transmission electron microscopy, and atomic force microscopy (Farago, 1982).

## 4.4. Effect of Surface Roughness on Diffusion Bonding

A literature review of the role of surface roughness on the solid state diffusion bonding process for different material systems is presented in this section. Pilling (1988) postulated a model to predict the time required to achieve full interfacial contact between the mating surfaces under isostatic conditions. The model was verified for Ti-6Al-4V material system under different bonding conditions. It was concluded that the bonding times were insensitive to temperature and pressure within the superplastic temperature range. However, the time required to attain full interfacial contact between the

mating surfaces seemed to depend substantially on the magnitude of both short wavelength roughness and long wavelength waviness of the mating surfaces. The 4 different surface conditions used in the study were 2.1 μm and 0.6 μm; 2.5μm and 1.3 μm; 4.5 μm and 22 μm; and 100 μm and 20 μm for the wavelength and amplitude of the roughness respectively.

Islam and Ridley (1998) studied the effects of varying temperature, pressure, time, and surface finish on the diffusion bonding of microduplex stainless steel Avesta 2205. Bond quality was characterized by employing light microscopy, compressive lap shear testing, and SEM fractography, whereas, surface roughness was measured by using an atomic force microscope. The 2 levels of roughness were 0.2 μm amplitude with a wavelength of 8 μm and 0.45 μm amplitude with a wavelength of 14 μm. It was found that the bonding time was reduced by increasing temperature and/or pressure and by decreasing the surface roughness.

Nagano and Wakai (1994) investigated the effect of surface roughness on superplastic diffusion bonding of a $ZrO_2/Al_2O_3$ composite. Three different surface finishes of the composite were obtained by using no. 200, 400, and 600 diamond wheels. The centerline mean roughnesses of the samples were 0.28 μm, 0.17 μm, and 0.11 μm respectively. Bonding strength was evaluated by a 4-point bending test. Bonding interface was inspected by an SEM and the residual voids in the bonding interfaces were evaluated with an ultrasonic

inspection system. Smoother surfaces were shown to yield higher bonding strengths.

Cox, Kim, and Carpenter (2002) investigated the effect of surface roughness on the diffusion bonding of single-phase austenitic stainless steel. The substrates were mechanically polished, lapped and the native oxide layer was removed by ion beam cleaning. Surface roughness was measured by atomic force microscope. Three different root mean square roughnesses of 0.5 nm, 1.5 nm, and 3 nm were obtained by employing a combination of mechanical polishing/ lapping and ion beam cleaning. The smoothest surface finish required the shortest bonding time for void free bonding interfaces. Transmission electron microscopy (TEM) was used to inspect the bonding interfaces for voids.

Yang, Chiu, Lee, and Sun (1998) explored the effect of temperature, pressure, time, vacuum, and surface roughness on solid state diffusion bonding of superplastic 7475 aluminum alloy. Six different surface roughnesses ranging from 0.17 μm to 1.08 μm were obtained by chemical cleaning and mechanical polishing. The quality of the bond was characterized by lap shear stress. Bond quality increased with increasing temperature, pressure, time, vacuum, and decreasing surface roughness.

Kurasawa, Takatsu, Sato, Kuroda, Sugimoto, and Tamura (1996) studied the effect of temperature, pressure, heat treatment and surface roughness on the diffusion bonding of grade F82H ferritic steel. Specimens

were divided into two groups on the basis of surface roughness; first group had a surface roughness of 0.5 μm whereas the surface roughness of the second group ranged from 7.8 to12.8 μm. For the smoother surface three temperature and pressure levels of 1060° C and 3.0 MPa, 950° C and 5.0 MPa, and 850° C and 12.0 MPa were executed. Heat treatment included normalizing at 1040° C for 30 minutes and tempering at 740° C for 2 hours. The quality of bond was characterized by tensile test. Smoother mating surfaces showed a yield strength comparable to the base metal at all three levels of temperature and pressure. For the rougher surfaces sufficient diffusion bonding was not achieved at 1050° C under a pressure of 3.0 MPa.

Zuruzi, Li, and Dong (1999) investigated the effects of surface roughness on the diffusion bonding of Al alloy 6061 in air. The 2 levels of center line mean surface roughness were 0.84 μm and 0.18 μm. An interface treatment step was carried out when the sample reached the target temperature of 450° C. The step involved inducing relative motion at the bonding surfaces by rotating the specimen through 360° about the axis of the specimen under the application of a compressive pressure. The rougher substrates yielded a 140% better ultimate tensile strength than the smoother surface which was attributed to the interface treatment step. However, voids were observed at the bonding interface of rougher substrates which were attributed to the air entrapment between the surfaces. Tensile strength comparable to the bulk material was obtained for holding time of 75 minutes for the rougher surface. An increase or

decrease in the holding time showed a drop in the tensile strength of the material. It was recommended to obtain a controlled roughness for diffusion bonding to achieve similar ultimate tensile strength of the bond as the bulk material.

Harvey, Partridge, and Lurshay (1986) studied the factors affecting the shear strength of solid state diffusion bonds between silver-coated clad Al-Zn-Mg-alloy. Samples were prepared by means of chemical mechanical polishing with five different roughnesses. Shear strength of the bonds increased with a decrease in roughness.

Enjo, Ikeuchi, and Akikawa (1982) studied the effect of the roughness of faying surfaces on the early process of diffusion welding of aluminum, copper, and titanium. Center line mean roughness of 0.34 μm, 0.40 μm, and 0.71 μm were obtained for all three materials by using 1500, 800, and 600 emery papers respectively. Electric resistance across the bonding interface was measured while the samples were heated at a constant rate from room temperature. The readings were analyzed by constriction resistance theory. The variation of electric resistance was divided into three stages; stage 1 was from room temperature to 220° C, stage 2 was from 220° C to 500° C, and stage 3 was from 500° C to 630° C. Welding pressure was 0.2 $kg/mm^2$. It was concluded that the disruption of oxide films and the metal to metal contact on the faying surface increased with increasing roughness with increase metal to metal contact being the highest in the first stage, decreasing in the second

stage, and then increasing again in the third stage. The formation of voids also increased with an increase in roughness of the mating surfaces. This result was attributed to that fact that the rougher surface had fewer contact spots to begin with thus had a larger potential of an increased metal to metal contact under an increasing temperature and application of pressure. It was also observed that oxide film on the surface of aluminum required much greater deformation of asperities as compared to titanium and copper. The bond strength was not characterized in this research.

Somekawa, Watanabe, and Higashi (2003) studied the grain size dependence on diffusion bonding behavior in superplastic magnesium alloy. A fine-grain and coarse-grain specimen of Mg-Al-Zn alloy AZ31 were prepared with grain sizes of 11 μm and 28 μm respectively. Experimental conditions included a bonding temperature of 673 K, bonding pressure ranged from 2.0 to 10 MPa, and bonding time was varied from 0.5 to 5.0 hours. Diffusion bonding quality was characterized by using lap shear tests. It was found that the fine-grain specimen achieved a better diffusion bond than the coarse grain specimen. Maximum lap shear strength ratio of 0.92 was achieved at 3.0 MPa and 2 hours of bonding time for the smaller grain size specimen and 0.90 at 5.0 MPa and 3 hours for the larger grain size specimen. Lap shear strength ratio of less than 0.6 resulted in a poor bond strength. This finding was in line with the fact that superplastic deformation is a grain size dependent phenomenon.

In an extension of the previous study, Somekawa and Higashi (2003) explored the optimal surface roughness condition on diffusion bonding for fine-grain and coarse-grain Mg-Al-Zn alloy. Different surface roughnesses ranging from 4.5 μm to 30.4 μm for fine-grain and 4.5 μm to 30.7 μm for coarse-grain samples were obtained by using different alumina particles. Bonding time was varied from 10 minutes to 6 hours. It was observed by carrying out lap shear tests that the optimal surface roughness in terms of bonding time was close to the grain size of the material. The lap shear strength ratio increased up to the ratio of surface roughness to grain size equal to 1, beyond this point lap shear strength remained constant.

Jauhari, Ogiyama, and Tsukuda (2003) studied the effects of temperarute, pressure, time, and surface roughness on the quality of the bond between superplastic stainless steel and carbon steel. An evaluation of bonding conditions at two roughnesses of 0.32 μm and 1.5 μm by carrying tensile strength suggested that smoother mating surface yielded a strength equal to the parent metal in a shorter period of time. It was also verified in the study that increasing the surface roughness increases the volume fraction of voids in the bonding interface resulting in a decrease in the bonding strength.

Chen, Fan, Reif (2002) analyze possible mechanisms of copper wafer bonding with respect to the position and alignment of the asperities. The study was conducted on N-type (100) Si wafers with a 50 nm film of tantalum and 300 nm layer of copper. Bonding conditions of 4000 mbar at 400° C were

applied for 30 minutes. The surface roughness of the wafers, i.e. the roughness of the Cu film, was measured as 1.5 nm with an atomic force microscope. The roughness was not uniform all along the surface of the wafer. The bonded interface was characterized by transmission electron microscopy. A schematic of the first mechanism, called "peak-to-peak" bonding mechanism, is shown in Figure 4.3. In this mechanism, the roughness of both mating surfaces was same at 1.5 nm. In a peak to peak alignment of asperities, the contact area between the two surfaces was small and the deformation of elastic spheres was easy, resulting in an atomic scale distance between the mating surfaces. Interdiffusion of Cu atoms with higher kinetic energy was facilitated between the surfaces with a simultaneous grain growth. The bond line at the interface disappeared giving way to a homogeneous region with a non-distinct interface.

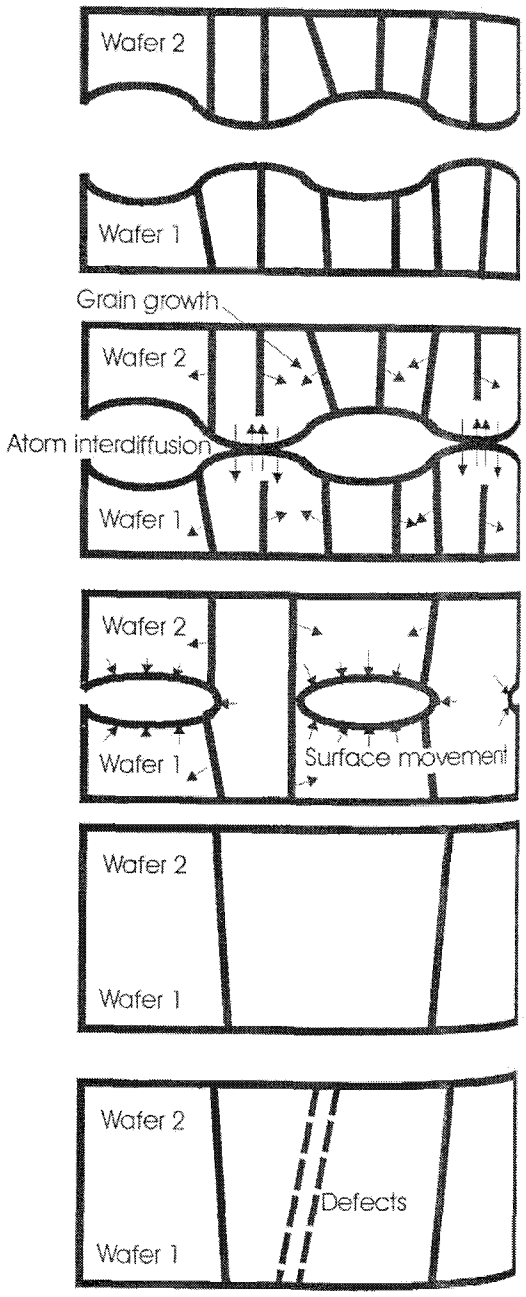


Figure 4.3. Schematic of "peak-to-peak" bonding mechanism (Chen et al., 2002)

In the second mechanism, known as "peak-to-valley" mechanism, as the normal load is not perpendicular to the contact area, the force acting on the

contact area is smaller than the normal load. Both mating surfaces had the same scale roughness. At high temperature, the atoms were more energetic and kept moving along the interface until the two surfaces matched each other. After annealing grain growth occurred and bonding was achieved in the form of a zigzag pattern. A schematic of "peak-to-valley" mechanism is shown is Figure 4.4.

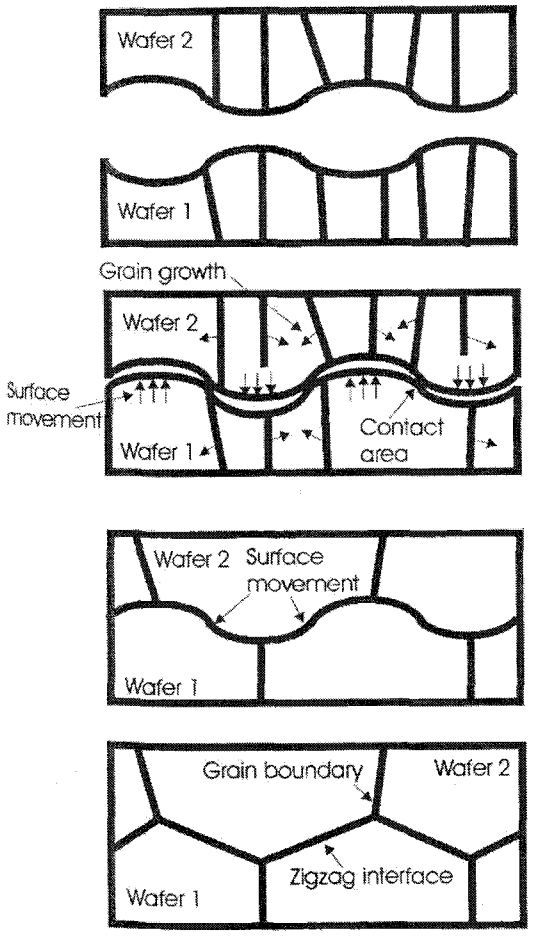


Figure 4.4. Schematic of "peak-to-valley" bonding mechanism (Chen et al., 2002)

In the third mechanism, termed as "different-scale-roughness" mechanism, the roughness of the two surfaces were not the same resulting in a random and mismatched positioning of the peaks and valleys of the two surfaces. Although, the asperities were decreased by the application of bonding pressure as the two surfaces were squeezed together, some voids remained at the interface. These voids were reduced by further annealing, leaving a distinct bonding interface. The schematic of "different-scale-roughness" mechanism is shown in Figure 4.5. In conclusion, surface roughness was regarded as an important parameter in the initial steps of bonding.

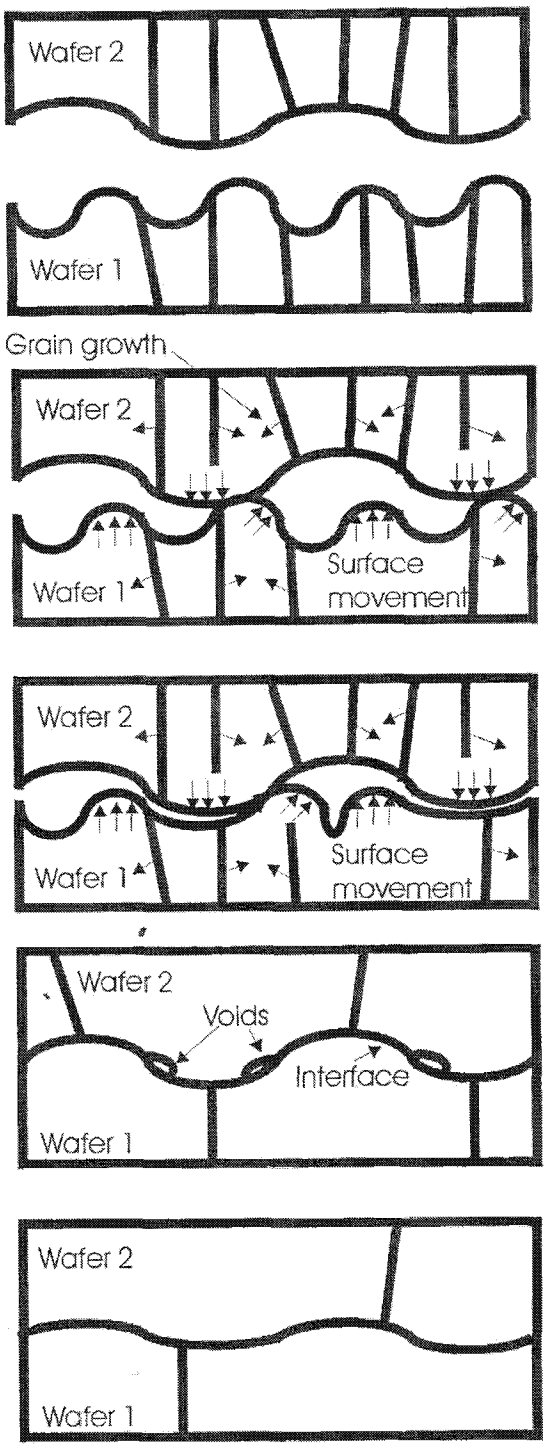


Figure 4.5. Schematic of "different scale roughness" bonding mechanism (Chen et al., 2002)

In a diffusion bonding study of silicon nitride to titanium, Lumus and Drew (2000) concluded that in case of high surface roughness atomic diffusion occurs where the mating surfaces are in contact with each other, whereas no mass transport occurs in regions not in contact with each other, requiring surface diffusion, plastic deformation, or creep as mechanisms for void elimination.

The literature review shows that smoother surfaces result in better bond quality, stronger bonds, better yield and shear strengths, and fewer voids for the same time, temperature and pressure conditions. It is also observed that increasing pressure and temperature, and decreasing surface roughness result in a shorter bonding time. An important aspect of surface roughness is the horizontal span of $R_a$ described as short wavelength roughness by Ridley (1988), which is found to be more important than $R_a$ itself. This phenomenon is described in the theoretical model section of this research. The void formation in the previous research by Kanlayasiri (2003) was likely caused by surface roughness.

## 4.5. Problem Statement

Kanlayasiri (2003) showed that Ni-assisted heterogeneous diffusion bonding resulted in reasonable channel uniformity. However, as shown in Figure 4.6., the bond lines were characterized as inhomogeneous with many voids. In addition to poor quality bond lines, the samples were found to have

carbon contamination which is known to embrittle NiAl. Other problems with this approach included the difficulty of handling 7.5 μm Ni foil as a diffusion brazing mechanism to assist in diffusion bonding.

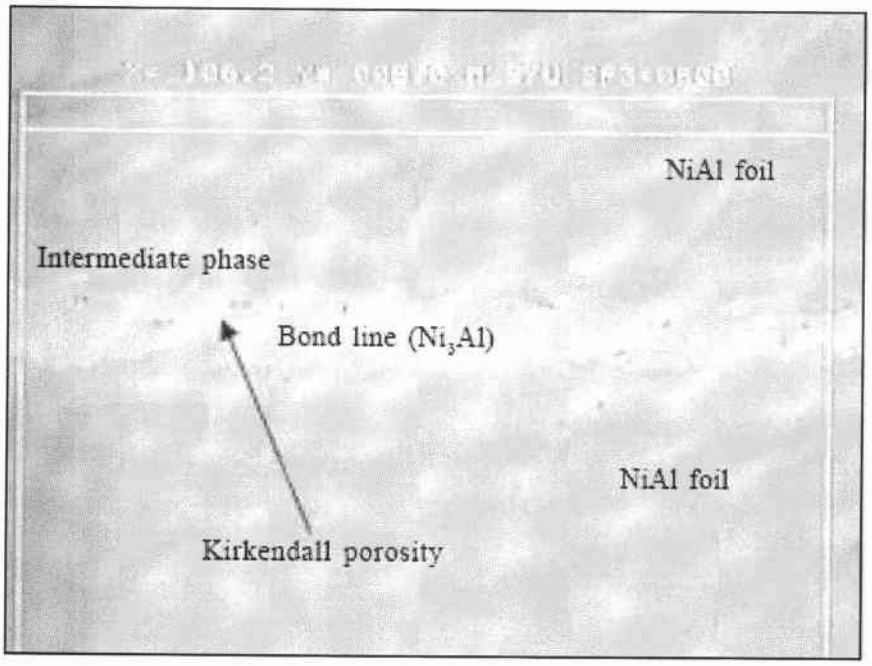


Figure 4.6. Diffusion bonded NiAl (Kanlayasiri, 2003)

### 4.5.1. Inert Platens

One contribution of this research is the use of ground inert platens during NiAl synthesis to reduce the roughness of NiAl laminae, thereby providing a means to minimize bond voids. Boron nitride is known to be inert and non reactive with Al. Hot pressed boron nitride sheets are made by densification of powder. They can be used up to a temperature of 2500° C and have a compressive strength of 30 to 120 MPa. They can be machined to close tolerances (Goodfellow, 2004). Further, these platens were also used during

the diffusion bonding experiments. Using these platens for synthesis and diffusion bonding, instead of graphite platens, eliminates carbon inclusions into the matrix of NiAl, which is known to embrittle NiAl (George and Liu, 1990).

### 4.5.2. Bond Homogeneity

Bond homogeneity is important and was something that Kanlayasiri (2003) struggled with in his research, as can be seen in Figure 4.6. The time to homogenize a NiAl bond for an appropriate range of the thickness can be determined by Fick's second law (Callister, 2000). Solution to Fick's second law is given as:

$$\frac{C_x - C_0}{C_s - C_0} = 1 - erf\left(\frac{x}{2\sqrt{Dt}}\right) \qquad (1)$$

where

$C_s$ = Surface concentration of element

$C_o$ = Initial uniform concentration of element

$C_x$ = Concentration of element at distance

$x$ = Distance from surface

$D$ = Diffusivity of diffusing solute

One implication of this formula is the need to reduce the thickness (represented by '$x$') of the Ni layer used for heterogeneous diffusion bonding. One means of doing this is the use of Ni electroplating.

### 4.5.3. Electroplating and Leveling

Use of heterogeneous material as a diffusion aid in diffusion bonding is well documented (e.g., Moore et al., 1993; Nakao et al., 1991). Kanlayasiri (2003) used a 7.5 μm thick Ni foil as a diffusion bonding aid in the diffusion bonding of NiAl. However, handling such a thin foil was cumbersome. In this research, it is proposed to use a thin layer of electroplated Ni on the NiAl substrates which would eliminate the difficulty of handling such a thin foil. This method will also provide some degree of control over the thickness of deposition. Hence, different thicknesses of the deposition can be evaluated in aiding the diffusion bonding process.

Electroplating has also been used as a smoothening process for rough surfaces. The process is referred to as leveling and is defined as the progressive reduction of surface roughness during deposition (Lowenheim, 1974). Leveling occurs when more deposition takes place in microrecesses than in micropeaks. Leveling can be achieved either by the use of chemical additives or in certain cases without using any chemical additives; the former is known as true leveling whereas the latter is known as geometric leveling. (Lowenheim, 1974). Aroyo (1995) showed that with pulse plating, maximum leveling power (LP) was obtained with a Watts nickel bath at 5 Hz where LP was defined as the ratio of the difference in the center line average roughnesses of the substrate and the plated surface and the thickness of the plate. A leveling power of 0.035 was obtained at a frequency of 5 Hz with a forward pulsed

current. This essentially means an improvement of 3.5% of the deposited film thickness. Current density was 4 A/dm$^2$ and pulse duration was 10 msec.

## 4.6. Thesis Statement

Microlaminated NiAl structures with embedded micro-scale geometry can be produced with better bond quality and compositional integrity than existing methods outlined in the literature specifically Kanlayasiri (2003). These improvements will be achieved by investigating several process developments:

i. Improving the surface conditions of NiAl foils.

ii. Reducing the thickness of Ni films for diffusion bonding.

In particular, better surface conditions will be pursued through the use of smooth, inert bonding platens used during the synthesis of the NiAl foils. Thinner film thickness will be pursued through the use of Ni electroplating. The desired improvements will be demonstrated using the criteria below through the experiments described in this chapter:

i. Bond quality – homogeneous joints and reduced void count.

ii. Compositional integrity – minimization of tertiary elements.

## 4.7. Theoretical Model

The objective of the theoretical model is to predict the conditions necessary for void-free diffusion bonded NiAl. The model will also give an

insight into the dynamics of diffusion bonding mechanism. An isostatic diffusion bonding model for superplastic materials was synthesized from Dr. John Pilling's research on diffusion bonding of superplastic materials with his permission (Pilling, 1988; and Pilling, Ridley, and Islam 1996). Hori, Tokizane, and Furushiro (1991) defined superplasticity as:

> "Superplasticity is the ability of a polycrystalline material (metallic, ceramic, intermetallic, or composite) to exhibit very high tensile elongations before failure."

Nieh and Wadsworth (1999) explained that superplastic materials generally have a high value of strain-rate sensitivity exponent $m$ during tensile deformation. Mathematically, it is characterized by the constitutive equation

$$\sigma = k\varepsilon^m$$

where $\sigma$ is the true flow stress, $k$ is a constant, and $\varepsilon$ is a true strain rate. Superplastic alloys have an $m$ value greater than 0.33, where as most metals and alloys have an $m$ value less than 0.2. NiAl has been shown to have superplastic behavior at elevated temperatures (Du, X. H., Guo, J. T., and Zhou, B. D., 2001; Du, X., and Wu, B., 2005; and Guo, J. T., Chen, R. S., Du, X. H., Li, G. S., and Zhou, L. Z., 2005).

In diffusion bonding, the points of contact between the mating surfaces collapse on application of an external pressure until the cross-sectional area can support the applied pressure, resulting in a planar array of voids. In order to calculate the time required to achieve full interfacial contact between the two surfaces, the stress distribution of the material surrounding the voids needs

to be determined. To facilitate this, the shape of the voids has been approximated by an upright cylinder such that the cross-sectional area of the cylinder is equal to the void projected on the bond interface. The initial height or the diameter of the cylinder is twice the amplitude of surface roughness (Pilling et al., 1996). During diffusion bonding, the voids are filled by two processes; the time dependent plastic collapse of voids and the mass transfer from bond to void by diffusion. Elasticity theory was employed to determine the stress gradients in the cylinder wall. These were averaged to account for any relaxation in the stress gradient by superplastic flow. Radial, circumferential, and axial stresses in the cylinder for a given void fraction are given by:

$$\sigma_r = \left(p - \frac{2\gamma}{r_o}\right)\left(\frac{\sqrt{f}-1}{1-f}\right) \tag{2}$$

$$\sigma_c = \left(-p - \frac{2\gamma}{r_o}\right)\left(\frac{\sqrt{f}+1}{1-f}\right) \tag{3}$$

$$\sigma_z = \frac{-p}{1-f} \tag{4}$$

where:

$\sigma_r$ = Radial stress in the cylinder wall

$\sigma_c$ = Circumferential stress in the cylinder wall

$\sigma_z$ = Axial stress in the cylinder wall

$p$ = Applied pressure

$\gamma$ = Surface tension

$r_o$ = Initial void radius

$f$ = void fraction

In B2 aluminides steady-state creep rate is usually expressed as a form of Dorn equation (Noebe, Bowman, and Nathal, 1993)

$$\dot{\varepsilon} = A\left(\frac{p}{E}\right)^n \exp\left(\frac{-Q}{RT}\right) \tag{5}$$

where:

$\dot{\varepsilon}$ = Effective plastic strain rate

$p$ = Applied pressure

$E$ = Young's modulus

$n$ = Stress exponent of a given creep mechanism

$Q$ = Activation energy for creep

$R$ = Gas constant

$A$ = constant related to such variables as microstructure, stacking fault, or antiphase- boundary energy

Axial and radial strain rates ($\dot{\varepsilon}_r$ and $\dot{\varepsilon}_z$) are determined by using the Levy-von Mises associated flow rule as:

$$\dot{\varepsilon}_r = \dot{\varepsilon}\left(\frac{\sigma_r - \frac{\sigma_c + \sigma_z}{2}}{\sigma_e}\right) \tag{6}$$

$$\dot{\varepsilon}_z = \dot{\varepsilon}\left(\frac{\sigma_z - \frac{\sigma_c + \sigma_r}{2}}{\sigma_e}\right) \tag{7}$$

where $\sigma_e$ is Von Mises effective stress given by (Pilling, 1988; Ugural and Fenster, 1987).

$$\sigma_e = \sqrt{\left(\frac{1}{2}\right)\left[(\sigma_r - \sigma_c)^2 + (\sigma_c - \sigma_z)^2 + (\sigma_z - \sigma_r)^2\right]} \tag{8}$$

Determination of the radial and axial stresses enables the establishment of the rate of reduction of area fraction of voids *f*. The kinetics of the void closure process by plastic collapse is given by:

$$\left[\frac{df}{dt}\right]_{plasticity} = -2\dot{\varepsilon}_r(1-f) \tag{9}$$

The total rate of change in the area of interfacial voids with time, as a result of diffusion from the bond interface (volume diffusion) and from the grain boundaries are given by:

$$\left[\frac{df}{dt}\right]_{vol} = -\frac{4\Omega D_v}{kT}\left[\frac{f}{\ln\left(\frac{1}{f}\right) - \frac{1-f}{2}}\right]\frac{1}{r_o^2}p \tag{10}$$

$$\left[\frac{df}{dt}\right]_{gb} = -\frac{2\Omega D_{gb}\delta}{kT}\left[\frac{f}{\ln\left(\frac{1}{f}\right) - \frac{1-f}{2}}\right]\frac{1}{r_o^2}p\left(\frac{1+\frac{h_o f}{d}}{h_o f}\right) \tag{11}$$

where:

$\Omega$ = Atomic volume

$D_v$ = Volume diffusion coefficient

$D_{gb}\delta$ = Grain boundary diffusion coefficient

$d$ = Grain size

$k$ = Boltzmann's constant

$T$ = Bonding temperature

$h_o$ = Initial void height

Apart from the center line average roughness $R_a$, the model also takes into account the short wavelength asperities $\lambda$ which is the span of a peak or valley of the roughness measured horizontally shown in Figure 4.7.

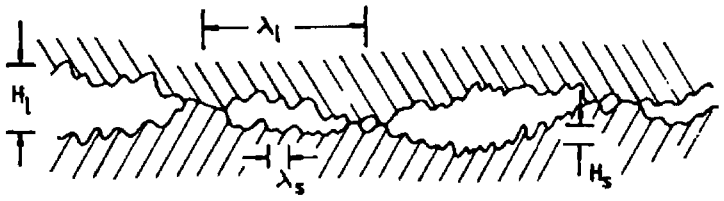


Figure 4.7. Schematic of interfacial geometry showing short term asperities denoted by $\lambda_s$ and long term waviness by $\lambda_l$ (Pilling, 1988)

The initial void radius $r_o$ was taken as half of $\lambda$ whereas initial void height is twice the $R_a$. The rate of reduction of voids for the power law creep mechanism (9) as well as for volume (10) and grain boundary (11) diffusion are added. Numerical integration of the reciprocal of this sum yields the bonding time for a given void fraction.

$$\left[\frac{df}{dt}\right]_{total} = \left[\frac{df}{dt}\right]_{plasticity} + \left[\frac{df}{dt}\right]_{vol} + \left[\frac{df}{dt}\right]_{gb} \tag{12}$$

$$t = \int_{0.99}^{0} \left[\frac{df}{dt}\right]_{total} \tag{13}$$

A computer simulation shown in Appendix A was written in Matlab to carry out the calculations. Alternatively, duration of bonding is given as an input in the simulation to give the resulting void fraction as the output.

### 4.7.1. Model Validation

The model was validated by reproducing the results from the data for Super Alpha-2, provided in Pilling et al. (1996) in a computer simulation. The diffusion bonding conditions for Pilling et al. were varied between temperatures of 950° C and 1050° C and pressures of 5 to 20 MPa. The surface roughness had an amplitude of 0.65 μm and a wavelength of 15 μm. The bonding time was set at 2 hours. Other physical properties of Super Alpha-2 taken from Pilling et al. (1996) are given in Table 4.3.

Table 4.3. Physical properties of Super Alpha-2 (Pilling et al., 1996)

| **Property** | **Units** | **Value** | |
|---|---|---|---|
| | | **$\alpha_2(\alpha)$** | **β** |
| Melting point ($T_m$) | K | 1875 | |
| Atomic volume ($\Omega$) | $m^3$ | $1.7 \times 10^{-29}$ | $1.81 \times 10^{-29}$ |
| Strain rate ($\dot{\varepsilon}$) | $s^{-1}$ | $1.28\times10^{9} \exp\left(\frac{-308000}{RT}\right)\sigma^{2.05}$ | |
| Volume diffusion ($D_v$) | $m^2 s^{-1}$ | $5.9\times10^{-3} \exp\left(\frac{-330000}{RT}\right)\sigma^{2.05}$ | |
| Grain boundary diffusion ($D_{gb}\delta$) | $m^3 s^{-1}$ | $3\times10^{-12} \exp\left(\frac{-202000}{RT}\right)\sigma^{2.05}$ | |
| Surface energy ($\gamma$) | $J m^{-2}$ | 1.8 | |
| Volume fraction β | T in K | $-4.593 + 0.0041T$ for $1120 \leq T \leq 1365$ | |
| Grain size ($d$) | μm | 5 | |

A computer simulation was written in Matlab to duplicate the plot for the conditions given above. The results matched the plots given in the publication, as shown in Figure 4.8.

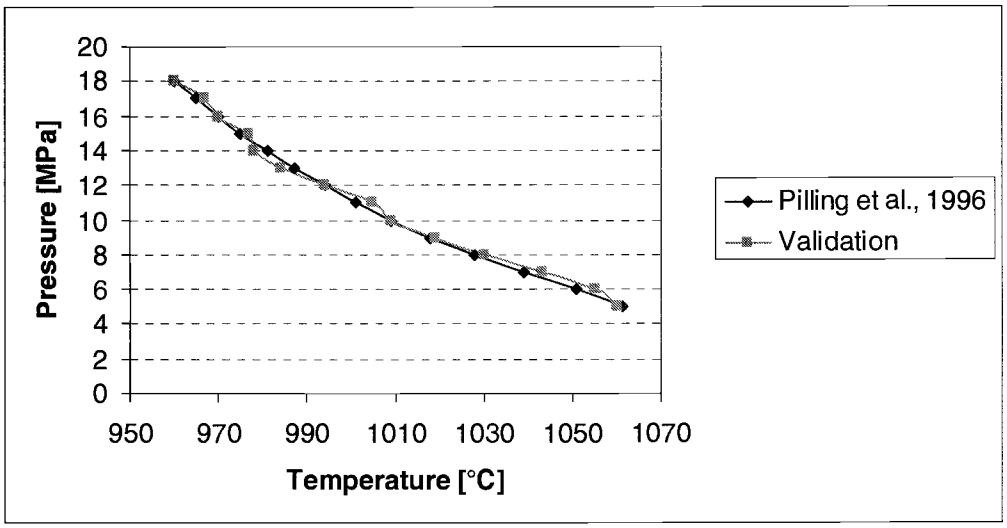


Figure 4.8. Comparison of published Pressure-Temperature curve from Pilling et al. (1996) and results obtained from Matlab simulation

### 4.7.2. Application of Model to NiAl

The model was applied to the diffusion bonding of NiAl at a temperature of 800° C under a pressure of 20 MPa for a duration of 8 hours. The values used for the matching surface roughness $R_a$ of the electroplated NiAl laminae was 0.95 μm and the wavelength of the asperities λ was 30 μm. Physical properties of NiAl are given in Table 4.4. The resulting void fraction was found to be 0.00 after 8 hours which essentially means a void free bond interface.

Table 4.4. Physical properties of NiAl

| **Property** | **Units** | **Value** |
|---|---|---|
| Melting point ($T_m$) | K | 1955<br>(Brandes et al., 1992) |
| Atomic volume ($\Omega$) | $m^3$ | $2.4 \times 10^{-29}$<br>(Noebe et al., 1993 ; Stoloff et al., 1996 ; Carter 1979) |
| Strain rate ($\dot{\varepsilon}$) | $s^{-1}$ | $2.7\times10^{14}\times\exp\left(\frac{-314000}{RT}\right)\times\left(\frac{p}{E_T}\right)^{2.0}$<br>(Noebe et al., 1993 ; Stoloff et al., 1996 ; Raj et al., 1995) |
| Volume diffusion ($D_v$) | $m^2 s^{-1}$ | $3.2\times10^{-3}\times\exp\left(\frac{-200000}{RT}\right)$<br>(Noebe et al., 1993; Callister, 2000) |
| Grain boundary diffusion ($D_{gb}\delta$) | $m^3 s^{-1}$ | $10^{\left(\left(\frac{-0.6279\times10^4}{T}\right)-4.4604\right)}\times5\times10^{-10}$<br>(Mishin et al., 1997 ; Gale et al., 2004) |
| Surface energy ($\gamma$) | $J m^{-2}$ | 2.65<br>(Lozovoi et al., 2001 ; Kuznetsov et al., 1998) |
| Grain size ($d$) | μm | 25<br>(Kanlayasiri, 2003) |

Matlab simulation was run to estimate the model sensitivity to different diffusion bonding parameters. Starting from the bonding conditions which give us zero void fraction, bonding temperature, time and pressure were reduced by 10 percent and amplitude and wavelength of surface roughness were increased by an increment of 10 percent, as shown in Figure 4.9. A void fraction of 0.00

was obtained at 800° C, 20 MPa, and 8 hours. The amplitude and wavelength of surface roughness were 0.95 μm and 30 μm, respectively.

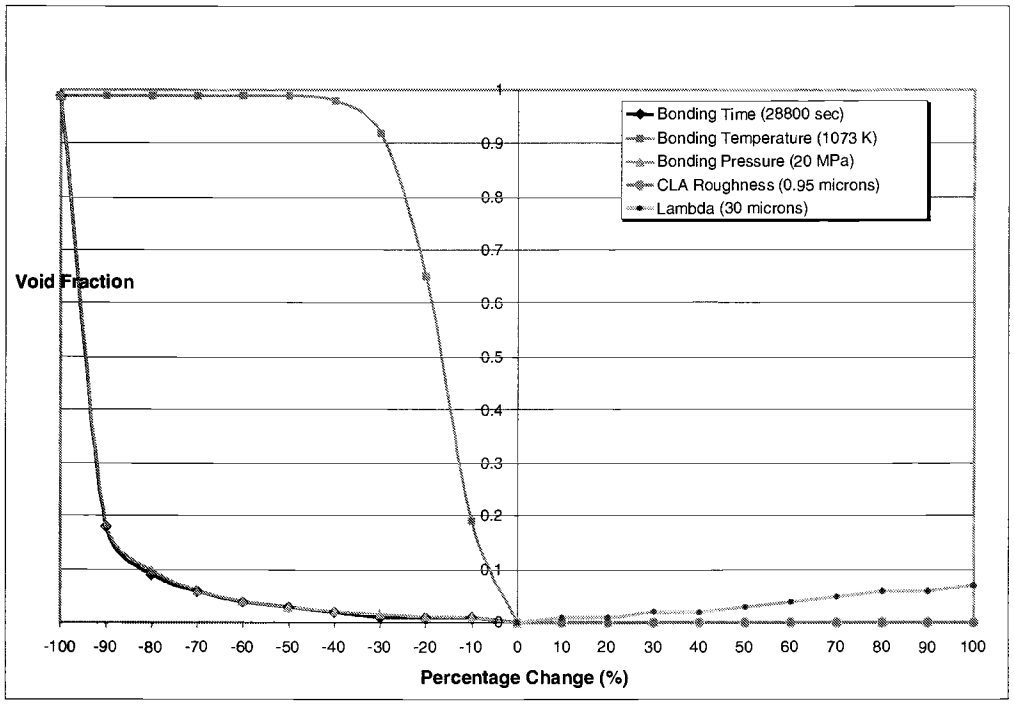


Figure 4.9. Theoretical model's sensitivity to bonding parameters.

As expected, the model was found to be most sensitive to temperature, followed by equal sensitivity to pressure and time, for NiAl at the given bonding parameters. It is interesting to note that the wavelength (λ) of surface roughness has a more profound effect on the resulting void fraction than the amplitude ($R_a$). This is consistent with the results shown by Pilling et al. (1996) for Super Alpha-2. It was found from the computer simulation that the most dominant mechanism in reduction of void fraction is time-dependent plastic flow followed by volume diffusion and grain boundary diffusion. A plot

of these results is shown in Appendix B. This result is consistent with the observation made by Derby and Wallach (1982); Orhan et al. (1999); and Pilling et al., (1988, 1996). Calculations by employing Fick's second law, given in section 4.5.2., reveal that a Ni thickness of up to 4.8 μm can be homogenized into NiAl in an 8 hour cycle at 800° C.

## 4.8. Experimental Approach

Several parameters influence the quality of diffusion bonding including temperature, pressure, time, surface texture, and environment. In a state of the art study Kanlayasiri (2003) determined a good set of parameters for temperature, pressure, and time. With environment being on the order of 0.01 Pa vacuum, role of surface texture in diffusion bonding of NiAl laminae is of prime importance for investigation. Thus the objective of this study is to show that improved smoothness of the surfaces will result in an improved bond. In order to do so role of the surface roughness of the bonding fixture in the final surface roughness of the synthesized NiAl was investigated. To accelerate the diffusion process, the effect of nickel braze thickness as a diffusion aid was on the on the diffusion bonding of NiAl laminae was also studied. Two levels each of surface roughness and electroplated nickel thickness were employed to study these effects.

Elemental foils of commercially pure (99%) aluminum and nickel were used as the starting materials to synthesize nickel aluminide intermetallic

substrates. In order to get 50at% of Ni and Al in 1:1 stoichiometric NiAl, ratio of thicknesses of the elemental foils were calculated as 2:3 for Ni and Al respectively (Kanlayasiri, 2003). Thus a foil of 50.8 μm thick Ni was sandwiched between two 38 μm Al foils. Elemental foils were sheared and cleaned with acetone, methanol, and deionized water. The foils were stacked in a boron nitride fixture in Al-Ni-Al sequence for tack bonding. Tack bonding was conducted at 500° C under a pressure of 3.9 MPa for 15 minutes in a vacuum of about 0.01 Pa. The heating rate was set at 10° C/min. Temperature profile of the tack bonding cycle is shown in Figure 4.10.

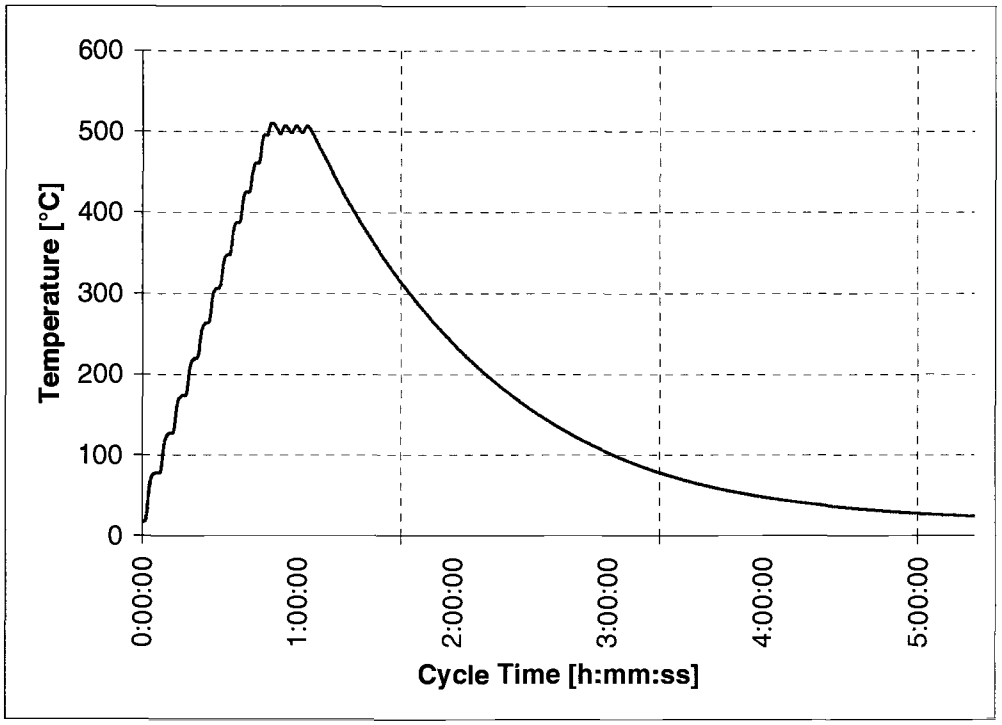


Figure 4.10. Temperature profile of NiAl tack bonding cycle

After the tack bonding step, the edges of the laminae were trimmed to get rid of the unbonded regions. Next, synthesis of the laminae was performed by annealing laminae at 1000° C for 10 hours under minimal pressure in a vacuum environment. A mass of about 100 grams was put on top of the PBN platen to prevent the sample from warping as reported by Kanlayasiri (2003). The heating rate was set at 10° C/min. To ensure a smooth impression of the PBN platens on the NiAl sample, a pressure of 3.9 MPa was applied during the cooling of the sample at 375° C for 15 minutes. The brittle to ductile transition temperature (BDTT) range of polycrystalline NiAl is widely reported between 300° C and 350°C at $10^{-4}$/s strain rate (Ebrahimi and Hoyle, 1997; Bergmann and Vehoff, 1995; Margevicius and Cotton, 1995). Temperature profile of the NiAl synthesis cycle is shown in Figure 4.11.

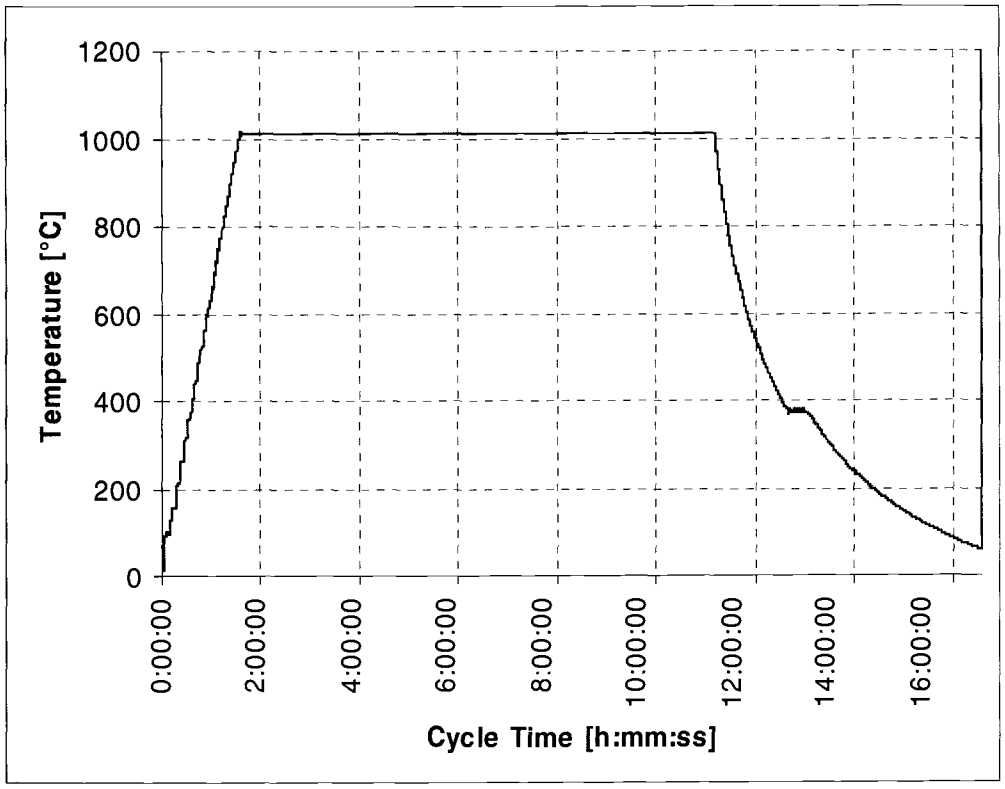


Figure 4.11. Temperature profile of NiAl synthesis cycle

Diffusion aid was deposited on the synthesized NiAl laminae by electroplating Ni on the surfaces. The electroplating procedure included anodic cleaning in a NaOH bath, activation of electroplating by Woods Ni strike, and electroforming in a nickel sulfamate bath. Within the NaOH bath, the electroplating circuit was run in reverse, with the sample to be electroplated being the anode and nickel plate being the cathode. This was done to remove oxides and other foreign particles from the surface. About 125 g of NaOH was stirred into 500 ml to prepare the solution. The reverse current was 30 mA and it was run for about 8 minutes. After rinsing with deionized water, the sample was put in the Woods nickel strike, which was used as an activation step to

initiate electroplating of nickel. The bath was comprised of 35 ml of HCl, 130 ml of $NiCl_2$ and 260 ml of deionized water. A forward current of 13mA was run through the solution for about 1.5 minutes. Next, the sample was placed in the nickel sulfamate solution, after rinsing with deionized water, for the electroforming step. Nickel sulfamate solution was prepared by mixing 1.4 liters of commercially available nickel sulfamate solution with 38 grams of boric acid. The pH range of the solution should be in the range of 3.8-4.5 which can be increased or decreased by 0.1 by adding 0.06g/L sulfamic acid or 0.04g/L of nickel carbonate. A forward current of 22 mA with a pulse duration of 10 ms having a frequency of 5 Hz was used for several hours, depending on the desired thickness of the nickel plate on the NiAl substrate. Surface roughness of the substrate was determined by taking a surface roughness profile of both sides of the substrate by a profilometer, both before and after the nickel electroplating. Two nickel plated NiAl substrate were diffusion bonded at 800° C with a heating rate of 10° C/min, under a pressure of 20.6 MPa for 8 hours. Temperature profile of NiAl diffusion bonding cycle is shown in Figure 4.12.

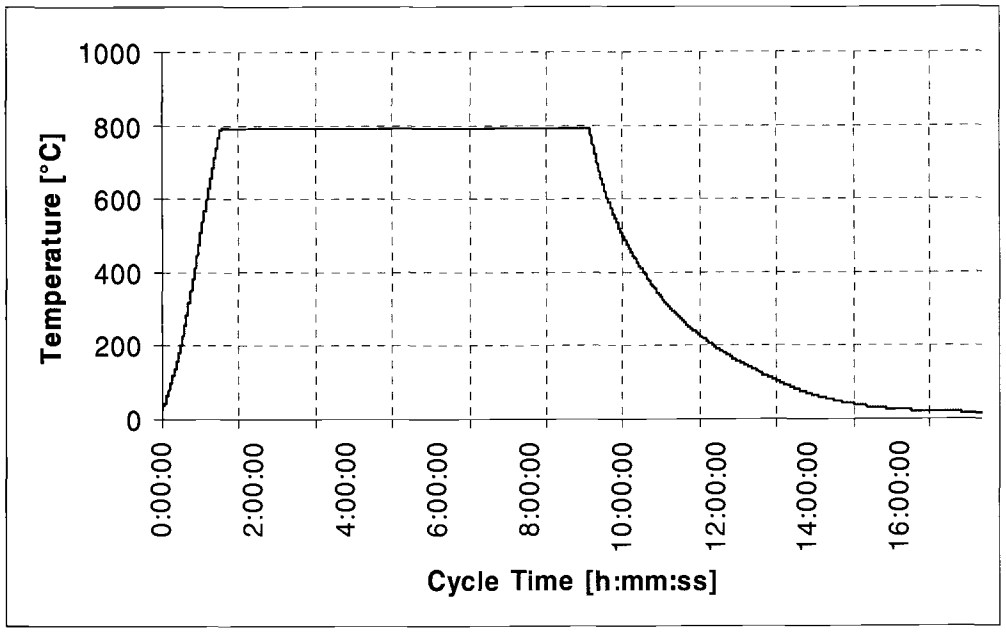


Figure 4.12. Temperature profile of NiAl diffusion bonding cycle

Using a Dektak contact profilometer with a 2.5 μm radius stylus, the surface profiles were taken before and after the tack bonding, synthesis and electroplating cycles to determine the center line average roughness of the laminae surfaces. The bonding quality was determined by optical microscope and scanning electron microscopy. The quality of bond can be quantified by linearized bonding ratio (LBR). Zuruzi et al. (1999) defined LBR as the percentage of bond line length with gaps less than 0.25 μm relative to the total length of the bond interface.

## 4.9. Results and Discussion

### 4.9.1. Nickel Thickness

To obtain two different thicknesses of the nickel plate, electroplating of NiAl laminae was carried out for 50 and 100 minutes. The results of the nickel electroplating are shown in Figures 4.13, 4.14, 4.15, and 4.16. Nickel plate thicknesses of 2 μm on the side facing the anode and 1.4 μm on the side away from the anode were obtained after 50 minutes of electroplating shown in Figures 4.13 and 4.14 respectively. Thicknesses of 4 μm and 2.5 μm were obtained after 100 minutes, for the same electroplating conditions, shown in Figures 4.15 and 4.16.

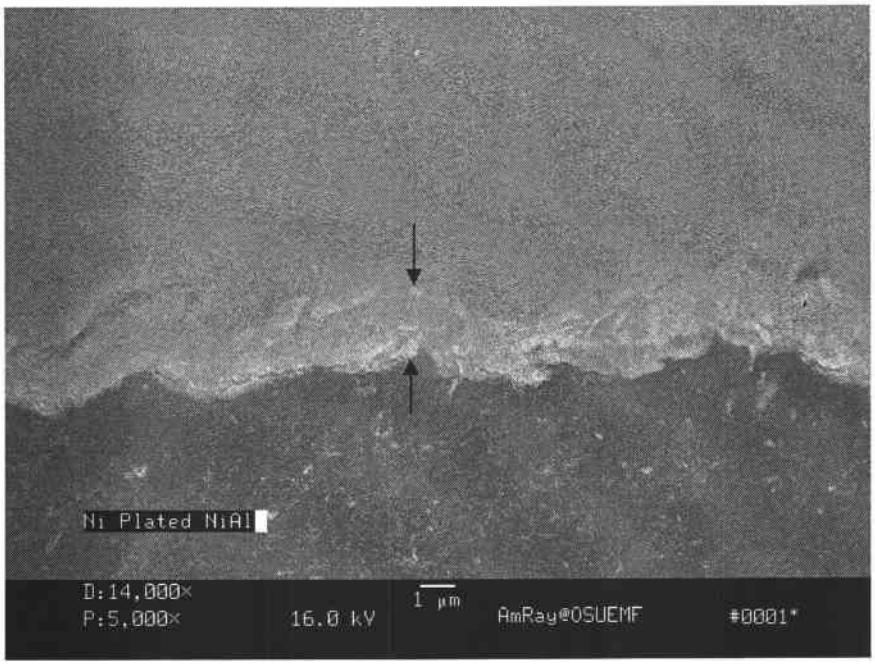


Figure 4.13. Scanning electron mircrograph of Ni deposition on the side facing the anode after 50 minutes (5000X)

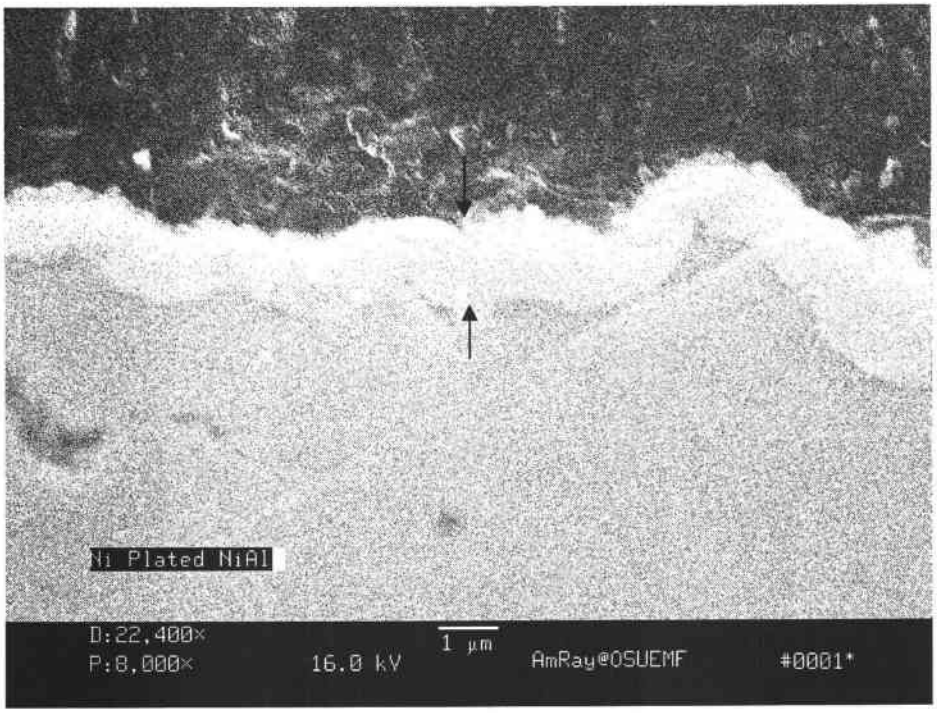


Figure 4.14. Scanning electron mircrograph of Ni deposition on the side away from the anode after 50 minutes (8000X)

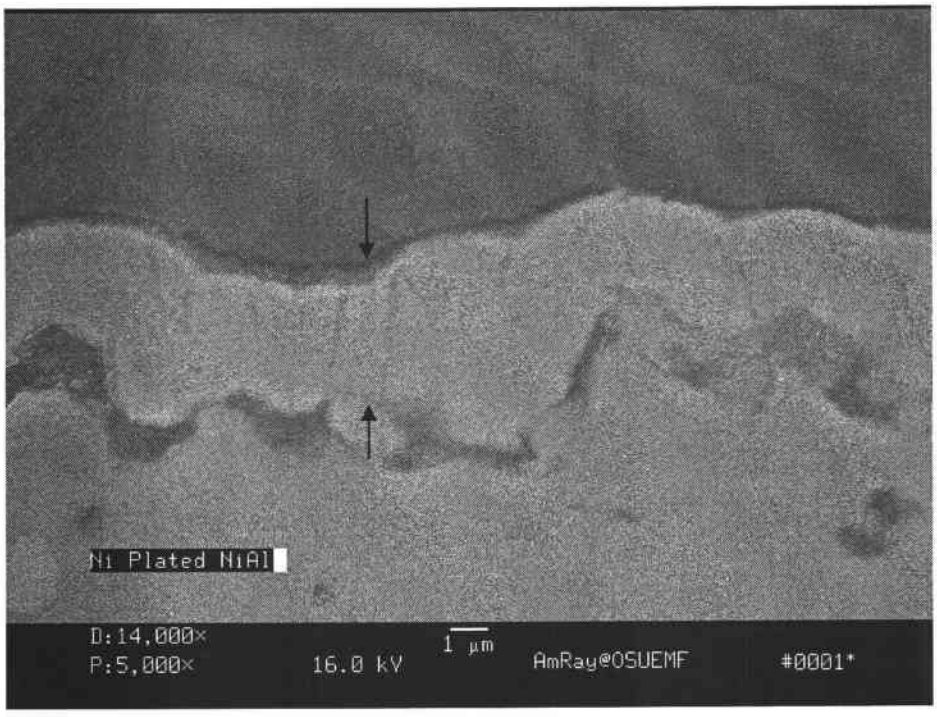


Figure 4.15. Scanning electron mircrograph of Ni deposition on the side facing the anode after 100 minutes (5000X)

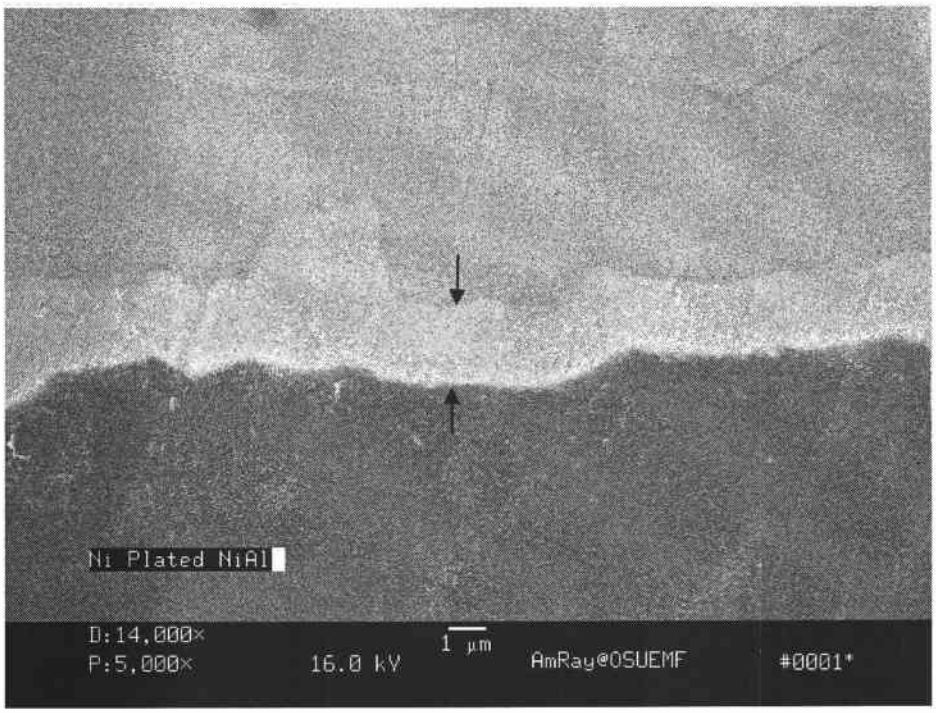


Figure 4.16. Scanning electron mircrograph of Ni deposition on the side away from the anode after 100 minutes (5000X)

### 4.9.2. Surface Roughness

To obtain two different levels of surface roughness in NiAl laminae, several pyrolytic boron nitride platens with an average surface roughness of about 0.3 µm (low) and 1.2 µm (high) were purchased from General Electric Advanced Ceramics. To determine center line average surface roughness ($R_a$), surface profiles of PBN platens as well as NiAl laminae were taken before and after tack bonding, synthesis, and in case of NiAl, electroplating cycles. Profiles were taken with surface profilometer with 4 mm scan length in accordance with ISO 4288. Averages of low and high levels of PBN platens

are plotted in Figure 4.17. A standard deviation of ±σ is shown as an error bar in the plot.

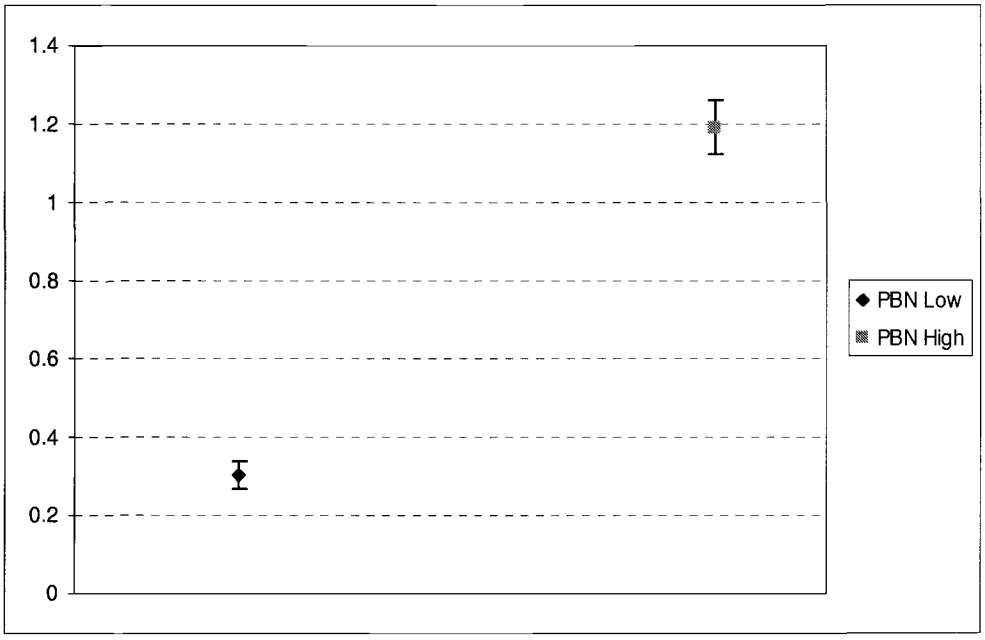


Figure 4.17. Averages of CLA surface roughness ($R_a$) of PBN platens

No significant difference in the $R_a$ of PBN platens was observed after tack bonding and synthesis cycles. Average $R_a$ of 0.38 μm and 0.85 μm were obtained on NiAl laminae after the tack bonding cycle shown in Figure 4.18.

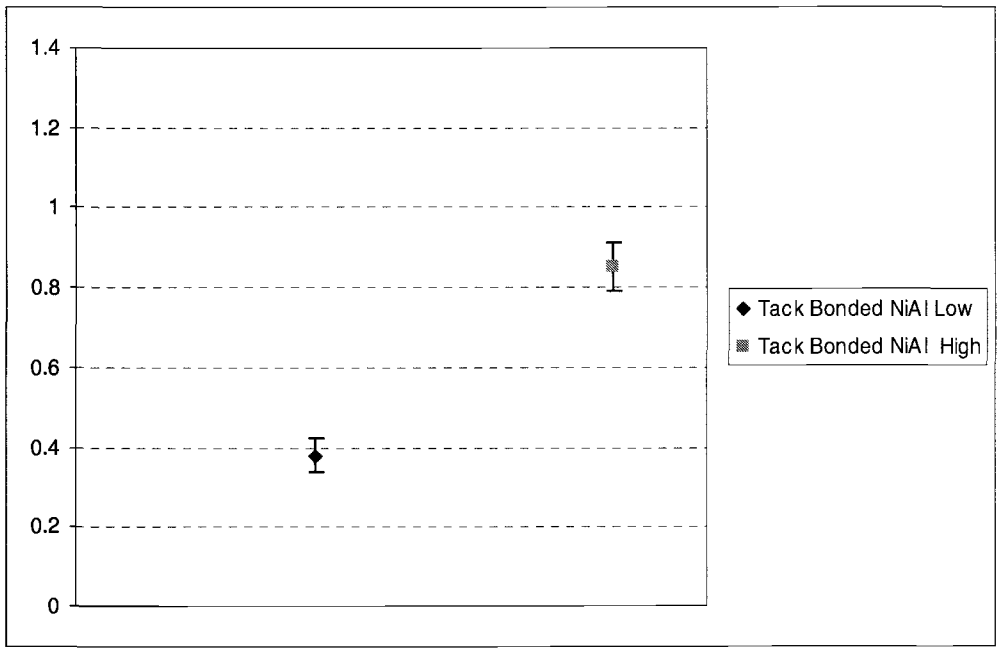


Figure 4.18. Averages of CLA surface roughness ($R_a$) of NiAl laminae after tack bonding

Average $R_a$ of 0.69 μm and 0.95 μm were obtained on NiAl laminae after the synthesis cycle shown in Figure 4.19. A marked increase in the resulting $R_a$ of low level NiAl after the synthesis cycle may be attributed to the Kirkendall effect.

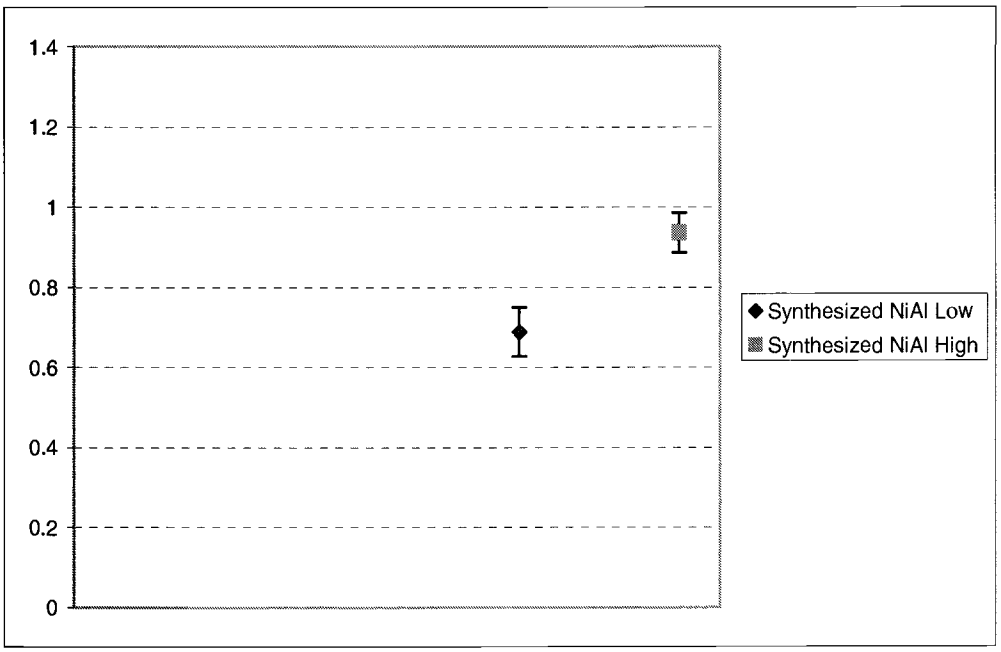


Figure 4.19. Averages of CLA surface roughness ($R_a$) of NiAl laminae after synthesis

Both low and high surface roughness NiAl laminae were electroplated with nickel for 50 and 100 minutes to obtain two different thicknesses of nickel. Average $R_a$ of 0.85 μm and 0.97 μm were obtained on low and high surface roughness NiAl laminae respectively after 50 minutes, as shown in Figure 4.20. An increase in the $R_a$ of low level lamina can be attributed to the phenomenon of leveling which requires a certain threshold of the deposited plate thickness, to achieve an improvement in the surface roughness.

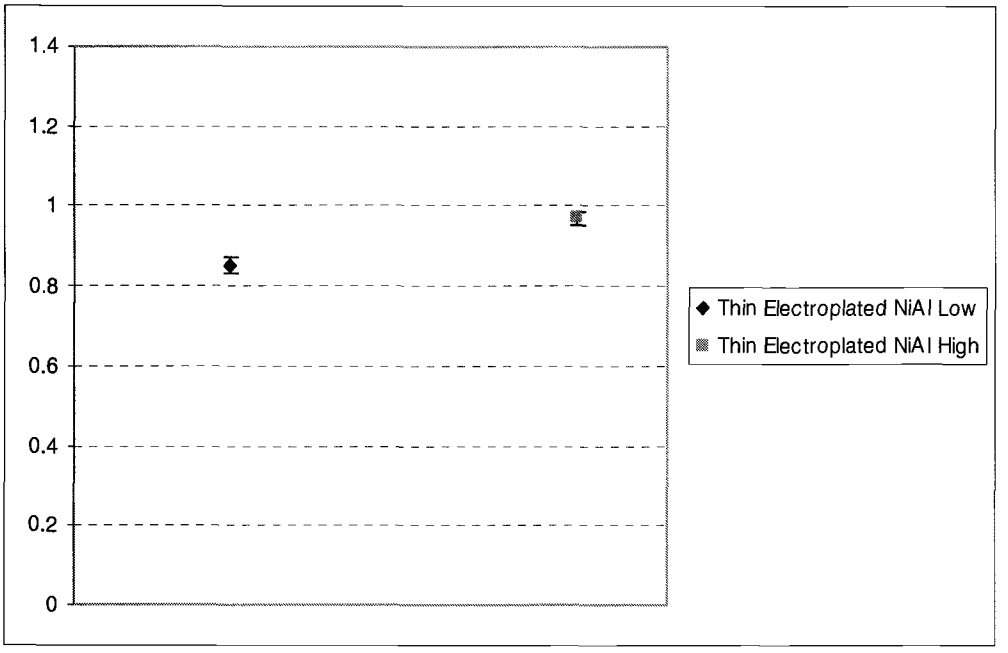


Figure 4.20. Averages of CLA surface roughness ($R_a$) of NiAl laminae after electroplating for 50 minutes

Average $R_a$ of 0.81 μm and 0.96 μm were obtained on low and high surface roughness respectively after 100 minutes, as shown in Figure 4.21.

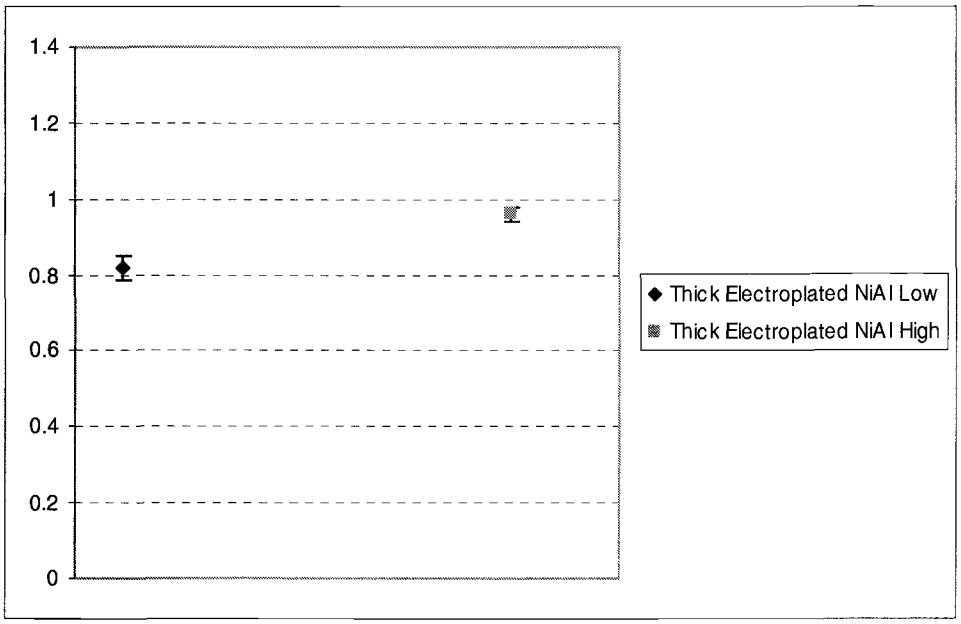


Figure 4.21. Averages of CLA surface roughness ($R_a$) of NiAl laminae after electroplating for 100 minutes

Average CLA surface roughnesses and standard deviations of PBN platens and NiAl laminae are shown in Figure 4.22 and 4.23. A standard deviation of $\pm\sigma$ is shown as error bars in the plots.

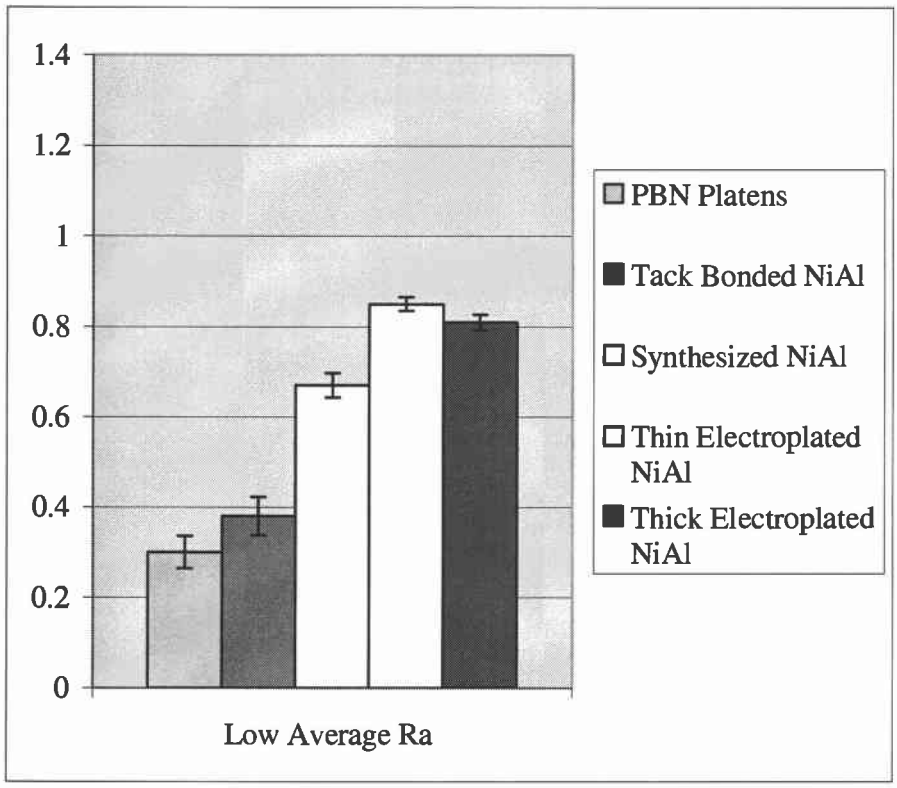


Figure 4.22. Average $R_a$ and standard deviation of low level PBN and NiAl laminae

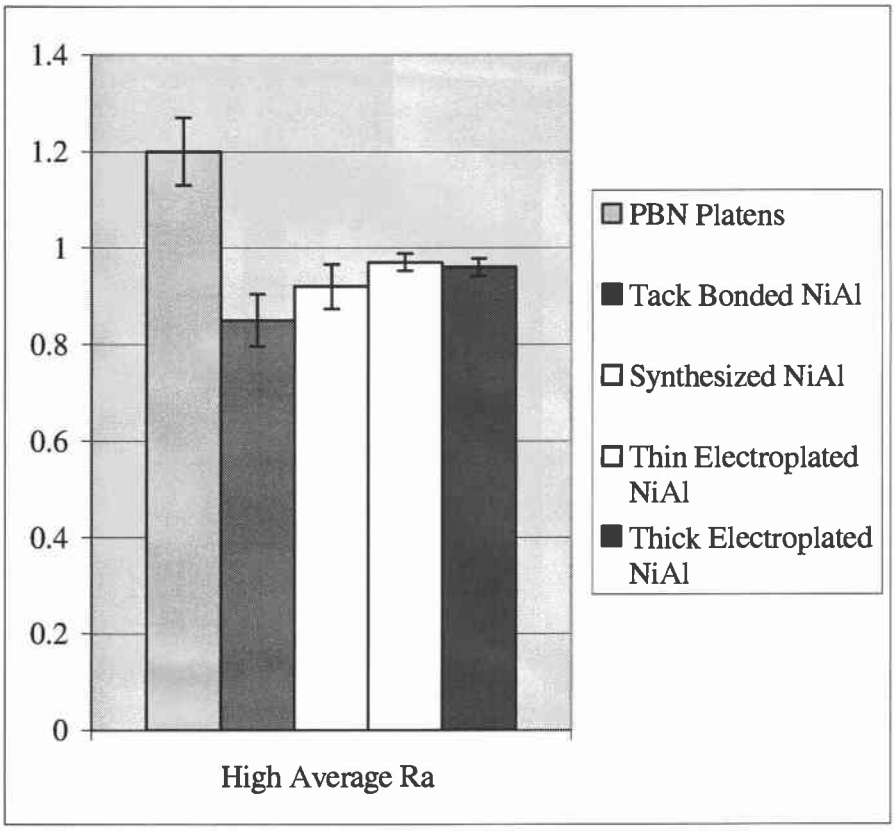


Figure 4.23. Average $R_a$ and standard deviation of high level PBN and NiAl laminae

Compared to the results from Kanlayasiri (2003), smoother surface roughness on NiAl laminae was obtained. However in case of 0.3 $R_a$ (low level), PBN platens desired results were not obtained. There was a significant increase in $R_a$ from tack bonding to synthesis to electroplating cycles. On the other hand, in case of 1.20 $R_a$ (high level) platens, the tack bonded NiAl laminae showed a better $R_a$ than the platens. Nickel electroplating on the surfaces of NiAl laminae further deteriorated the $R_a$ in both low and high levels. As leveling is a progressive process, a certain minimum thickness of

deposition is required to achieve geometric leveling (Lowenheim, 1974). The deposited layers of 2 μm and 4 μm were not thick enough to actually improve the surface roughness.

### 4.9.3. Void Fraction of Bond Line

Electroplated NiAl samples were diffusion bonded with synthesized NiAl laminae of the corresponding surface roughness. The four combinations of surface roughness and nickel-plate thickness employed for diffusion bonding of NiAl are tabulated below.

Table 4.5. Table of $R_a$, λ, and thickness of nickel plate

| | Average CLA $R_a$ and λ | | | | | | | | |
|---|---|---|---|---|---|---|---|---|---|
| | Synthesized NiAl | | | | Electroplated NiAl | | | | Thickness of Nickel Plate |
| | $R_a$ | Std. Dev. | λ | Std. Dev | $R_a$ | Std. Dev. | λ | Std. Dev | |
| No. | μm | μm | μm | μm | μm | μm | μm | μm | μm |
| 1. | 0.67 (low) | 0.027 | 15 | 1 | 0.85 μm (low-thin) | 0.015 | 20 | 1 | 2 |
| 2. | 0.92 (high) | 0.046 | 30 | 1 | 0.97 μm (high thin) | 0.018 | 31 | 1 | 2 |
| 3. | 0.67 (low) | 0.027 | 15 | 1 | 0.81 μm (low-thick) | 0.017 | 19 | 1 | 4 |
| 4. | 0.92 (high) | 0.046 | 30 | 1 | 0.96 μm (high-thick) | 0.018 | 29 | 1 | 4 |

Micrographs obtained from the metallographic studies of the diffusion bonded NiAl are shown in Figures 4.24, 4.25, 4.26, and 4.27.

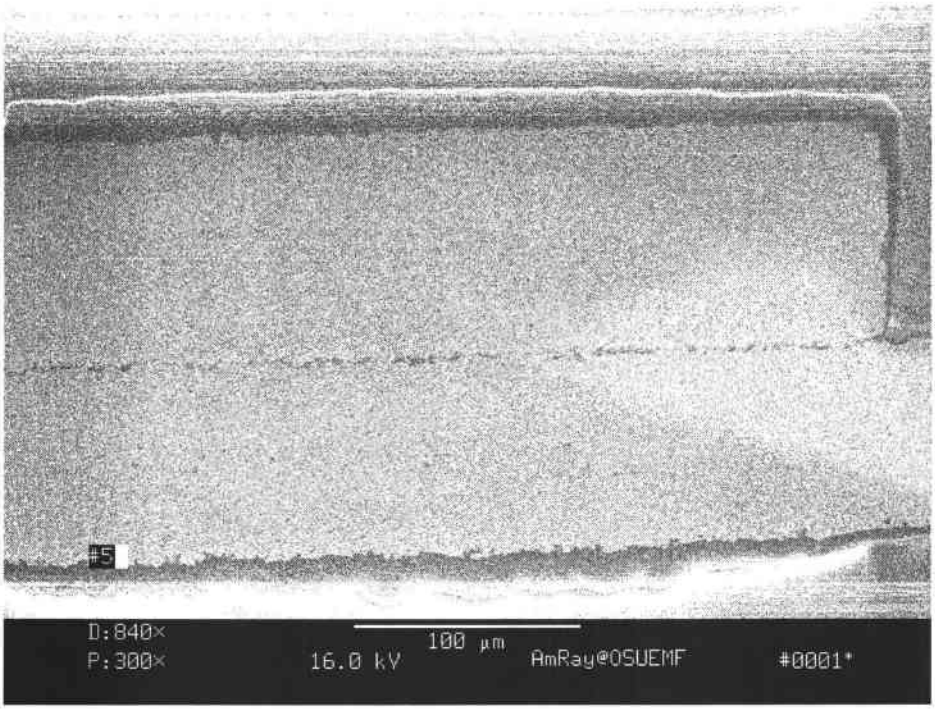


Figure 4.24. Scanning electron micrograph of the cross-section of diffusion bonded NiAl #1 (300x)

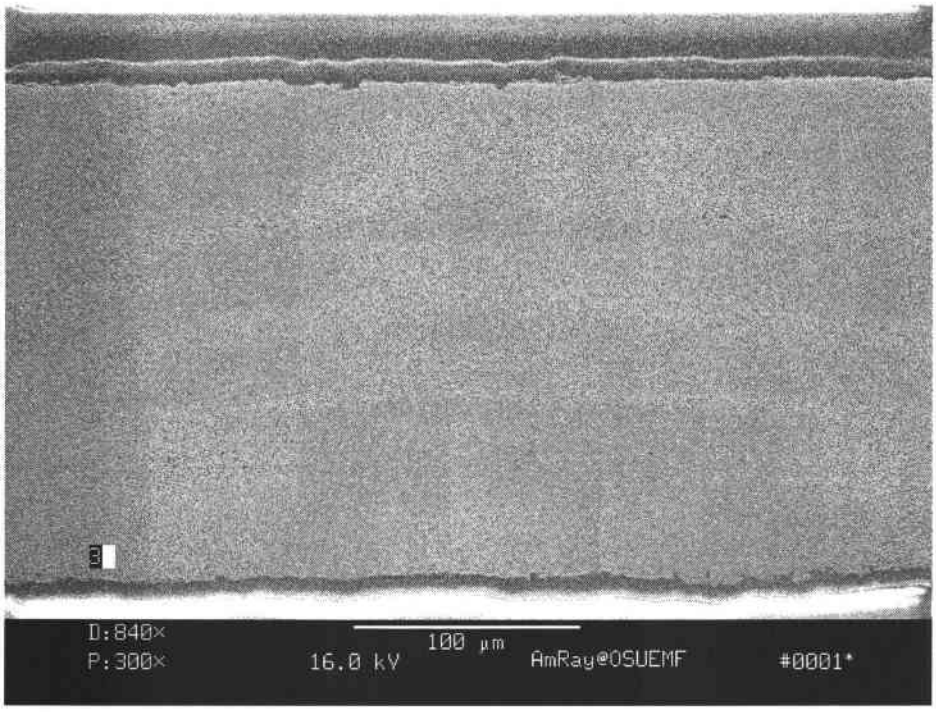


Figure 4.25. Scanning electron micrograph of the cross-section of diffusion bonded NiAl #2 (300x)

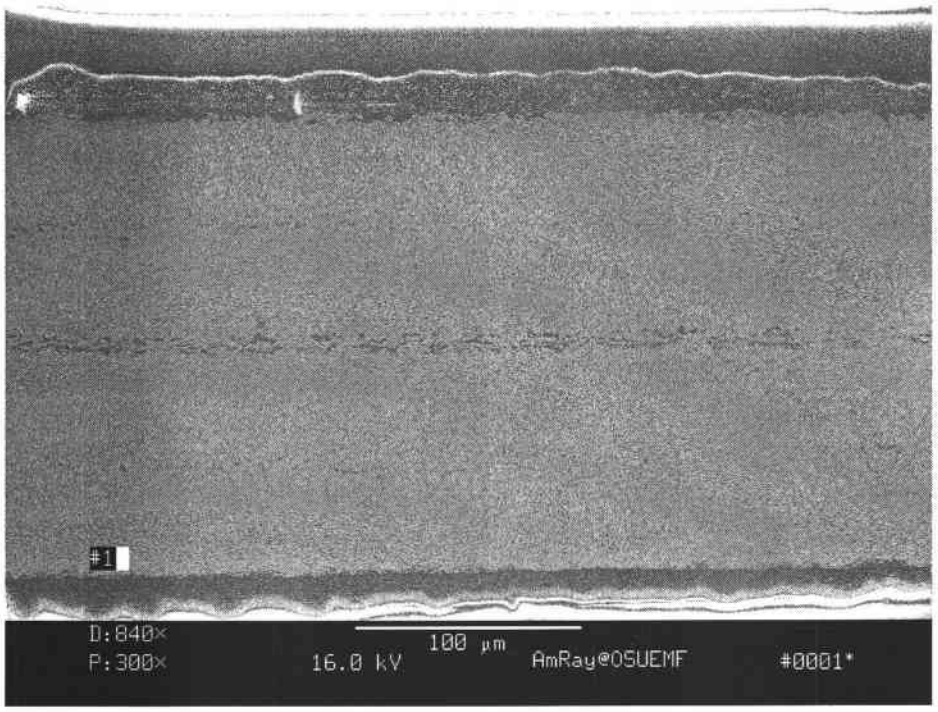


Figure 4.26. Scanning electron micrograph of the cross-section of diffusion bonded NiAl #3 (300x)

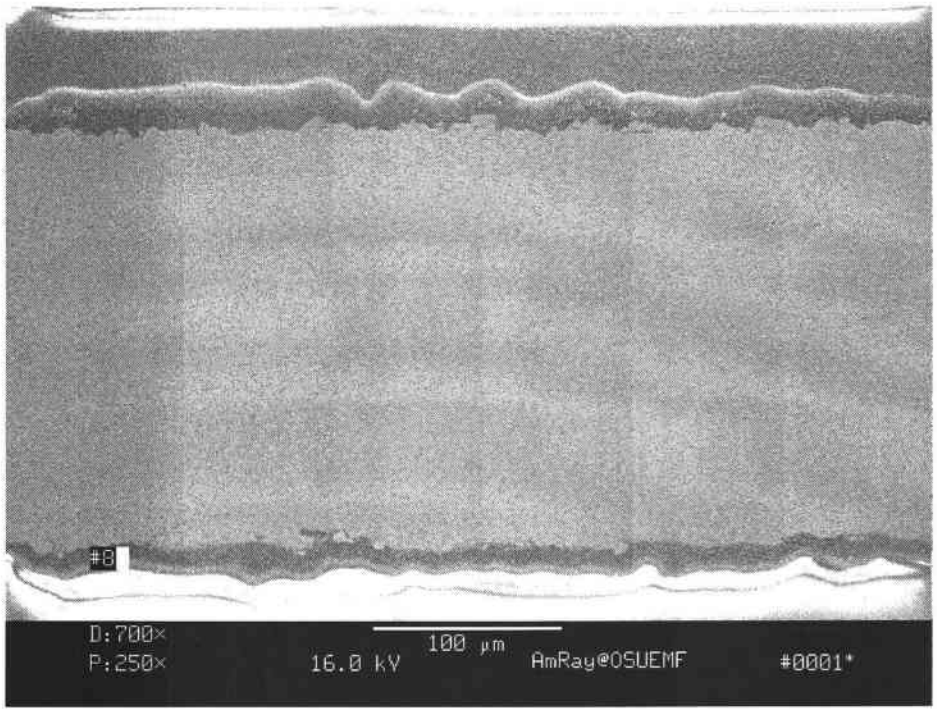


Figure 4.27. Scanning electron micrograph of the cross-section of diffusion bonded NiAl #4 (300x)

In case of NiAl sample 1, due to a difference of 26% in the $R_a$ of two laminae a bond line with voids is obvious in Figure 4.24. This phenomenon has been explained by Chen et al. (2002) and is described in section 4.4 of this chapter. NiAl 1 fits into the case of "different-scale-roughness" mechanism of diffusion bonding. The $R_a$ of the two mating surfaces were not the same, resulting in a random and mismatched positioning of the peaks and valleys of the two surfaces. Although, the asperities were decreased by the application of bonding pressure as the two surfaces were squeezed together, some voids remained at the interface. The schematic of "different-scale-roughness" mechanism is shown in Figure 4.28.

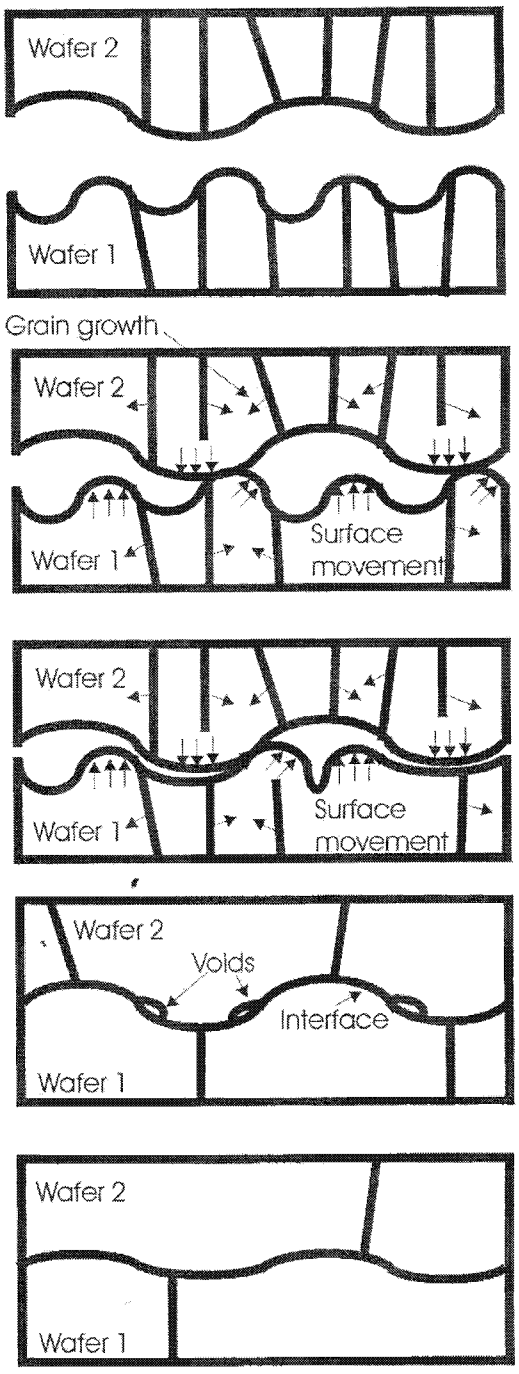


Figure 4.28. Schematic of "different scale roughness" bonding mechanism (Chen et al., 2002)

In case of sample 2, a difference of just 5% in the $R_a$ of the laminae yields a void free bond with no bond line in Figure 4.25. According to Chen et al. (2002) this would most probably fall under "peak-to-peak" bonding mechanisms. In a peak to peak alignment of asperities, the contact area between the two surfaces is small and the deformation of elastic spheres is easy, resulting in an atomic scale distance between the mating surfaces. Interdiffusion of atoms with higher kinetic energy is facilitated between the surfaces with a simultaneous grain growth. The bond line at the interface disappears, giving way to a homogeneous region with a non-distinct interface. A schematic of "peak-to-peak" mechanism is shown is Figure 4.29.

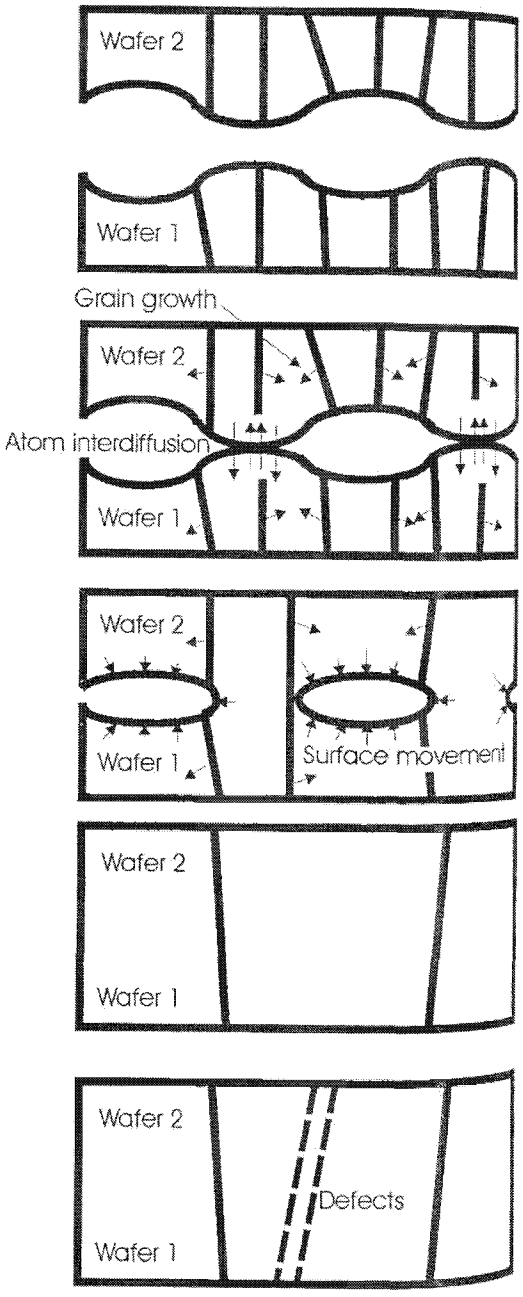


Figure 4.29. Schematic of "peak-to-peak" bonding mechanism (Chen et al., 2002)

A 20 % difference in the Ra of laminae in sample 3 resulted in joint with voids shown in Figure 4.26. A void free interface was obtained in sample 4 because of a matching $R_a$ of within 4%, shown in Figure 4.27. The void fraction is an improvement over Kanlayasiri's (2003) bond line as shown in Figure 4.30. Bonding conditions used were the same, with the exception of Ra, which was about 1.5 μm in Kanlayasiri.

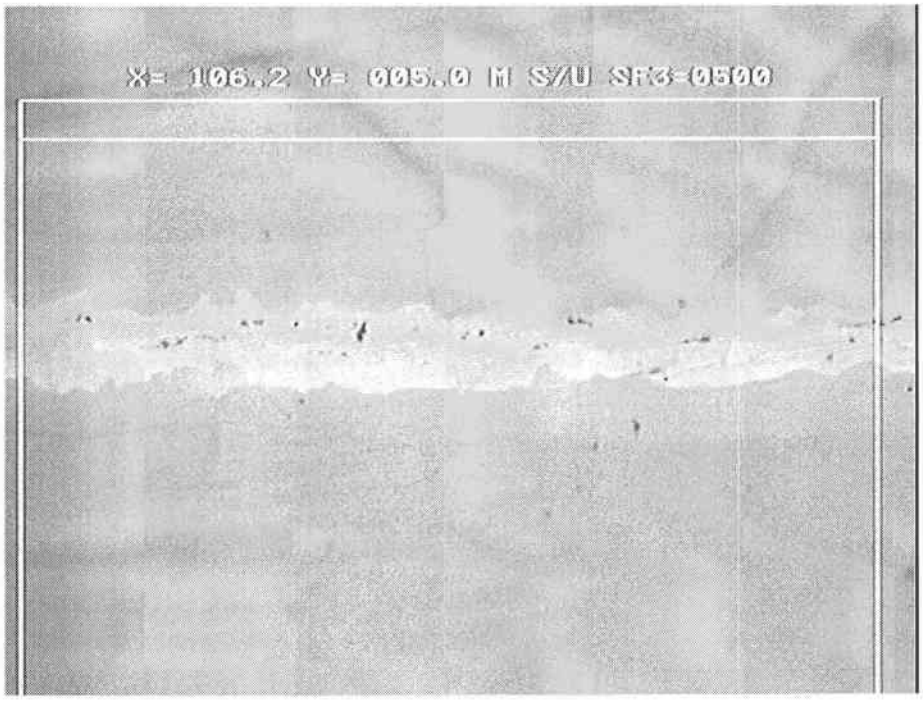


Figure 4.30. Diffusion bonded NiAl (Kanlayasiri, 2003)

### 4.9.4. Homogeneity of Bond Line

To determine the homogeneity of the diffusion bonded NiAl samples, point EDS (electron-diffraction spectroscopy) analysis was carried out at the

top, bottom, and the bonding interface of the bonded samples. The fifth set of data is from previous research by Kanlayasiri (2003). For Kanlayasiri, the synthesis and diffusion bonding cycles were the same as the current study, however instead of nickel plating, a thin foil of nickel with a thickness of about 7.5 μm was used as a diffusion aid. Atomic percentage of nickel and aluminum are shown in Table 4.6. Weight percentage of nickel and aluminum can be found in Appendix C. The spectrographs of the point EDS can be found in Appendix D.

Table 4.6. Point EDS analysis of the diffusion bonded samples

| Sample No. | | **Al at%** | **Ni at%** |
|---|---|---|---|
| 1. | Top | 59.61 | 40.38 |
| | Bond | 56.97 | 43.02 |
| | Bottom | 53.42 | 46.57 |
| 2. | Top | 60.22 | 39.77 |
| | Bond | 51.85 | 48.14 |
| | Bottom | 60.29 | 39.70 |
| 3. | Top | 54.93 | 45.06 |
| | Bond | 51.10 | 48.89 |
| | Bottom | 59.77 | 40.22 |
| 4. | Top | 58.05 | 41.94 |
| | Bond | 36.21 | 63.78 |
| | Bottom | 54.13 | 45.86 |
| 5. | Top | 62.71 | 37.28 |
| | Bond | 66.19 | 33.80 |
| | Bottom | 63.72 | 36.27 |

From the binary phase diagram of NiAl shown in Figure 4.1, NiAl phase exists within a range of 45 to 59 at% Ni or 41 to 55 at% Al at room temperature. For all the samples in this study, the composition of nickel and

aluminum lie within the range or within 4% of NiAl range. The accuracy of point EDS is known to be 5-10%. The previous study by Kanlayasiri (2003) lay in the $Ni_2Al_3$ or an intermediate phase between $Ni_2Al_3$ and $NiAl_3$.

Kanlayasiri (2003) summarized the kinetics of phase transformation during the reactive diffusion of NiAl synthesis as follows:

$$Ni + 3Al \rightarrow NiAl_3$$

$$NiAl_3 + Ni \rightarrow Ni_2Al_3$$

$$Ni_2Al_3 + Ni \rightarrow 3NiAl$$

$$NiAl + 2Ni \rightarrow Ni_3Al$$

$$Ni_3Al \rightarrow \text{ intermediate phase} \rightarrow NiAl$$

Considering the progression of the synthesis, it may be worthwhile to extend the dwell time at the annealing temperature to progress from $Ni_2Al_3$ to NiAl.

### 4.9.5. Compositional Analysis of NiAl

A wavelength dispersive spectroscopic (WDS) study of the synthesized NiAl lamina fabricated in PBN platens showed a reduction in carbon contents as compared to the lamina fabricated in the graphite platens. Averages of the atomic percentages of nickel, aluminum, and other inclusions for the synthesized NiAl in graphite platens, in PBN platens, as well as the atomic composition of nickel electroplated NiAl are shown in Table 4.7. The first four samples were not tested for oxygen. Elements of concern among inclusions are

boron and carbon. Both boron and carbon embrittle the NiAl (George and Liu, 1990). Although there is a trace amount of boron on the surface of NiAl formed in PBN platens, there is substantial amount of carbon on the surface and cross-section of NiAl formed in PBN platens. There could be two reasons for this. First, the carbon inclusion may have been absorbed from the graphite heating elements in the vacuum hot press. Second, as the samples were mounted in epoxy, some carbon might have been read by the X-ray beam from the hydrocarbons in the epoxy.

Table 4.7. Table of WDS analysis of synthesized and electroplated samples

| | **N** | **B** | **C** | **Al** | **Ni** | **O** | **S** |
|---|---|---|---|---|---|---|---|
| | at% | at% | at% | at% | at% | at% | at% |
| Surface of NiAl formed in PBN platens | 4.01 | 0.21 | 5.79 | 49.71 | 40.26 | - | - |
| Cross-section of NiAl formed in PBN platens | 4.36 | 0.00 | 9.581 | 43.88 | 42.49 | - | - |
| Surface of NiAl formed in graphite platens | 1.50 | 0.00 | 52.98 | 37.36 | 8.414 | - | - |
| Cross-section of NiAl formed in graphite platens | 4.00 | 0.00 | 6.89 | 48.44 | 40.97 | - | - |
| Surface of Ni electroplated NiAl | 6.61 | 0.00 | 7.07 | 0.005 | 85.02 | 2.29 | 0.105 |
| Cross-section of Ni electroplated NiAl | 3.92 | 0.00 | 10.00 | 45.20 | 39.27 | 2.31 | 0.049 |

### 4.9.6. Theoretical Model

The theoretical model, presented in section 4.7, was applied to the diffusion bonding of NiAl at a temperature of 800° C under a pressure of 20 MPa for a duration of 8 hours. The matching $R_a$ of the synthesized and electroplated NiAl laminae was 0.95 μm and the wavelength of the asperities λ was 30 μm. The resulting void fraction was 0.00 after 8 hours which essentially means a void free bond interface. In the experimental research, the results were verified and can be seen from samples 2 and 4 in Figures 4.25 and 4.27. This is an improvement over Kanlayasiri's (2003) bond at the same bonding conditions, with the exception of $R_a$ which was about 1.5 μm, shown in Figure 4.31.

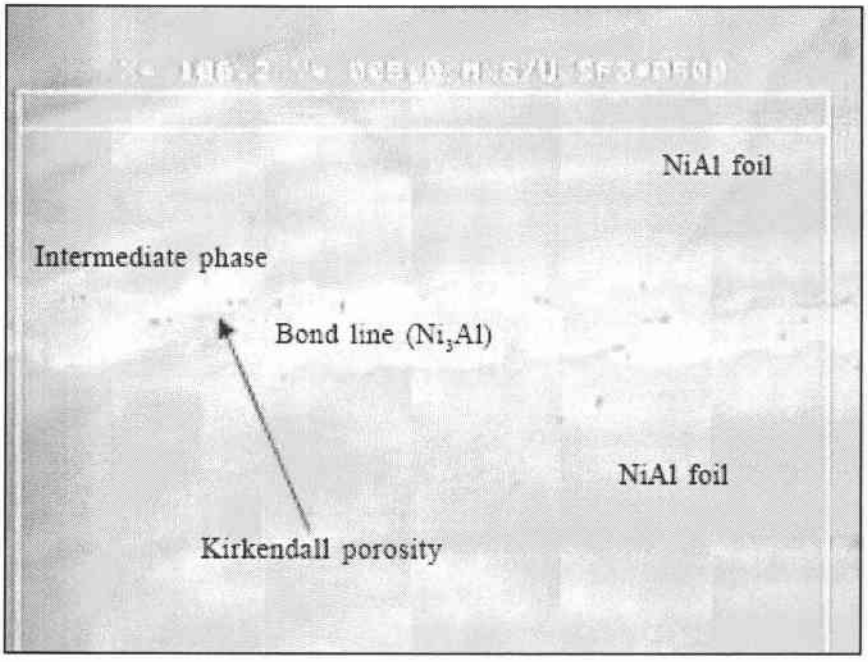


Figure 4.31. Diffusion bonded NiAl (Kanlayasiri, 2003)

From the results, condition #2 of NiAl seems to be the best with low void fraction and has excellent homogeneity with little carbon contamination. It is expected that the NiAl synthesis route used here and reported elsewhere could be replaced with a more economical synthesis approach such as the rolling and annealing of NiAl shim (250 μm) from Ni and Al powder. This expectation is based on interactions with industrial sheet material suppliers. Therefore, the surface roughness and Ni-plating specifications developed as a result of this research will help to steer future efforts needed to develop this synthesis approach.

## 4.10. Conclusions

The work presented here found that it is possible to produce homogenized, void-free, diffusion-bonded NiAl samples without carbon contamination. Control of bond line voids and carbon contamination was brought about by the use of smooth, inert PBN platens used during synthesis and bonding to reduce the surface roughness and contamination of foils. In addition, Ni-electroplating was used to control the thickness of Ni layers used as a diffusion aid. Theoretical results were found to be good predictors both for homogenization of samples as well as void elimination.

In particular, one parameter investigated in this research was foil surface roughness and its effects on bond quality in the diffusion bonding process. Due to the surface geometry of the bonded objects, modeling of diffusion bonding of metallic or intermetallic foils is much more difficult than the modeling of sintering of particles in powder metallurgy. In powder metallurgy, the surface geometry of the particles is round or close to round facilitating the geometric modeling of particles. In contrast, in metallic or intermetallic foils, a planar array of peaks and valleys as well as non-uniform distribution of these peaks and valleys is encountered, which leads to mismatched mating surfaces. An isostatic diffusion bonding model was synthesized from prior work and employed to understand the effect of different bonding parameters in the diffusion bonding process. It was learned from this model that the wavelength of the surface asperities has a much more profound

effect on void fraction than the amplitude of the asperities. Also, the prediction of the theoretical model was found to be consistent with experimental results for surfaces with similar roughness conditions. However, for samples with mismatched roughnesses, it was found that diffusion bonding results significantly deviated from the model. This has profound implications for the producers of future NiAl foils. It is expected that the roughness wavelength and perhaps the amplitude of the foils would need to have less than 20% variation with excellent bonding results around 5% variation. The theoretical model was shown to be most sensitive to the variation in bonding temperature followed by equal sensitivity to bonding pressure and bonding time, in the case of NiAl diffusion bonding.

An improvement in the bond quality and the homogeneity of the bonded laminae, over previous NiAl research by Kanlayasiri (2003), was demonstrated by decreasing the surface roughness of the mating surfaces through the use of smoother pyrolytic boron nitride platens. A significant reduction in carbon contamination was also achieved by using PBN platens instead of graphite platens to hold the laminae. A thin nickel layer was deposited on NiAl laminae, as a diffusion aid by means of electroplating, to expedite the diffusion bonding process.

## 4.11. References

Alman, D. E., (1994), "Reaction Synthesis of Ni-36.8 at% Al," Journal of Materials Science Letters, 13: 483-486.

Alman, D. E., Dogan, C. P., Hawk, J. A., and Rawers, J. C., (1995), "Processing, Structure and Properties of Metal-Intermetallic Layered Composites," Materials Science and Engineering A: Structural Materials: Properties, Microstructure and Processing, A192/193(pt 2): 624-632.

Aroyo, M. S., (1995), "Leveling in Pulse Plating with Brighteners: Synergistic Effect of Frequency and Hydrodynamically Active Additives," Plating & Surface Finishing, 82(11): 53-57.

"ASM Metal Handbook, Volume 2, Properties and Selection: Nonferrous Alloys and Special Purpose Materials," (1990), American Society for Metals, Metals Park, Ohio, pp. 914-920.

Bergmann, G. and Vehoff, H., (1995), "Effect of Environment on the Brittle-to-Ductile Transition of Precracked NiAl Single and Polycrystal," Materials Science and Engineering A: Structural Materials: Properties, Mircrostructures and Processes, A192-19(pt1): 309-315.

Berkowitz, A. E., Jaumot, f. E., and Nix, F. C., (1954), "Diffusion of $Co^{60}$ in Some Ni-Al Alloys Containing Excess Vacancies," Physical Review, 95(4): 1185-1189.

Callister Jr., W. D., (2000), "Materials Science and Engineering: An Introduction," 5th Edition, John Wiley & Sons, Inc., New York, pp. 92-111.

Carter, G. F., (1979), "Principles of Physical and Chemical Metallurgy," American Society of Metal, Ohio, pp. 27.

Chen, K. N., Fan, A., and Reif, R., (2002), "Interfacial Morphologies and Possible Mechanisms of Copper Wafer Bonding," Journal of Materials Science, 37(16): 3441-3446.

Cox, M. J., Kim, M. J., and Carpenter, R. W., (2002), "Interface Nanochemistry Effects on Stainless Steel Diffusion Bonding," Metallurgical and Materials Transactions A, 33(2): 437-442.

Dallas, D. B. (Editor-in-Chief) (1976), "Tool and Manufacturing Engineers Handbook," Third Edition, Society of Manufacturing Engineer, McGraw-Hill Book Company, New York, USA.

Derby, B. and Wallach, E. R., (1982), "Theoretical Model for Diffusion Bonding," Metal Science, 16: 49-56.

Du, X. H., Guo, J. T., and Zhou, B. D., (2001), "Superplasticity of Stoichiometric NiAl With Large Grains," Scripta Materialia, 45(1): 69-74.

Du, X., and Wu, B., (2005), "Continuous Dynamic Recrystallization of Extruded NiAl Polycrystals During Superplastic Deformation Process," Metallurgical and Materials Transactions A: Physical Metallurgy and Materials Science, 36(12): 3343-3351.

Ebrahimi, F. and Hoyle, T. G., (1997), "Brittle-to-Ductile Transition in Polycrystalline NiAl," Acta Materialia, 45(10): 4193-4204.

Ehrfeld, W., Hessel, V., and Lowe, H., (2000), "Microreactors: New Technology for Modern Chemistry," Wiley-VCH, New York.

Enjo, T., Ikeuchi, K., and Akikawa, N., (1982), "Effect of the Roughness of Faying Surface on the Early Process of Diffusion Welding - Study of the Early Process Of Diffusion Welding by Means of the Electric Resistance Measurement (Report II)," Transactions of JWRI (Japanese Welding Research Institute), 11(2): 49-57.

Farago, F. T., (1982), "Handbook of Dimensional Mesurement," Second Edition, Industrial Press Inc., New York, USA.

Gale, W. F., and Totemeier, T. C. (Ed.), (2004), "Smithells Metals Reference Book," 8th Edition. Elsevier, New York, pp 13-7.

George, E. P. and Liu, C. T., (1990), "Brittle Fracture and Grain Boundary Chemistry of Microalloyed NiAl," Journal of Materials Research, 5(4): 754-762.

Goodfellow (2004), Goodfellow Corporation, Accessed on December 2004, http://www.goodfellow.com/csp/active/gfHome.csp

Guo, J. T., Chen, R. S., Du, X. H., Li, G. S., and Zhou, L. Z., (2005), "Microstructural Evolution and Deformation Mechanisms for Superplaticity of NiAl Intermetallic," Materials Science Forum, 475-479(IV): 2995-2998.

Harvey, J., Partridge, P. G., and Lurshay, A. M., (1986), "Factors Affecting the Shear Strength of Solid State Diffusion Bonds Between Silver-Coated Clad Al-

Zn-Mg Alloy (Aluminium Alloy 7010)," Materials Science and Engineering, 79(2): 191-199.

Hori, S., Tokizane, M., and Furushiro, N., (1991), "Superplasticity in Advanced Materials," The Japan Society of Research on Superplasticity, Osaka, Japan.

Islam, M. F., and Ridley, N., (1998), "Isostatic Diffusion Bonding of a Microduplex Stainless Steel," Scripta Materialia, 38(8): 1187-1193.

ISO 4287, (1997), "Geometric Product Specification (GPS) – Surface Texture: Profile Method – Terms, Definitions and Surface Texture Parameters," International Organization for Standardization, Geneve, Switzerland.

ISO 4288, (1996), ""Geometric Product Specification (GPS) – Surface Texture: Profile Method – Rules and Procedures for the Assessment of Surface Texture," International Organization for Standardization, Geneve, Switzerland.

Janikowski, S. K., Gombert, D., Soelberg, N. R., Harrup, M., and Jovanovich, G., (2002), "Catalytic Steam Reforming in a Microreactor," Presentation to Idaho National Engineering and Environmental Laboratory," May 22-23.

Jauhari, I., Ogiyama, H., and Tsukuda, H., (2003), "Solid State Diffusion Bonding of Superplastic Duplex Stainless Steel with Carbon Steel," Materials Science Research International, 9(2): 154-159.

Kalpakijan, S. and Schmid, S. R., (2001), "Manufacturing Engineering and Technology," 4th Edition, Prentice-Hall, Inc., New Jersey, USA. pp. 812-813.

Kanlayasiri, K. and Paul, B. K., (2004), "A Nickel Aluminide Microchannel Array Heat-Exchanger for High Temperature Applications," Journal of Manufacturing Processes, 6(1): 17-25.

Kanlayasiri, K., (2003), "Development of Nickel Aluminide (NiAl) Microchannel Array Devices for High Temperature Applications," Ph.D. Dissertation, Industrial and Manufacturing Engineering, Oregon State University.

Kazakov, N. F., (1985), "Diffusion Bonding of Materials," First Edition, Pergamon Press, New York, USA.

Kearns, W. H., (1980), "Welding Handbook: Resistance and Solid-State Welding and Other Joining Processes," 7th edition, Volume 3, American Welding Society, Miami, Florida, USA.

Kurasawa, T., Takatsu, H., Sato, S., Kuroda, T., Sugimoto, S., and Tamura, M., (1996), "Diffusion Bonding of Reduced Activation Ferritic Steel F82H for Demo Blanket Application," Journal of Nuclear Materials, 233-237(Pt A): 313-318.

Kuznetsov, V. M., Kadyrov, R. I., and Rudenskii, G. E., (1998), "Calculation of Surface Energy of Metals and Alloys by the Electron Density Functional Method," Journal of Materials Science and Technology, 14(4): 320-322.

Lemus, J., and Drew, R. A. L., (2000), "Diffusion Bonding of Silicon Nitride to Titanium," British Ceramic Transactions, 99(5): 200-205.

Loweneheim, F. A. (editor), (1974), "Modern Electroplating," 3rd Editon, John Wiley & Sons, Inc., New York.

Lozovoi, A. Y., Alavi, A., and Finnis, M. W., (2001), "Surface Energy and the Early Stages of Oxidation of NiAl(110)," Computer Physics Communication, 137: 174-194.

Margevicius, R. W. and Cotton, J. D., (1995), "Study of the Brittle-to-Ductile Transition in NiAl by Texture Analysis," Acta Materialia, 43(2): 645-655.

Massalski, T. B., Singleton, M. F., Marray, J. L., and Nash, P., (1990), "Binary Alloy Phase Diagrams," American Society for Metals, Metals Park, Ohio, pp.183.

Mishin, Y., and Farkas, D., (1997), "Atomistic Simulation of Grain Boundary Structure and Diffusion in B2 NiAl," Materials Research Society Symposium Proceedings, 458: 21-26.

Moore, T. J. and Kalinowski, J. M., (1993), "Diffusion Brazing NiAl With Self-Generated Filler Metal" Materials Research Society Symposium Proceedings, 288: 1173-1178.

Nagano, T., and Wakai, F., (1994), "Relationship Between Surface Roughness and Bonding Strength in Superplastic Diffusion Bonding," Journal of the Ceramic Society of Japan, International Edition, 102(7): 690-693.

Nakao, Y., Shinozaki, K., and Hamada, M., (1991), "Diffusion Bonding of Intermetallic Compound TiAl," ISIJ International, 31(10): 1260-1266.

Nieh, T. G. and Wadsworth, J., (1999), "Fine Structure Superplastic Intermetallics," International Materials Review, 44(2): 59-75.

Noebe, R. D., Bowman, R. R., and Nathal, M. V., (1993), "Physical and Mechanical Properties of the B2 Compound NiAl," International Materials Review, 38(4): 193-232.

Orhan, N., Aksoy, M., and Eroglu, M., (1999), "A New Model for Diffusion Bonding and Its Application to Duplex Alloys," Materials Science and Engineering, A271: 458-468.

Ortego, J. D., Richardson, J. T., and Twigg, M. V., (1997), "Catalytic Steam Reforming of Chlorocarbons: Methyl Chloride," Applied Catalysis B:Environmental, (12)(4): 339-355.

Philibert, J., (1991), "Reactive Diffusion in Thin Films," Applied Surface Science, 53:74-81.

Pilling, J., (1988), "The Kinetics of Isostatic Diffusion Bonding in Superplastic Materials," Materials Science and Engineering, 100: 137-144.

Pilling, J., Ridley, N., and Islam, M. F., (1996), "On the Modelling of Diffusion Bonding in Materials: Superplastic Super Alpha-2," Materials Science and Engineering A: Structural Materials: Properties, Microstructure and Processing, A205(1-2): 72-78.

Raj, S.V. and Farmer, S. C., (1995), "Characteristics of a New Creep Regime in Polycrystalline NiAl," Metallurgical and Materials Transaction A: Physical Metallurgy and Materials Science, 26A(2): 343-356.

Rawers, J. C., Hansen, J. S., Alman, D. E., and Hawk, J. A., (1994), "Formation of Sheet Metal-Intermetallic Composites by Self-Propagating High-Temperature Reactions," Journal of Materials Science Letters, 13: 1357-1360.

Schwartz, M. M., (1979), "Metal Joining Manual," McGraw-Hill, New York, USA.

Somekawa, H., and Higashi, K., (2003), "The Optimal Surface Roughness Condition on Diffusion Bonding," Materials Transactions, 44(8): 1640-1643.

Somekawa, H., Watanabe, H., and Higashi, K., (2003), "The Grain Size Dependence on Diffusion Bonding Behavior in Superplastic Mg Alloys," Materials Transactions, 44(4): 496-503.

Stoloff, N. S., and Sikka V. K. (editors) (1996), "Physical Metallurgy and Processing of Intermetallic Compounds," Chapman and Hall, New York, NY, pp. 217.

Ugural, A. C. and Fenster, S. K., (1987), "Advanced Strength and Applied Elasticity," 2nd Edition, Elsevier Science Publishing Co, Inc., New York, pp.

Veeco, (2000), "Dektak 3 Surface Profile Measuring System: Installation, Operation, and Maintenance Manual," Veeco Metrology Group, Santa Barbra, USA.

Wattanutchariya, W., (2002), "Application of Buckling Behavior to Evaluate and Control Shape Variation in High-Temperature Microlamination," Ph.D. Dissertation, Industrial and Manufacturing Engineering, Oregon State University.

Yang, C. F., Chiu, L. H., Lee, S. C., and Sun, J. Y., (1998), "Solid State and Transient Liquid Phase Diffusion Bonding of an Al-Zn-Mg Alloy," Proceedings of the National Science Council, Republic of China, Part A: Physical Science and Engineering, 22(1): 132-141.

Zuruzi, A. S., Li, H., and Dong, G., (1999), "Effects of Surface Roughness on the Diffusion Bonding of Al Alloy 6061 in Air," Materials Science and Engineering A, 270(2): 244-248.

# CHAPTER 5

# CONCLUSIONS AND FUTURE RESEARCH

## 5.1. Conclusions

This research dealt with issues related to the development of high temperature microchannel arrays from aluminide foils. Major issues in fabricating aluminide microchannel arrays include room temperature ductility of aluminide foils; flatness and surface roughness of foils; warpage and deformation of the microchannels due to application of bonding pressure; quality of bonded foils; and in the case of synthesized NiAl, homogeneity of the bonded matrix. The research was conducted on three intermetallic aluminide foils: single crystal $Ni_3Al$ foil, an ordered intermetallic phase in the nickel aluminide system; FeAl, an ordered phase in the iron-aluminide system; and NiAl synthesized from commercially pure Ni and Al, the other ordered intermetallic phase in the nickel aluminide system.

In the first part of this study, the potential for making high temperature microchannel devices was demonstrated through the use of pre-fabricated single crystal $Ni_3Al$ foil. A two-fluid counter flow microchannel array was fabricated from cold rolled, single crystal $Ni_3Al$ foil. A leak-proof device,

tested under a pressure of more than one atmosphere, was successfully fabricated. Metallographic studies of the cross-section of the bonded foils did not show any bond line or voids at the bonding interface. Furthermore, no cracks or major heat affected zone were observed after patterning the microchannel geometry on the foils. However, cost is a major issue in mass production of high temperature devices from single crystal $Ni_3Al$ foils.

The second part of this research investigated the potential for fabricating two-fluid counter flow microchannel array from relatively more inexpensive and thus economical FeAl foil, made via a powder metallurgy route. This particular foil had some room temperature ductility as opposed to previously available FeAl foils which were brittle at room temperature. One motivation for this research was to explore the possibility for other types of aluminide foils, for instance NiAl, to be produced by following the same route as FeAl. Metallographic studies of the array showed void free, sound bond interfaces. However, a marked deformation was observed in the microchannel geometry. This deformation and warpage could be the effect of the applied bonding pressure at an elevated temperature and may be eliminated by optimizing the bonding conditions. Another issue with this foil was its surface flatness at room temperature. The foils were flattened under an excessive pressure for a short duration, at room temperature, which may have introduced some stresses in the foil.

The third part of this research dealt with understanding the diffusion bonding conditions necessary to produce sound, homogeneous joints using NiAl foils. NiAl has the highest melting point of the common aluminide phases. In addition, NiAl has been demonstrated to have excellent corrosion resistance for high temperature reactions such as hydrocarbon steam reforming. Also, materials vendors believe that economical powder roll compaction methods similar to those of the FeAl foil could be developed for NiAl. Consequently, efforts were made to specify the foil conditions and bonding aids necessary to produce sound, homogeneous joints. NiAl foils were synthesized from commercially pure Ni and Al foils for this investigation.

One parameter investigated in this research was foil surface roughness and its effects on bond quality in the diffusion bonding process. Due to the surface geometry of the bonded objects, modeling of diffusion bonding of metallic or intermetallic foils is much more difficult than the modeling of sintering of particles in powder metallurgy. In powder metallurgy, the surface geometry of the particles is round or close to round facilitating the geometric modeling of particles. In contrast, in metallic or intermetallic foils, a planar array of peaks and valleys as well as non-uniform distribution of these peaks and valleys is encountered, which leads to mismatched mating surfaces. An isostatic diffusion bonding model was synthesized from prior work and employed to understand the effect of different bonding parameters in the diffusion bonding process. It was learned from this model that the wavelength

of the surface asperities has a much more profound effect on void fraction than the amplitude of the asperities. Also, the prediction of the theoretical model was found to be consistent with experimental results for surfaces with similar roughness conditions. However, for samples with mismatched roughnesses, it was found that diffusion bonding results significantly deviated from the model. This has profound implications for the producers of future NiAl foils. It is expected that the roughness wavelength and perhaps the amplitude of the foils would need to have less than 20% variation with excellent bonding results around 5% variation. The theoretical model was shown to be most sensitive to the variation in bonding temperature followed by equal sensitivity to bonding pressure and bonding time, in the case of NiAl diffusion bonding.

An improvement in the bond quality and the homogeneity of the bonded laminae, over previous NiAl research by Kanlayasiri (2003), was demonstrated by decreasing the surface roughness of the mating surfaces through the use of smoother pyrolytic boron nitride platens. A significant reduction in carbon contamination was also achieved by using PBN platens instead of graphite platens to hold the laminae. A thin nickel layer was deposited on NiAl laminae, as a diffusion aid by means of electroplating, to expedite the diffusion bonding process.

## 5.2. Future Research

This research investigated the potential for using aluminide foils to fabricate high temperature devices. It successfully demonstrated that nickel and iron aluminide foils can be used to make high aspect ratio, high temperature devices. Future research can contribute towards improving the processing parameters; improving dimensional and compositional integrity; optimizing surface roughness standards to achieve sound economical bonds; and investigating the role of alloying elements in improving the physical properties of the foil.

One future research possibility is to improve the flatness of FeAl foils. It may also be helpful to increase the room temperature ductility of the foil. This will facilitate the patterning as well as diffusion bonding process of the laminae. Optimization of the bonding parameters will contribute towards the elimination of warpage and deformation of the microchannels.

In case of NiAl, it is advisable to decrease the amplitude and wavelength of the peaks and valleys of surface roughness asperities, to facilitate the bonding process. Achieving uniformity in distribution of surface roughness, throughout the surface of the foil, will contribute to better bond quality. Uniform thin nickel layers should be deposited on both mating surfaces to expedite the diffusion bonding process. In case of cold rolling, rolling conditions have a significant affect on the surface characteristics transferred on the sheets (Ma, Tieu, Lu, and Jiang, 2002). Various terms have

been used to characterize surface asperities and distribution of these asperities. Liv (1996) characterized the surface profile in cold rolling of foils as grooves, gorges, shingles, cross-hatches, and rolling ridges. To obtain smoother and uniform surfaces, it is recommended to investigate the effect of rolling parameters and conditions on the deformation sequence of the asperities on the rolled aluminide foils.

The role of alloying elements should be investigated to improve the room temperature ductility of NiAl foil. For instance in FeAl, addition of chromium improved the room temperature ductility; zirconium additions achieved grain refinement; whereas boron increased the grain boundary cohesion and suppressed the inter-granular fracture. Molybdenum, tantalum, and niobium have shown to improve the high temperature strength and creep resistance of the FeAl foils. These alloying elements have a critical range; outside this range they are either ineffective or detrimental to the properties of the alloy (Deevi, Sastry, and Sikka, 2001; Sikka, Vishwanath, and McKamey, 1993).

## 5.3. References

Deevi, S. C., Sastry, D. H., and Sikka, V.K., (2001), "Alloy Development and Industrial Processing of Iron Aluminide Sheets," Proceedings of the International Symposium on Structural Intermetallics, 111-119.

Kanlayasiri, K., (2003), "Development of Nickel Aluminide (NiAl) Microchannel Array Devices for High Temperature Applications," Ph.D. Dissertation, Industrial and Manufacturing Engineering, Oregon State University.

Liv, G., (1996), "Development of Surface Topography During Cold Rolling of Twin-Roll Cast Aluminium," Wear, 192: 216-227.

Ma, B., Tieu, A. K., Lu, C., and Jiang, Z., (2002), "An Experimental Investigation of Steel Surface Characteristic Transfer by Cold Rolling," Journal of Materials Processing Technology, 125-126: 657-663.

Sikka, V. K., Viswanathan, S., and McKamey, C. G., (1993), "Development and Commercialization Status of $Fe_3Al$ Based Intermetallic Alloys," Proceedings of the First International Symposium on Structural Intermetallics Structural Intermetallics," The Materials Society, Warrendale, PA, pp. 483-491.

# BIBLIOGRAPHY

"ASM Metal Handbook, Volume 2, Properties and Selection: Nonferrous Alloys and Special Purpose Materials," (1990), American Society for Metals, Metals Park, Ohio, pp. 914-920.

Akash, A., Nair, B., Minnick, K., Wilson, M., and Hartvigsen, J., (2004), "HAS-CERCANAM: A New Material with a Continuous Nanopore Network," Materials Research Society Symposium, 788: 359-363.

Alman, D. E., (1994), "Reaction Synthesis of Ni-36.8 at% Al," Journal of Materials Science Letters, 13: 483-486.

Alman, D. E., Dogan, C. P., Hawk, J. A., and Rawers, J. C., (1995), "Processing, Structure and Properties of Metal-Intermetallic Layered Composites," Materials Science and Engineering A: Structural Materials: Properties, Microstructure and Processing, A192/193(pt 2): 624-632.

Alman, D.E. and Dogan, C.P., (1995), "Intermetallic Sheets Synthesized from Elemental Ti, Al, and Nb Foils," Metallurgical and Materials Transactions A, 26A: 2759-62.

Alman, D.E., (1996), "Fabrication, Structure and Properties of Aluminum-Aluminide Layered Composites," Materials Research Society Symposium – Proceeding, 434: 255-260.

Ameel, T. A., Warrington, R. O., Wegneg, R. S., and Drost, M. K., (1997), "Miniaturization Technologies Applied to Energy System," Energy Conversion Management, 38(10-13): 969-982.

Aroyo, M. S., (1995), "Leveling in Pulse Plating with Brighteners: Synergistic Effect of Frequency and Hydrodynamically Active Additives," Plating & Surface Finishing, 82(11): 53-57.

Banovic, S. W., DuPont, J. N., Tortorelli, P.F., and Marder, A.R., (1999), "Role of Aluminum on the Weldability and Sulfidation Behavior of Iron-Aluminum Cladding," Welding Journal, 78(1): 23s-30s.

Banovic, S. W., Dupont, J.N., and Marder, A. R., (2001), "Experimental Evaluation of Fe-Al Claddings in High-Temperature Sulfidizing Environments," Welding Journal, 80(3): 63s-70s.

Bergmann, G. and Vehoff, H., (1995), "Effect of Environment on the Brittle-to-Ductile Transition of Precracked NiAl Single and Polycrystal," Materials Science and Engineering A: Structural Materials: Properties, Mircrostructures and Processes, A192-19(pt1): 309-315.

Berkowitz, A. E., Jaumot, f. E., and Nix, F. C., (1954), "Diffusion of $Co^{60}$ in Some Ni-Al Alloys Containing Excess Vacancies," Physical Review, 95(4): 1185-1189.

Brandes, E.A. and Brook, G.B. (Ed.), (1992), "Smithells Metals Reference Book," 1992, 7th edition.

Callister Jr., W. D., (2000), "Materials Science and Engineering: An Introduction," 5th Edition, John Wiley & Sons, Inc., New York, pp. 92-111.

Carter, G. F., (1979), "Principles of Physical and Chemical Metallurgy," American Society of Metal, Ohio, pp. 27.

Chaumat, G., Moret, F., and Gasse, A., (1995), "SiC Brazing for Ceramic Heat Exchangers," DVS-Berichte, 166:217-219.

Chen, K. N., Fan, A., and Reif, R., (2002), "Interfacial Morphologies and Possible Mechanisms of Copper Wafer Bonding," Journal of Materials Science, 37(16): 3441-3446.

Clemens, H., Lorich, A., Eberhardt, N., Glatz, W., Knabl, W., and Kestler, H., (1999), "Technology, Properties and Applications of Intermetallic γ-TiAl Based Alloys," Zeitschrift fuer Metallkunde/Materials Research and Advanced Techniques, 90(8): 569-580.

Cox, M. J., Kim, M. J., and Carpenter, R. W., (2002), "Interface Nanochemistry Effects on Stainless Steel Diffusion Bonding," Metallurgical and Materials Transactions A, 33(2): 437-442.

Dallas, D. B. (Editor-in-Chief) (1976), "Tool and Manufacturing Engineers Handbook," Third Edition, Society of Manufacturing Engineer, McGraw-Hill Book Company, New York, USA.

David, S. A., Horton, J. A., McKamey, C. G., Zacharia, T., and Reed, R. W., (1989) "Welding of Iron Aluminides," Welding Journal, 68(9): 372s-381s.

Deevi, S. C., (2000), "Powder Processing of FeAl Sheets by Roll Compaction," Intermetallics, 8: 679-685.

Deevi, S. C., Sastry, D. H., and Sikka, V.K., (2001), "Alloy Development and Industrial Processing of Iron Aluminide Sheets," Proceedings of the International Symposium on Structural Intermetallics, 111-119.

Demura, M., Kishida, K., Umezawa, O., George, E.P. and Hirano, T., (2000), "Ductile Thin Foil of $Ni_3Al$," Mechanical Properties of Structural Films, STP 1413, American Society for Testing and Materials, 248-261.

Demura, M., Suga, Y., Umezawa, O., Kishida, K., George, E. P., and Hirano, T., (2001), "Fabrication of $Ni_3Al$ Thin Foil by Cold-Rolling" Intermetallics, 9(2):157-167.

Derby, B. and Wallach, E. R., (1982), "Theoretical Model for Diffusion Bonding," Metal Science, 16: 49-56.

Drost, M. K., Call, C. J., Cuta, J. M., and Wegneg, R. S., (1997), "Microchannel Integrated Evaporator/Combustor Thermal Processes," Microscale Thermophysics Engineering, 1(4): 321-333.

Du, X. H., Guo, J. T., and Zhou, B. D., (2001), "Superplasticity of Stoichiometric NiAl With Large Grains," Scripta Materialia, 45(1): 69-74.

Du, X., and Wu, B., (2005), "Continuous Dynamic Recrystallization of Extruded NiAl Polycrystals During Superplastic Deformation Process," Metallurgical and Materials Transactions A: Physical Metallurgy and Materials Science, 36(12): 3343-3351.

Dunford, D. and Wisbey, A., (1993), "Diffusion Bonding of Advanced Aerospace Metallics," Materials Research Society Symposium Proceedings, 314: 39-50

Ebrahimi, F. and Hoyle, T. G., (1997), "Brittle-to-Ductile Transition in Polycrystalline NiAl," Acta Materialia, 45(10): 4193-4204.

Ehrfeld, W., Hessel, V., and Lowe, H., (2000), "Microreactors: New Technology for Modern Chemistry," Wiley-VCH, New York.

Enjo, T., Ikeuchi, K., and Akikawa, N., (1982), "Effect of the Roughness of Faying Surface on the Early Process of Diffusion Welding - Study of the Early Process Of Diffusion Welding by Means of the Electric Resistance Measurement (Report II)," Transactions of JWRI (Japanese Welding Research Institute), 11(2): 49-57.

Farago, F. T., (1982), "Handbook of Dimensional Mesurement," Second Edition, Industrial Press Inc., New York, USA.

Gale, W. F., and Totemeier, T. C. (Ed.), (2004), "Smithells Metals Reference Book," 8th Edition. Elsevier, New York, pp 13-7.

George, E. P. and Liu, C. T., (1990), "Brittle Fracture and Grain Boundary Chemistry of Microalloyed NiAl," Journal of Materials Research, 5(4): 754-762.

German, R. M. and Iacocca, R. G., (1996), "Powder Metallurgy Processing," Physical Metallurgy and Processing of Intermetallic Compound, Chapman & Hall, NewYork, pp. 605.

Ghezel-Ayagh, H., Daly, J. M., and Wang, Z. H., (2003), "Advances in Direct Fuel Cell / Gas Turbine Power Plants," American Society of Mechanical Engineers, International Gas Turbine Institute, Turbo Expo (Publication) IGTI, 2: 625-629.

Golberg, D., Demura, M. and Hirano, T., (1998), "Effects of Al-rich off-stoichiometry on the yield stress of binary Ni3Al single crystals," Acta Materialia, 46: 2695-2703.

Goodfellow (2004), Goodfellow Corporation, Accessed on December 2004, http://www.goodfellow.com/csp/active/gfHome.csp

Guo, J. T., Chen, R. S., Du, X. H., Li, G. S., and Zhou, L. Z., (2005), "Microstructural Evolution and Deformation Mechanisms for Superplaticity of NiAl Intermetallic," Materials Science Forum, 475-479(IV): 2995-2998.

Harvey, J., Partridge, P. G., and Lurshay, A. M., (1986), "Factors Affecting the Shear Strength of Solid State Diffusion Bonds Between Silver-Coated Clad Al-Zn-Mg Alloy (Aluminium Alloy 7010)," Materials Science and Engineering, 79(2): 191-199.

Hessel V., Ehrfeld, W., Golbig, K., Hoffmann, C., Lowe, H., and Storz, M., (1999), "High Temperature HCN Gerneration in a Complex Integrated Micro-Reaction System," Proceedings of IMRET3, 3RD International Conference on Microreaction Technology, Frankfurt.

Hori, S., Tokizane, M., and Furushiro, N., (1991), "Superplasticity in Advanced Materials," The Japan Society of Research on Superplasticity, Osaka, Japan.

Islam, M. F., and Ridley, N., (1998), "Isostatic Diffusion Bonding of a Microduplex Stainless Steel," Scripta Materialia, 38(8): 1187-1193.

ISO 4287, (1997), "Geometric Product Specification (GPS) – Surface Texture: Profile Method – Terms, Definitions and Surface Texture Parameters," International Organization for Standardization, Geneve, Switzerland.

ISO 4288, (1996), ""Geometric Product Specification (GPS) – Surface Texture: Profile Method – Rules and Procedures for the Assessment of Surface Texture," International Organization for Standardization, Geneve, Switzerland.

Janikowski, S. K., Gombert, D., Soelberg, N. R., Harrup, M., and Jovanovich, G., (2002), "Catalytic Steam Reforming in a Microreactor," Presentation to Idaho National Engineering and Environmental Laboratory," May 22-23.

Jauhari, I., Ogiyama, H., and Tsukuda, H., (2003), "Solid State Diffusion Bonding of Superplastic Duplex Stainless Steel with Carbon Steel," Materials Science Research International, 9(2): 154-159.

Jordan, A. D., Uwakweh, O. N. C., Maziasz, P. J., and Reed, R. W., (1999), "Weld Thermal Simulation and its Effect upon the Microstructure of As-Cast FeAl-Based Materials," Materials Characterization, 43(4): 227-233.

Juan, W., Yajiang, L., and Huiqiang, W., (2002), "Fine Structure at the Diffusion Welded Interface of $Fe_3Al$/Q235 Dissimilar Materials," Bulletin of Materials Science, 24(6): 639-642.

Juan, W., Yajiang, L., Huiqiang, W., and Jiangwei, R., (2002), "Micro-Image Analysis in the Diffusion-Bonded Zone of $Fe_3Al$/Q235 Carbon Steel Dissimilar Materials," Bulletin of Materials Science, 25(5): 367-370.

Juan, W., Yajiang, L., Huiqiang, W., and Jiangwei, R., (2002), "Micro-Image Analysis in the Diffusion-Bonded Zone of $Fe_3Al$/Q235 Carbon Steel Dissimilar Materials," Bulletin of Materials Science, 25(5): 367-370.

Kalpakijan, S. and Schmid, S. R., (2001), "Manufacturing Engineering and Technology," 4th Edition, Prentice-Hall, Inc., New Jersey, USA. pp. 812-813.

Kanlayasiri, K. and Paul, B. K., (2004), "A Nickel Aluminide Microchannel Array Heat-Exchanger for High Temperature Applications," Journal of Manufacturing Processes, 6(1): 17-25.

Kanlayasiri, K. and Paul, B. K., (2004), "A Nickel Aluminide Microchannel Array Heat-Exchanger for High Temperature Applications," Journal of Manufacturing Processes, 6(1): 17-25.

Kanlayasiri, K., (2003), "Development of Nickel Aluminide (NiAl) Microchannel Array Devices for High Temperature Applications," Ph.D.

Dissertation, Industrial and Manufacturing Engineering, Oregon State University.

Kazakov, N. F., (1985), "Diffusion Bonding of Materials," First Edition, Pergamon Press, New York, USA.

Kearns, W. H., (1980), "Welding Handbook: Resistance and Solid-State Welding and Other Joining Processes," 7th edition, Volume 3, American Welding Society, Miami, Florida, USA.

Kim, M., Yi, M. Zhong, J., Bau, H.H., Hu, H. and Ananthasuresh, S.G.K., (1998) "The Fabrication of Flow Conduits in Ceramic Tapes and the Measurement of Fluid Flow through These Conduits," Proceedings of the ASME Dynamic Systems and Controls Division, DSC, 66:171-177.

Knitter, R., Bauer, W., Linner-Kramer, B., and Hansojosten, E., (1999), "Rapid Manufacturing of Ceramic Microcomponents," EUROMAT 99, September 27-30, Munche, 14-18.

Kurasawa, T., Takatsu, H., Sato, S., Kuroda, T., Sugimoto, S., and Tamura, M., (1996), "Diffusion Bonding of Reduced Activation Ferritic Steel F82H for Demo Blanket Application," Journal of Nuclear Materials, 233-237(Pt A): 313-318.

Kuznetsov, V. M., Kadyrov, R. I., and Rudenskii, G. E., (1998), "Calculation of Surface Energy of Metals and Alloys by the Electron Density Functional Method," Journal of Materials Science and Technology, 14(4): 320-322.

Lagerstrom, G. and Xie, M., (2002), "High Performance and Cost Effective Recuperator for Micro-Gas Turbines," American Society of Mechanical Engineers, International Gas Turbine Institute, Turbo Expo (Publication) IGTI, 1: 1003-1008.

Lemus, J., and Drew, R. A. L., (2000), "Diffusion Bonding of Silicon Nitride to Titanium," British Ceramic Transactions, 99(5): 200-205.

Li, H., and Chaki, T. K., (1993), "Welding of a Two-Phase $Ni_3Al$ Alloy," Materials Research Society Symposium Proceedings, 288: 1167-1172.

Li, H., and Chaki, T. K., (1995), "Grain Boundary Melting and Hot Cracking in Weld HAZ of a Two-Phase $Ni_3Al$ Alloy Containing Zr," Materials Research Society Symposium - Proceedings, 364(1): 375-380.

Liv, G., (1996), "Development of Surface Topography During Cold Rolling of Twin-Roll Cast Aluminium," Wear, 192: 216-227.

Loweneheim, F. A. (editor), (1974), "Modern Electroplating," 3rd Editon, John Wiley & Sons, Inc., New York.

Lozovoi, A. Y., Alavi, A., and Finnis, M. W., (2001), "Surface Energy and the Early Stages of Oxidation of NiAl(110)," Computer Physics Communication, 137: 174-194.

Ma, B., Tieu, A. K., Lu, C., and Jiang, Z., (2002), "An Experimental Investigation of Steel Surface Characteristic Transfer by Cold Rolling," Journal of Materials Processing Technology, 125-126: 657-663.

Margevicius, R. W. and Cotton, J. D., (1995), "Study of the Brittle-to-Ductile Transition in NiAl by Texture Analysis," Acta Materialia, 43(2): 645-655.

Marshall, P. D., (2002), "Advanced Sensor Technologies for Micro- to Nano-Scale Biological Measurements," Proceedings of IEEE Sensors, 1(1): 466-471.

Massalski, T. B. (Editor-in-Chief), (1990), "Binary Alloy Phase Diagrams," ASM International, Materials Park, Ohio, pp. 148.

Massalski, T. B., Singleton, M. F., Marray, J. L., and Nash, P., (1990), "Binary Alloy Phase Diagrams," American Society for Metals, Metals Park, Ohio, pp.183.

Matson, D. W., Marin, P. M., Bennett, W. D., Stewart, D. C., and Bonham, C. C., (1999), "Laminated Ceramic Ccomponents for Micro Fluidic Applications," Proceedings of SPIE - The International Society for Optical Engineering, 3877: 95-100.

Matson, D. W., Martin, P., Stewart, D., Tonkovich, A., White, M., Zilka J., and Roberts, G., (1999), "Fabrication of Microchannel Chemical Reactors Using a Metal Lamination Process," Proceedings of IMRET3, 3RD International Conference on Microreaction Technology, Frankfurt.

Maziasz, P. J., Goodwin, G. M., Liu, C. T., and David, S. A. (1992), "Effects of Minor Alloying Elements on the Welding Behavior of FeAl Alloys for Structural and Weld-Overlay Cladding Applications," Scripta Metallurgic, 27(12): 1835-1840.

McKamey, C. G., (1996), "Iron Aluminides," Physical Metallurgy and Processing of Intermetallic Compound, Chapman & Hall, New York, pp. 351-391.

Mishin, Y., and Farkas, D., (1997), "Atomistic Simulation of Grain Boundary Structure and Diffusion in B2 NiAl," Materials Research Society Symposium Proceedings, 458: 21-26.

Moore, T. J. and Kalinowski, J. M., (1993), "Diffusion Brazing NiAl With Self-Generated Filler Metal" Materials Research Society Symposium Proceedings, 288: 1173-1178.

Moore, T. J. and Kalinowski, J. M., (1993), "Diffusion Brazing NiAl With Self-Generated Filler Metal" Materials Research Society Symposium Proceedings, 288: 1173-1178.

Nagano, T., and Wakai, F., (1994), "Relationship Between Surface Roughness and Bonding Strength in Superplastic Diffusion Bonding," Journal of the Ceramic Society of Japan, International Edition, 102(7): 690-693.

Nair, B., Wislon, M., Akash, A., Crandallm J., Lewinsohn, C., Cutler, R., and Flinders, M., (2004), "Ceramic Microfabrication Techniques for Microdevices with Three-Dimensional Architecutre," Materials Research Society Symposium Proceedings, 782: 205-210.

Nakao, Y., Shinozaki, K., and Hamada, M., (1991), "Diffusion Bonding of Intermetallic Compound TiAl," ISIJ International, 31(10): 1260-1266.

Nakao, Y., Shinozaki, K., and Hamada, M., (1991), "Diffusion Bonding of Intermetallic Compound TiAl," ISIJ International, 31(10): 1260-1266.

Nieh, T. G. and Wadsworth, J., (1999), "Fine Structure Superplastic Intermetallics," International Materials Review, 44(2): 59-75.

Noebe, R. D., Bowman, R. R., and Nathal, M. V., (1993), "Physical and Mechanical Properties of the B2 Compound NiAl," International Materials Review, 38(4): 193-232.

Orhan, N., Aksoy, M., and Eroglu, M., (1999), "A New Model for Diffusion Bonding and Its Application to Duplex Alloys," Materials Science and Engineering, A271: 458-468.

Ortego, J. D., Richardson, J. T., and Twigg, M. V., (1997), "Catalytic Steam Reforming of Chlorocarbons: Methyl Chloride," Applied Catalysis B:Environmental, (12)(4): 339-355.

Paul, B. K., and Peterson, R. B., (1999), "Microlamination for Microtechnology Based Energy, Chemical, and Biological Systems," American Society of Mechanical Engineers, Advanced Energy Systems Division (Publication) AES, 39: 45-52.

Paul, B. K., Hasan, H., Dewey, T., Alman, D., and Wilson, R. D., (2002), "An Evaluation of Two Methods for Producing Intermetallic Microchannels,"

American Society of Mechanical Engineers, Micro-Electromechanical Systems Division Publication (MEMS), 261-266.

Paul, B.K., Hasan, H., Thomas, J., Wilson, R., and Alman, D., (2001), "Limits on Aspect Ratio in Two-fluid Micro-scale Heat Exchangers," Transactions of NAMRC XXIX, Gainesville, FL. 461-468.

Paul, B.K., Hasan, H., Thomas, J., Wilson, R., and Alman, D., (2001), "Limits on Aspect Ratio in Two-fluid Micro-scale Heat Exchangers," Transactions of NAMRC XXIX, Gainesville, FL. 461-468.

Peterson, R. B, (1999), "Numerical Modeling of Conduction Effects in Microscale Counterflow Heat Exchangers," Microscale Thermophysical Engineering, 3(1):17-30.

Peterson, R. B., (1998), "Size Limits for Regenerative Heat Engines," Microscale Thermophysical Engineering, 2: 121-131.

Philibert, J., (1991), "Reactive Diffusion in Thin Films," Applied Surface Science, 53:74-81.

Pilling, J., (1988), "The Kinetics of Isostatic Diffusion Bonding in Superplastic Materials," Materials Science and Engineering, 100: 137-144.

Pilling, J., Ridley, N., and Islam, M. F., (1996), "On the Modelling of Diffusion Bonding in Materials: Superplastic Super Alpha-2," Materials Science and Engineering A: Structural Materials: Properties, Microstructure and Processing, A205(1-2): 72-78.

Pint, B. A., Swindeman, R. W., More, K. L., Tortorelli, P. F., (2001) "Materials Selection for High Temperature (750°-1000°C) Metallic Recuperators for Improved Efficiency Microturbines," ASME Paper #2001-GT-445, presented at the International Gas Turbine & Aeroengine Congress & Exhibition, New Orleans, LA,

Raj, S.V. and Farmer, S. C., (1995), "Characteristics of a New Creep Regime in Polycrystalline NiAl," Metallurgical and Materials Transaction A: Physical Metallurgy and Materials Science, 26A(2): 343-356.

Rawers, J. C., Hansen, J. S., Alman, D. E., and Hawk, J. A., (1994), "Formation of Sheet Metal-Intermetallic Composites by Self-Propagating High-Temperature Reactions," Journal of Materials Science Letters, 13:1357-1360.

Rawers, J. C., Hansen, J. S., Alman, D. E., and Hawk, J. A., (1994), "Formation of Sheet Metal-Intermetallic Composites by Self-Propagating

High-Temperature Reactions," Journal of Materials Science Letters, 13: 1357-1360.

Ray, R., (1990), "Dipersion Strengthened Nickel Aluminide (NiAl) Alloys via Advanced Melt Spinning Technology," Metal Powder Report, 45(1): 56-59.

Santella, M. L, and David, S. A., (1985), "Study of HAZ Cracking in Ductile Aluminides," Abstracts **of** Papers Presented at 66th AWS Annual Meeting, 228-230.

Santella, M. L., David, S. A., and Horton, J. A., (1986), "Weldability of and Ni3Al Alloy," Advances in Welding Science and Technology - TWR '86: Proceedings of an International Conference on Trends in Welding Research, 629-633.

Sauthoff, G., (1995), "Intermetallics," Weinhem, New York, pp. 1-2, 38-40.

Sauthoff, G., (1995), "Intermetallics," Weinhem, New York, pp. 84-87.

Schwartz, M. M., (1979), "Metal Joining Manual," McGraw-Hill, New York, USA.

Sikka, V. K., (1996), "Processing of Aluminides," Physical Metallurgy and Processing of Intermetallic Compound, Chapman & Hall, New York, pp. 561-562.

Sikka, V. K., (1996), "Processing of Aluminides," Physical Metallurgy and Processing of Intermetallic Compound, Chapman & Hall, NewYork, pp. 598-599.

Sikka, V. K., Viswanathan, S., and McKamey, C. G., (1993), "Development and Commercialization Status of $Fe_3Al$ Based Intermetallic Alloys," Proceedings of the First International Symposium on Structural Intermetallics Structural Intermetallics," The Materials Society, Warrendale, PA, pp. 483-491.

Somekawa, H., and Higashi, K., (2003), "The Optimal Surface Roughness Condition on Diffusion Bonding," Materials Transactions, 44(8): 1640-1643.

Somekawa, H., Watanabe, H., and Higashi, K., (2003), "The Grain Size Dependence on Diffusion Bonding Behavior in Superplastic Mg Alloys," Materials Transactions, 44(4): 496-503.

Stoloff, N. S. and Alman, D. E., (1991), "Powder Processing of Intermetallic Alloys and Intermetallic Matrix Composites," Material Science and Engineering A, 144(1-2): 51-62.

Stoloff, N. S., and Sikka V. K. (editors) (1996), "Physical Metallurgy and Processing of Intermetallic Compounds," Chapman and Hall, New York, NY, pp. 217.

TeGrotenhuis W. E., Wegneg, R. S., Vanderwiel, D. P., Whyatt, G. A., Viswanath, V. V., Schielke, K. P. ,(2000), "Microreactor System Design for NASA In Situ Propellant Production Plant on Mars," AICHE Spring National Meeting, Atlanta, GA.

Thomas, J. and Paul, B. K., (2002), "Thermally-Enhanced Edge Registration (TEER) for Aligning Metallic Microlaminated Devices," Transactions of NAMRC XXX, West Lafayette, IN, 21-24.

Ugural, A. C. and Fenster, S. K., (1987), "Advanced Strength and Applied Elasticity," 2nd Edition, Elsevier Science Publishing Co, Inc., New York, pp.

Veeco, (2000), "Dektak 3 Surface Profile Measuring System: Installation, Operation, and Maintenance Manual," Veeco Metrology Group, Santa Barbra, USA.

Wallis, I. C., Ubhi, H. S., Bacos, M. P., Josso, P., Lindqvist, J., Lundstrom, D., and Wisbey, A., (2004), "Brazed Joints in γ TiAl Sheet: Microstructure and Properties," Intermetallics, 12(3): 303-316.

Wattanutchariya, W., (2002), "Application of Buckling Behavior to Evaluate and Control Shape Variation in High-Temperature Microlamination," Ph.D. Dissertation, Industrial and Manufacturing Engineering, Oregon State University.

Wilcox, D. L., Burdon, J. W., Changrani, R., Chou, c., Dai, S., Koripella, R., Oliver, M., Sadler, D., Allmen, P. V., and Zenhauasern, F., (2002), "Add Ceramic "MEMS" to the Pallet of Microsystem Technologies," Materials Research Society Symposium Proceedings, 687: 225-242.

Wilcox, D. L., Burdon, J. W., Changrani, R., Chou, c., Dai, S., Koripella, R., Oliver, M., Sadler, D., Allmen, P. V., and Zenhauasern, F., (2002), "Add Ceramic "MEMS" to the Pallet of Microsystem Technologies," Materials Research Society Symposium Proceedings, 687: 225-242.

Wright R. N., and Knobloe, J. R., (1990), "Influence of Alloying on the Microstructure and Mechanical Properties of P/M $Ni_3Al$," Acta Metalllurgica, 38(10): 1993-2001.

Yang, C. F., Chiu, L. H., Lee, S. C., and Sun, J. Y., (1998), "Solid State and Transient Liquid Phase Diffusion Bonding of an Al-Zn-Mg Alloy,"

Proceedings of the National Science Council, Republic of China, Part A: Physical Science and Engineering, 22(1): 132-141.

Zuruzi, A. S., Li, H., and Dong, G., (1999), "Effects of Surface Roughness on the Diffusion Bonding of Al Alloy 6061 in Air," Materials Science and Engineering A, 270(2): 244-248.

# APPENDICES

## Appendix A. Computer Simulation for an Isostatic Diffusion Bonding Model

```
upper = 0.99;

%printf('Enter 1 to calculate bonding time\n');
%printf('Enter anything else to calculate void fraction\n');
choice = input('Enter 1 to calculate bonding time, anything else to calculate the
void fraction\n');

if (choice == 1)
        lower=input('Enter the void fraction at which bonding is considered
DONE!! \n');
%       final = quad('total', upper, lower);
inc = 0.00001;
FINALSUM = 0;

counter = 1;
start = upper;
while(counter <= ((upper - lower)/inc) + 1)
   value(counter) = totalNIAL(start);
   FINALSUM = FINALSUM + value(counter).*inc;
   counter =counter + 1;
   start = start - inc;
end

-FINALSUM
-FINALSUM/3600

else
        tbond=input('Enter the bonding time - void fraction expected will be
output!! \n');
        counter = 1;
        inc = 0.001;
   tquad = 0;
   start = upper;
        while (counter >=1)
      tquad = tquad + totalNIAL(start)*inc;
      if (tbond < -tquad)
                        counter = 0;
                else
```

```
                start = start - inc;
            end
    end
        start
end


function [result] = totalNIAL(f)

        omega = 2.40625*10^(-29);                   %m3
        k = 1.38*10^(-23);                          %J/atom-K
        R = 8.314;                                  %J/mol-K
        Ra= 0.95*10^(-6);                           %m
        Lambda= 30*10^(-6);                         %m
        ro = Lambda/2;                              %m
        ho = 2*Ra;                                  %m
        d = 25*10^(-6);                             %m
        T = 1073;                                   %K
        p = 20*10^(6);                              %N/m2

        Tm =1955;                                   %K
        gamma = 2.65;                               %J/m2



        %*******Derived

        Dv = 3.2*10^(-3) * exp(-200000/ (R*T));     %m2/s


        Dgb = 10^((-0.06279*(10^4)/T) – 4.4604);    %m3/s

        E = 188 * 10^(9);                           %N/m2
        Et = E-E*(T-240)*(0.0002);                  %N/m2


        sigma_r = (p - 2*gamma/ro)*( (sqrt(f) - 1)/(1 - f));
        sigma_c = (-p - 2*gamma/ro)*( (sqrt(f) + 1)/(1 - f));
        sigma_z = -p/(1 - f);
        sigma_m = sqrt(0.5*((sigma_r - sigma_c)^2 + (sigma_c - sigma_z)^2
+(sigma_z - sigma_r)^2));
```

```
        e_dot= (2.7*10^(14)*(p/Et)^(2.0))*(exp(-314000/(R*T)));

        e_r_dot = e_dot*( (sigma_r - (sigma_c + sigma_z)/2)/sigma_m);
        e_z_dot = e_dot*( (sigma_z - (sigma_c + sigma_r)/2)/sigma_m);


        g1 = -2*e_r_dot*(1-f);
        g2 = ((-4*omega*Dv/(k*T))*(p/((ro^2)))*( f / (log(1/f)  - (1-f)/2)));
        g3 = ((-2*omega*Dgb/(k*T))*(p/((ro^2)))*( 1 / (log(1/f)  - (1-f)/2))*((1
+ ho*f/d)/ho*f) );

        result = 1/(g1 + g2 + g3);
end
```

# Appendix B. Plot Between Rate of Change in Void Fraction vs. Time

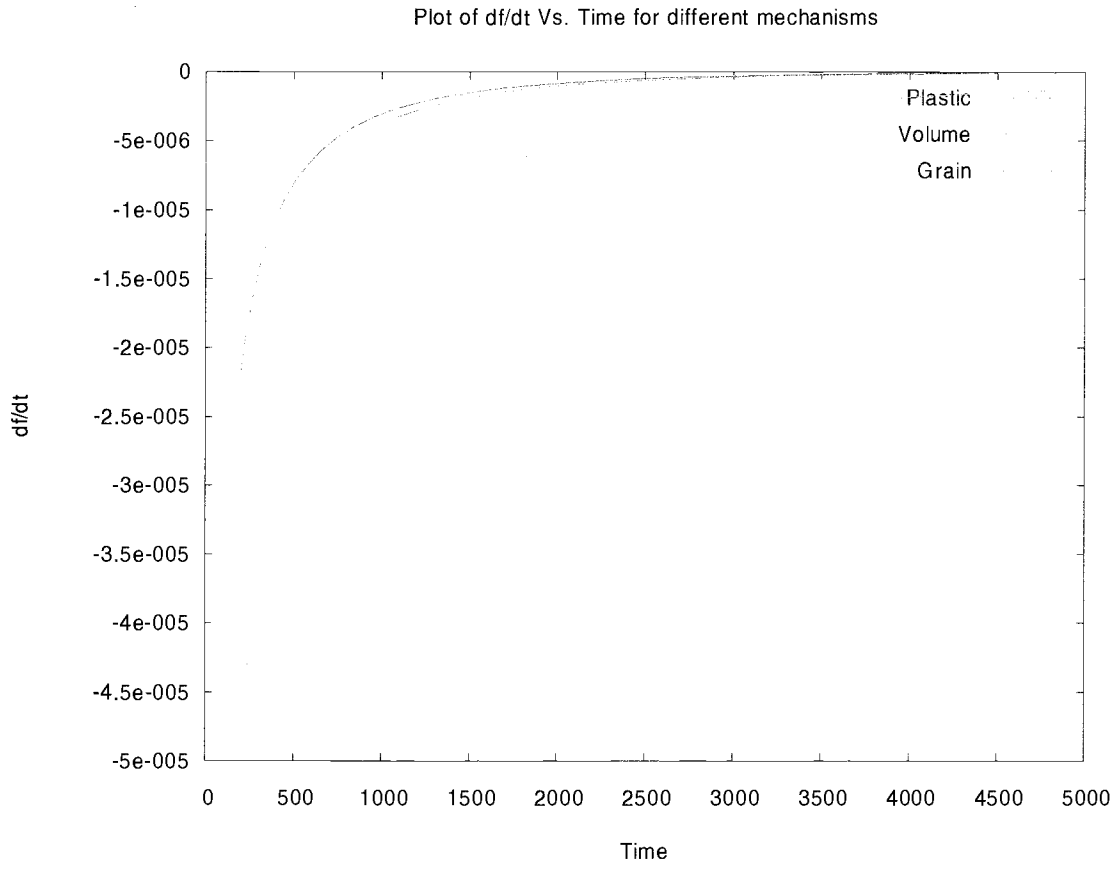

## Appendix C. Point EDS Analysis of the Diffusion Bonded Samples

| | | Al | Ni | Al | Ni |
|---|---|---|---|---|---|
| | | wt% | wt% | at% | at% |
| 1. | Top | 40.42 | 59.57 | 59.61 | 40.38 |
| | Middle | 37.84 | 62.158 | 56.97 | 43.02 |
| | Bottom | 34.52 | 65.47 | 53.42 | 46.57 |
| 2. | Top | 41.03 | 58.96 | 60.22 | 39.77 |
| | Middle | 33.11 | 66.88 | 51.85 | 48.14 |
| | Bottom | 41.11 | 58.88 | 60.29 | 39.70 |
| 3. | Top | 35.91 | 64.08 | 54.93 | 45.06 |
| | Middle | 32.45 | 67.54 | 51.10 | 48.89 |
| | Bottom | 40.58 | 59.41 | 59.77 | 40.22 |
| 4. | Top | 38.88 | 61.11 | 58.05 | 41.94 |
| | Middle | 20.69 | 79.30 | 36.21 | 63.78 |
| | Bottom | 35.17 | 64.82 | 54.13 | 45.86 |
| 5. | Top | 43.60 | 56.39 | 62.71 | 37.28 |
| | Middle | 47.37 | 52.62 | 66.19 | 33.80 |
| | Bottom | 44.67 | 55.32 | 63.72 | 36.27 |

## Appendix D. Point EDS Analysis of Diffusion Bonded NiAl Samples

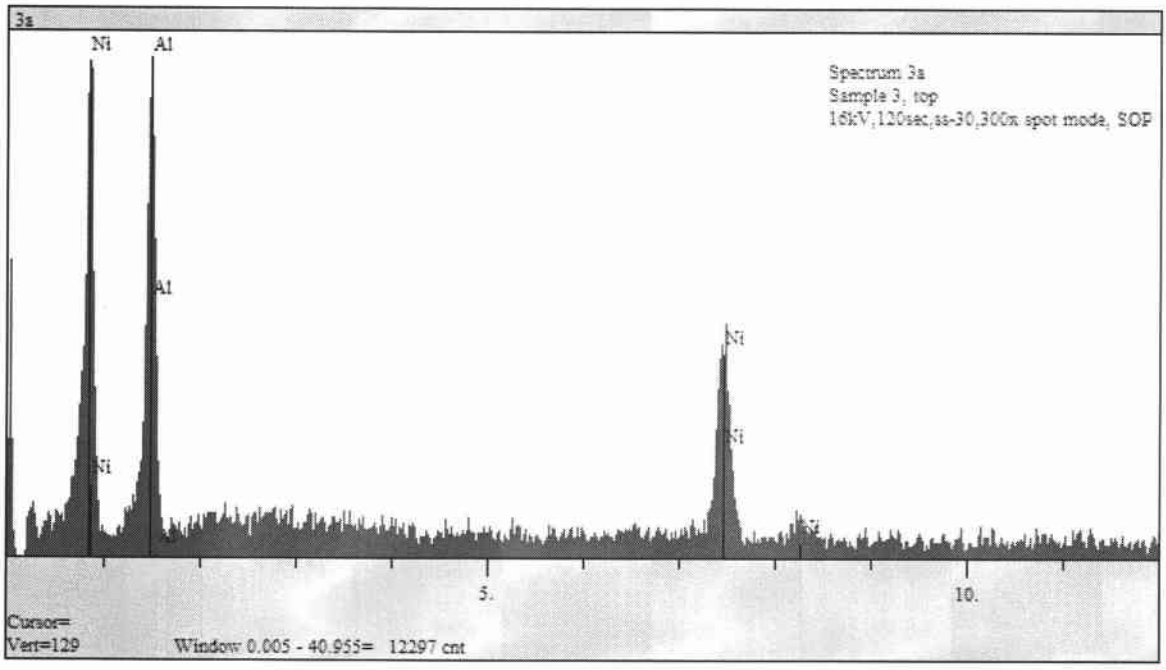


| Elt. | Line | Intensity (c/s) | Error 2-sig | Conc | Units | |
|---|---|---|---|---|---|---|
| Al | Ka | 10.02 | 0.614 | 40.427 | wt.% | |
| Ni | Ka | 6.19 | 0.519 | 59.573 | wt.% | |
| | | | | 100.000 | wt.% | Total |

kV 16.0
Takeoff Angle 17.6°
Elapsed Livetime 120.0

**Spectrograph of elemental composition of sample 1 top.**

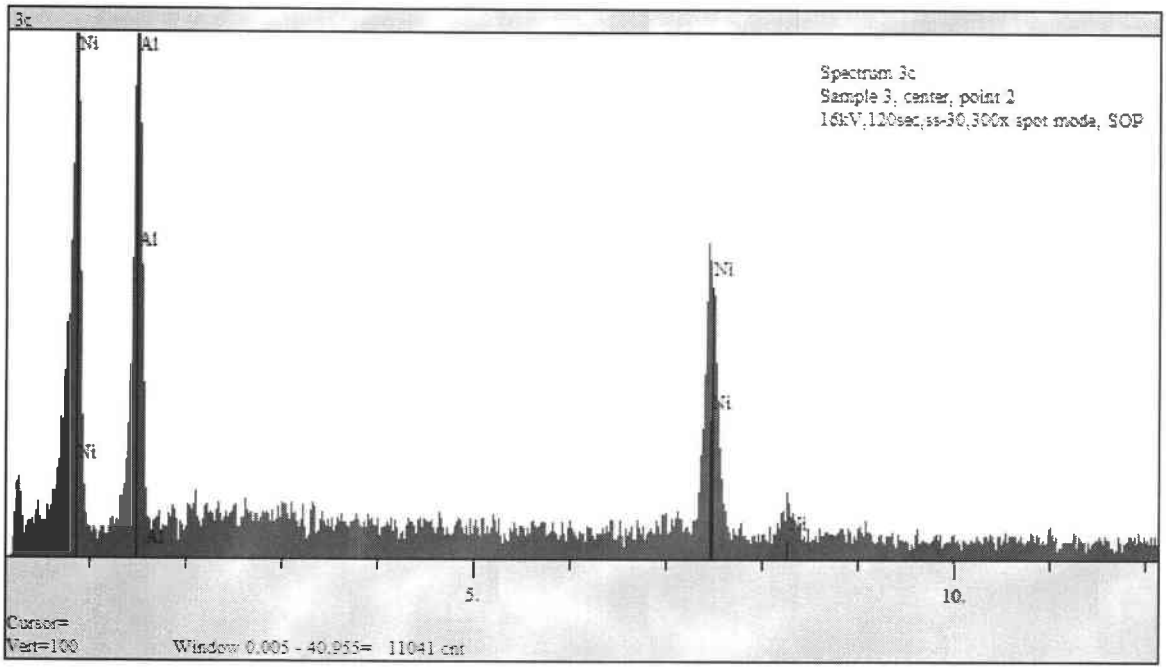


| Elt. | Line | Intensity (c/s) | Error 2-sig | Conc | Units | |
|---|---|---|---|---|---|---|
| Al | Ka | 8.98 | 0.587 | 37.842 | wt.% | |
| Ni | Ka | 6.37 | 0.520 | 62.158 | wt.% | |
| | | | | 100.000 | wt.% | Total |

kV 16.0
Takeoff Angle 17.6°
Elapsed Livetime 120.0

**Spectrograph of elemental composition of sample 1 middle.**

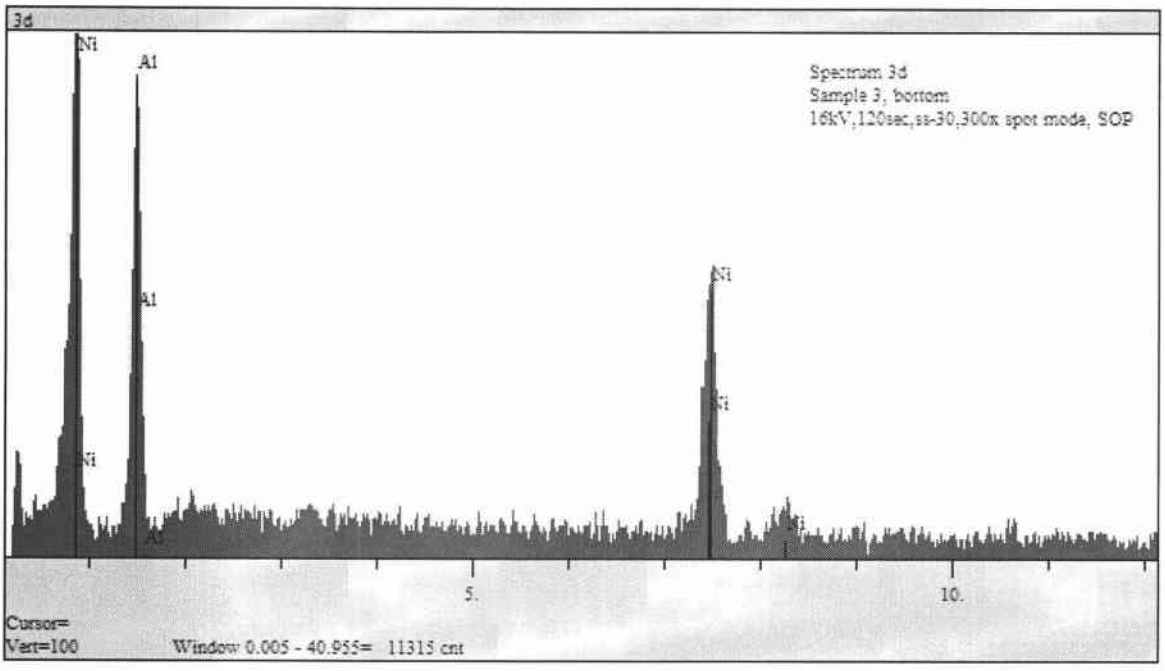


| Elt. | Line | Intensity (c/s) | Error 2-sig | Conc | Units | |
|---|---|---|---|---|---|---|
| Al | Ka | 7.36 | 0.533 | 34.529 | wt.% | |
| Ni | Ka | 6.26 | 0.513 | 65.471 | wt.% | |
| | | | | 100.000 | wt.% | Total |

kV 16.0
Takeoff Angle 17.6°
Elapsed Livetime 120.0

**Spectrograph of elemental composition of sample 1 bottom.**

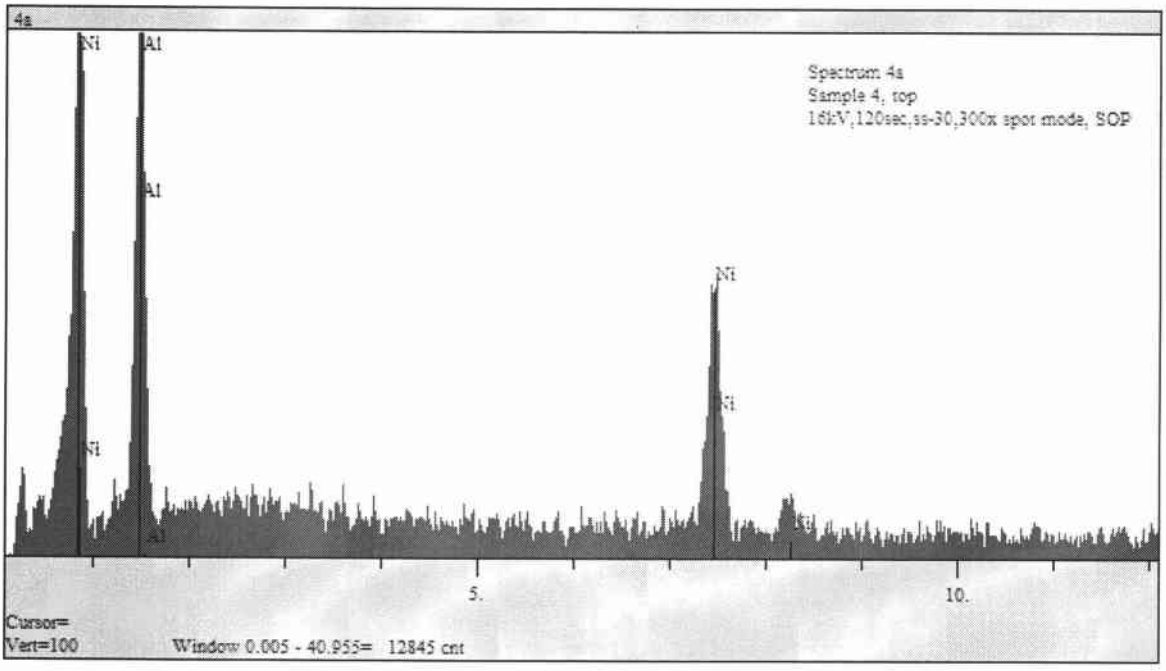


| Elt. | Line | Intensity (c/s) | Error 2-sig | Conc | Units | |
|---|---|---|---|---|---|---|
| Al | Ka | 10.23 | 0.615 | 41.037 | wt.% | |
| Ni | Ka | 6.12 | 0.508 | 58.963 | wt.% | |
| | | | | 100.000 | wt.% | Total |

kV 16.0
Takeoff Angle 17.6°
Elapsed Livetime 120.0

**Spectrograph of elemental composition of sample 2 top.**

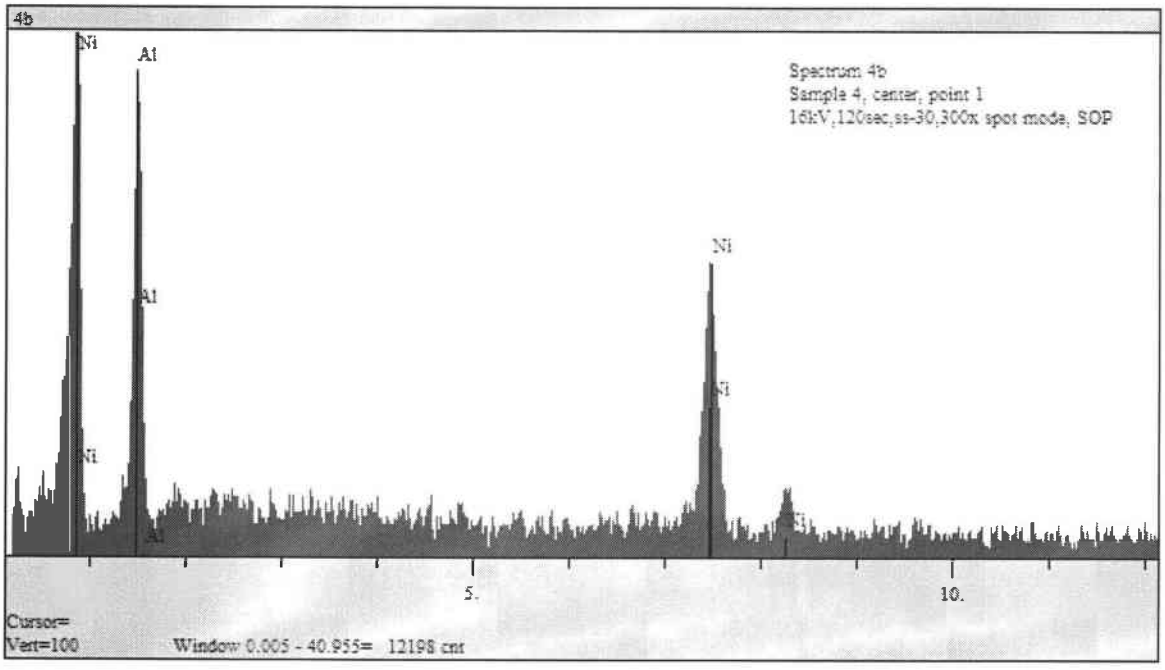


| Elt. | Line | Intensity (c/s) | Error 2-sig | Conc | Units | |
|---|---|---|---|---|---|---|
| Al | Ka | 7.03 | 0.531 | 33.115 | wt.% | |
| Ni | Ka | 6.46 | 0.527 | 66.885 | wt.% | |
| | | | | 100.000 | wt.% | Total |

kV 16.0
Takeoff Angle 17.6°
Elapsed Livetime 120.0

**Spectrograph of elemental composition of sample 2 middle.**

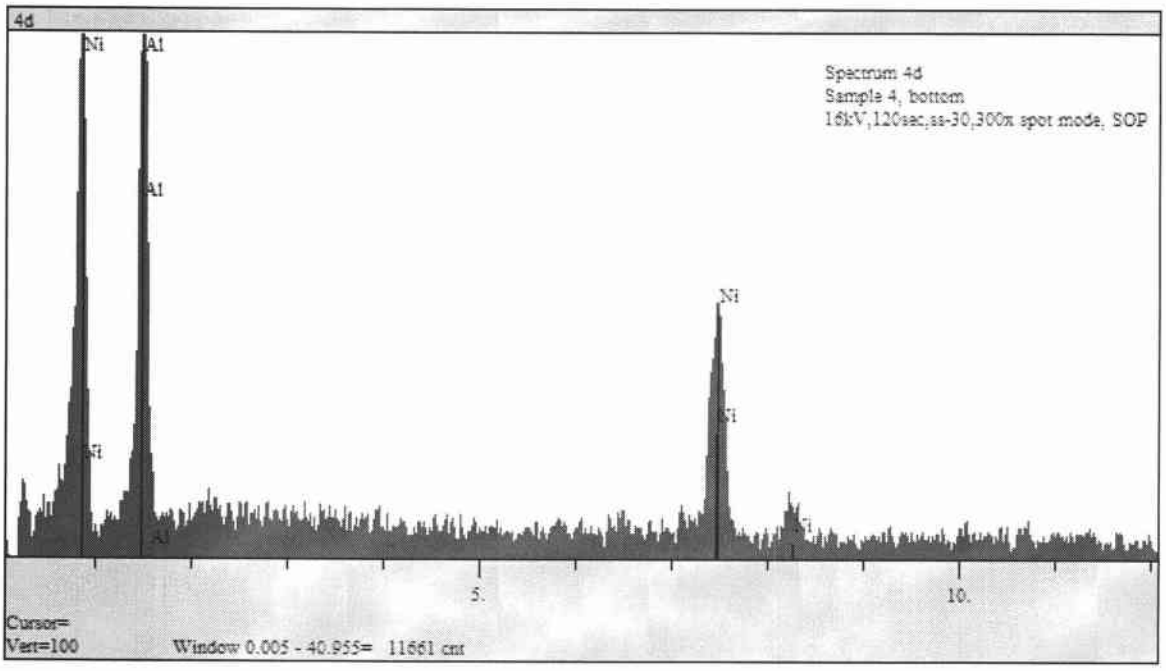


| Elt. | Line | Intensity (c/s) | Error 2-sig | Conc | Units | |
|---|---|---|---|---|---|---|
| Al | Ka | 9.93 | 0.601 | 41.115 | wt.% | |
| Ni | Ka | 5.91 | 0.486 | 58.885 | wt.% | |
| | | | | 100.000 | wt.% | Total |

kV 16.0
Takeoff Angle 17.6°
Elapsed Livetime 120.0

**Spectrograph of elemental composition of sample 2 bottom.**

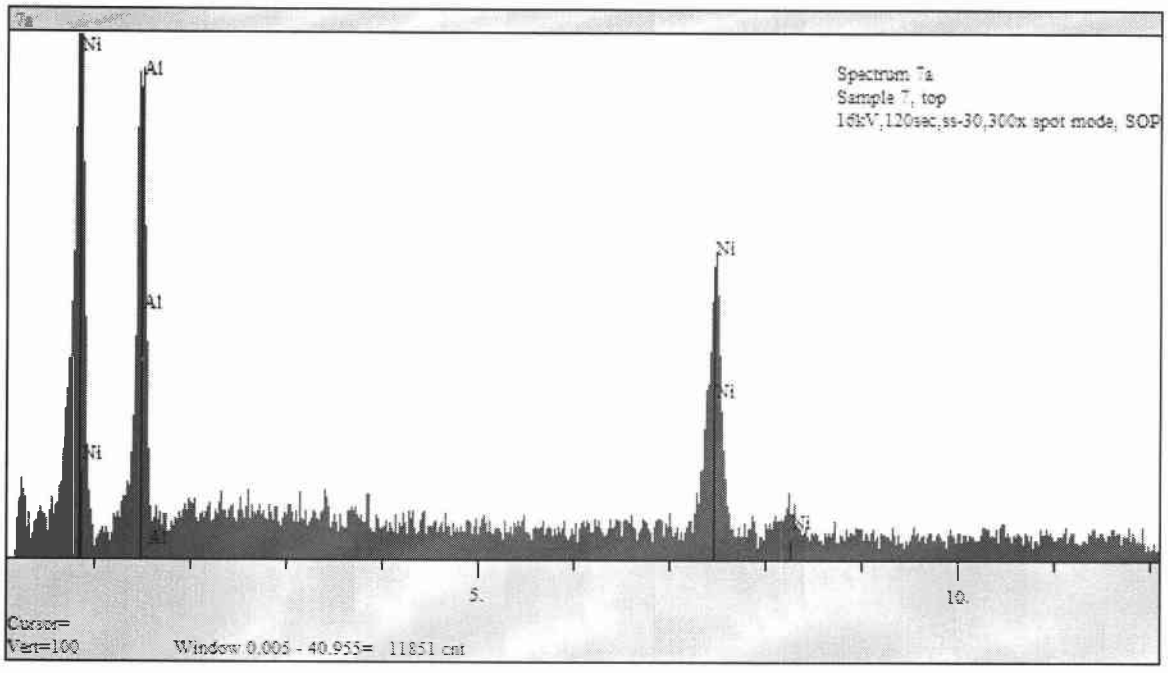


| Elt. | Line | Intensity (c/s) | Error 2-sig | Conc | Units | |
|---|---|---|---|---|---|---|
| Al | Ka | 7.92 | 0.550 | 35.911 | wt.% | |
| Ni | Ka | 6.24 | 0.502 | 64.089 | wt.% | |
| | | | | 100.000 | wt.% | Total |

kV 16.0
Takeoff Angle 17.6°
Elapsed Livetime 120.0

**Spectrograph of elemental composition of sample 3 top.**

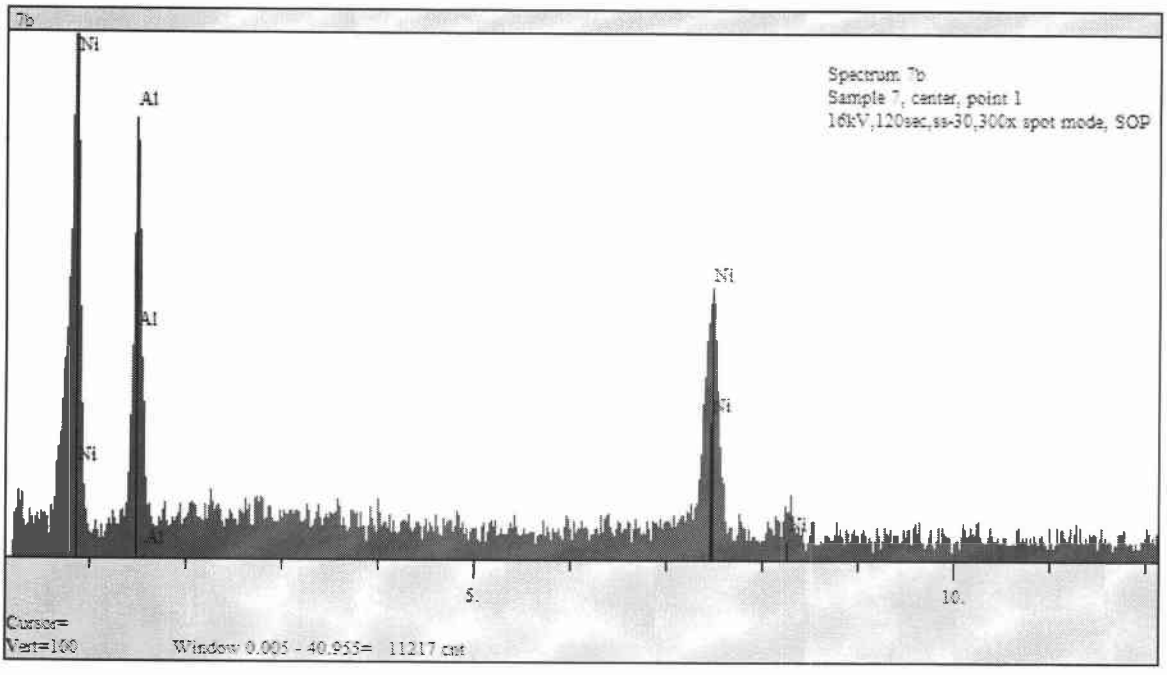


| Elt. | Line | Intensity (c/s) | Error 2-sig | Conc | Units | |
|---|---|---|---|---|---|---|
| Al | Ka | 6.20 | 0.503 | 32.454 | wt.% | |
| Ni | Ka | 5.91 | 0.507 | 67.546 | wt.% | |
| | | | | 100.000 | wt.% | Total |

kV 16.0
Takeoff Angle 17.6°
Elapsed Livetime 120.0

**Spectrograph of elemental composition of sample 3 middle.**

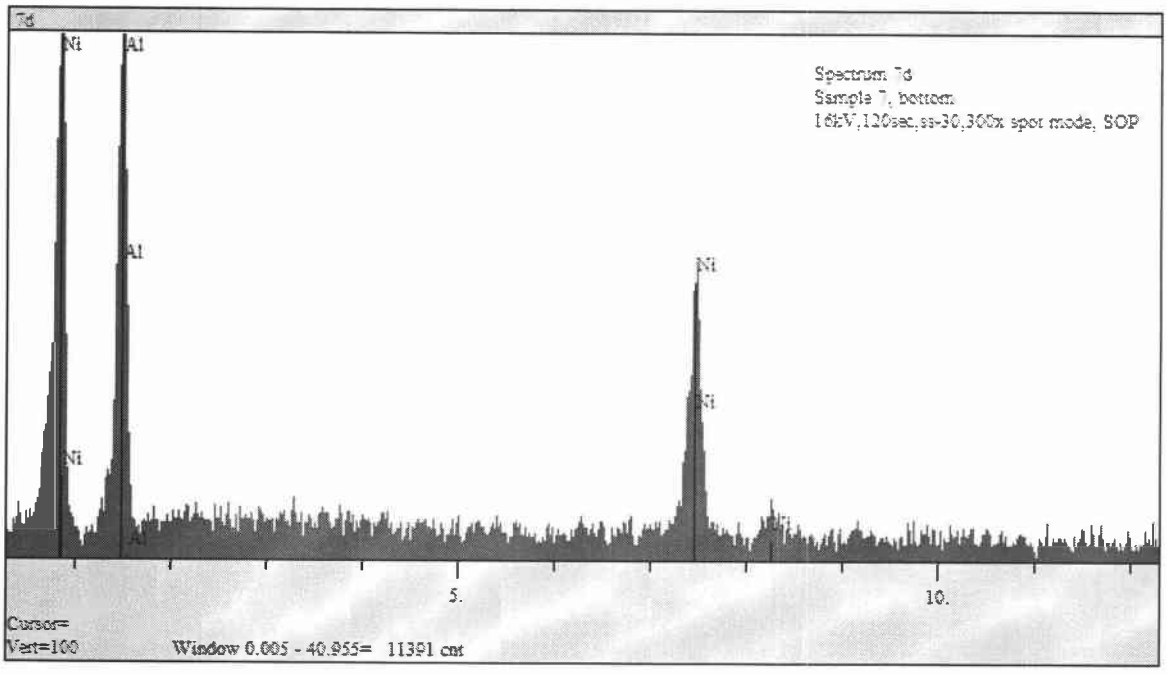


| Elt. | Line | Intensity (c/s) | Error 2-sig | Conc | Units | |
|---|---|---|---|---|---|---|
| Al | Ka | 9.19 | 0.588 | 40.582 | wt.% | |
| Ni | Ka | 5.63 | 0.495 | 59.418 | wt.% | |
| | | | | 100.000 | wt.% | Total |

kV 16.0
Takeoff Angle 17.6°
Elapsed Livetime 120.0

**Spectrograph of elemental composition of sample 3 bottom.**

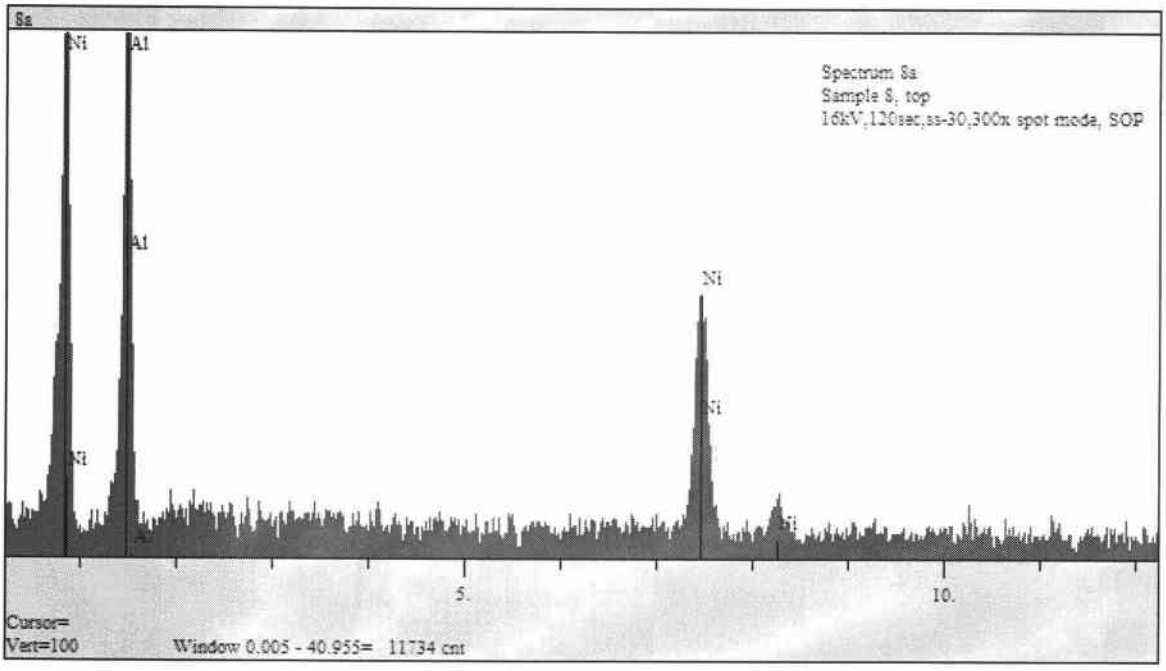


| Elt. | Line | Intensity (c/s) | Error 2-sig | Conc | Units | |
|---|---|---|---|---|---|---|
| Al | Ka | 8.84 | 0.585 | 38.889 | wt.% | |
| Ni | Ka | 5.93 | 0.505 | 61.111 | wt.% | |
| | | | | 100.000 | wt.% | Total |

kV 16.0
Takeoff Angle 17.6°
Elapsed Livetime 120.0

**Spectrograph of elemental composition of sample 4 top.**

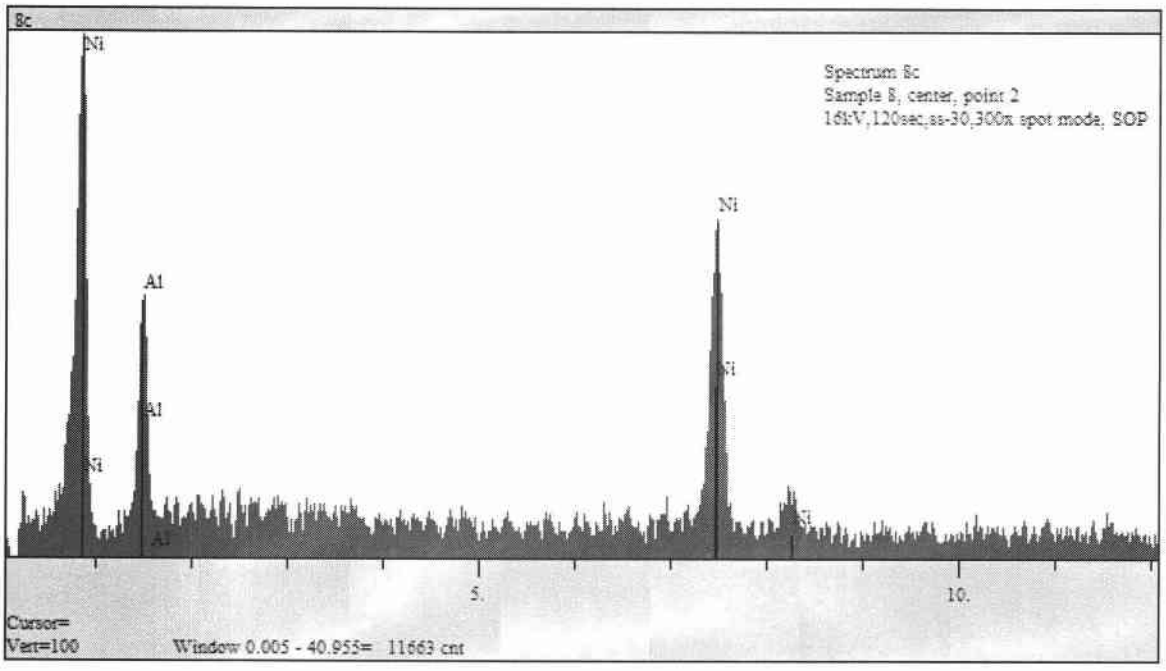


| Elt. | Line | Intensity (c/s) | Error 2-sig | Conc | Units | |
|---|---|---|---|---|---|---|
| Al | Ka | 3.53 | 0.393 | 20.697 | wt.% | |
| Ni | Ka | 6.97 | 0.544 | 79.303 | wt.% | |
| | | | | 100.000 | wt.% | Total |

kV 16.0
Takeoff Angle 17.6°
Elapsed Livetime 120.0

**Spectrograph of elemental composition of sample 4 middle.**

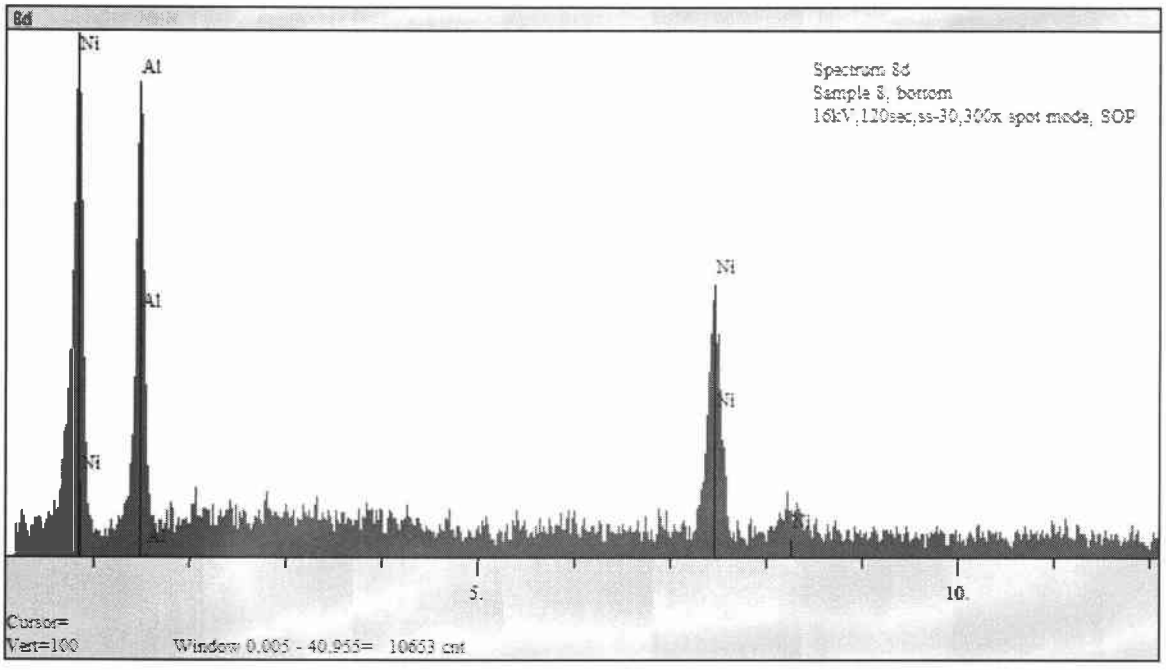


| Elt. | Line | Intensity (c/s) | Error 2-sig | Conc | Units | |
|---|---|---|---|---|---|---|
| Al | Ka | 6.97 | 0.525 | 35.173 | wt.% | |
| Ni | Ka | 5.71 | 0.513 | 64.827 | wt.% | |
| | | | | 100.000 | wt.% | Total |

kV 16.0
Takeoff Angle 17.6°
Elapsed Livetime 120.0

**Spectrograph of elemental composition of sample 4 bottom.**

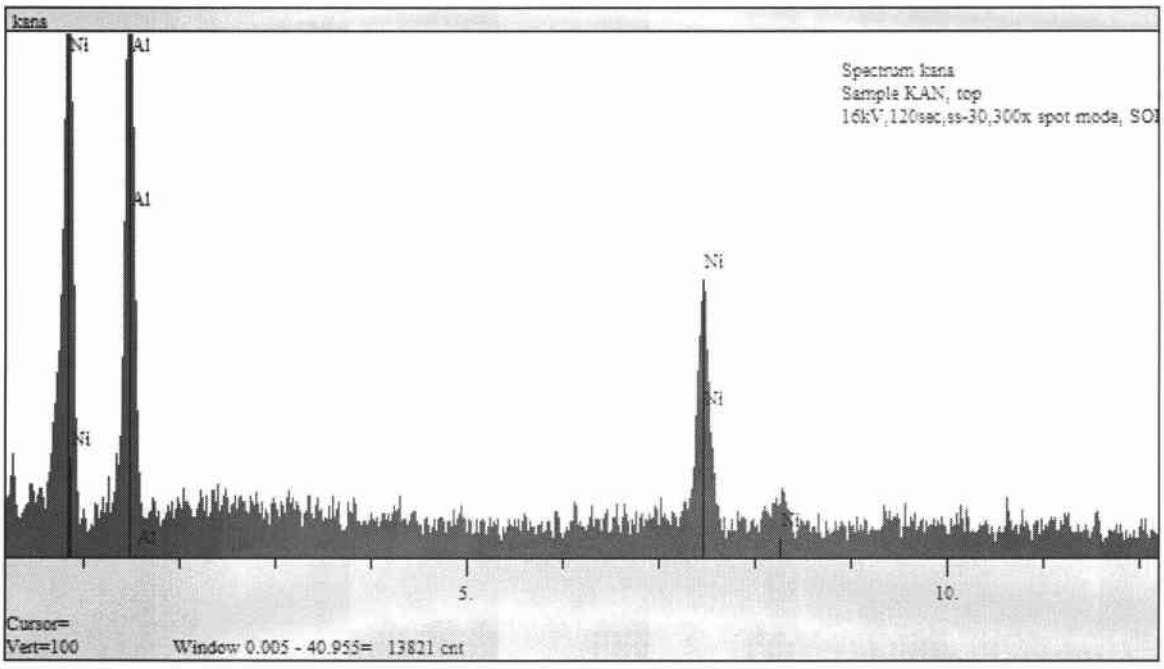


| Elt. | Line | Intensity (c/s) | Error 2-sig | Conc | Units | |
|---|---|---|---|---|---|---|
| Al | Ka | 10.58 | 0.624 | 43.606 | wt.% | |
| Ni | Ka | 5.53 | 0.495 | 56.394 | wt.% | |
| | | | | 100.000 | wt.% | Total |

kV 16.0
Takeoff Angle 17.6°
Elapsed Livetime 120.0

**Spectrograph of elemental composition of sample 5 top.**

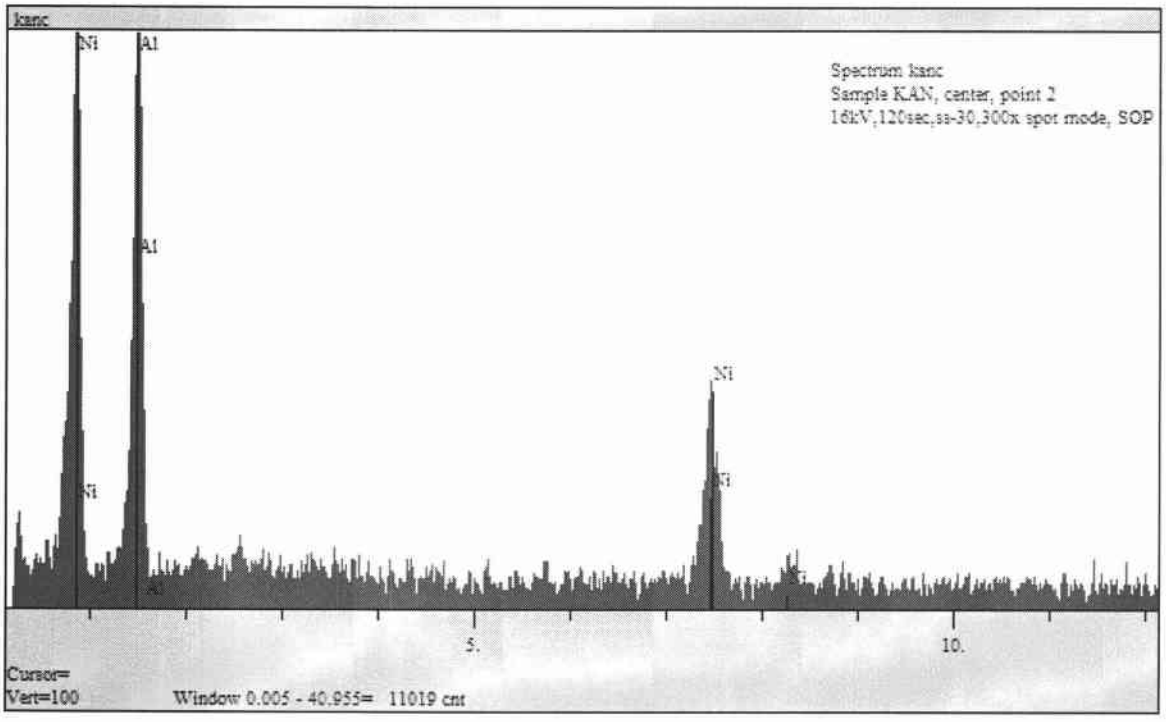


| Elt. | Line | Intensity (c/s) | Error 2-sig | Conc | Units | |
|---|---|---|---|---|---|---|
| Al | Ka | 9.42 | 0.591 | 47.376 | wt.% | |
| Ni | Ka | 4.04 | 0.437 | 52.624 | wt.% | |
| | | | | 100.000 | wt.% | Total |

kV 16.0
Takeoff Angle 17.6°
Elapsed Livetime 120.0

**Spectrograph of elemental composition of sample 5 middle.**

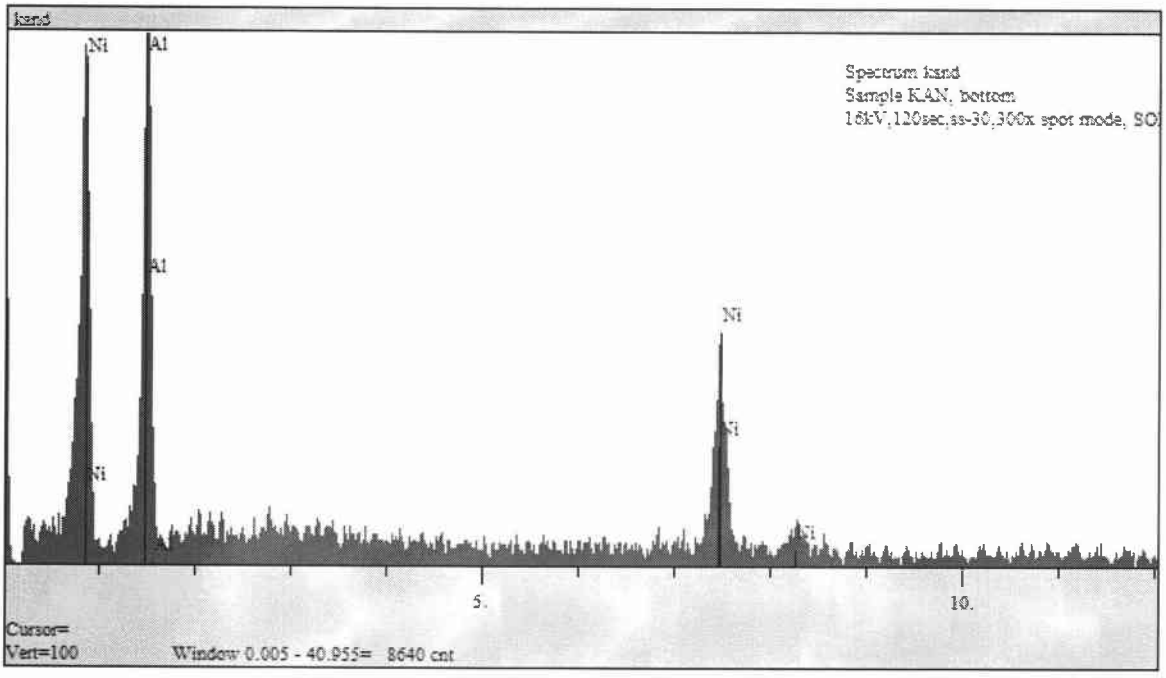


| Elt. | Line | Intensity (c/s) | Error 2-sig | Conc | Units | |
|---|---|---|---|---|---|---|
| Al | Ka | 8.38 | 0.567 | 44.672 | wt.% | |
| Ni | Ka | 4.14 | 0.434 | 55.328 | wt.% | |
| | | | | 100.000 | wt.% | Total |

kV 16.0
Takeoff Angle 17.6°
Elapsed Livetime 120.0

**Spectrograph of elemental composition of sample 5 bottom.**